NMR spectroscopy

- **Feb. 25: Introduction to NMR spectroscopy and instrumentation**
- **Feb 27: Field trip to NMRFAM, tour of NMR instruments (Mark Anderson)**
  - **Meet @9:45a in East Atrium of Biochemistry addition; 433 Babcock Dr.**
- **Mar 1: Basic theory of NMR**
- **Mar 4: Theory and application of MR flow imaging and related techniques**
- **Mar 6: Introduction to theory and practice of 2D NMR spectroscopy**
- **Mar 8: Assignments of an organic molecule using 2D NMR**

W. Milo Westler
Spring 2013

CBE 575:
Instrumental Analysis for Chemical Engineers

References

- The lecture notes CBE_575_2013.pdf are available.

- A couple of references dealing with the use of NMR imaging in engineering
  - Mantle, M. D. & Sederman, a. J. Dynamic MRI in chemical process and reaction engineering. Progress in Nuclear Magnetic Resonance Spectroscopy 43, 3–60 (2003).
  - Gladden, L. F. & Sederman, A. J. Recent advances in Flow MRI. Journal of magnetic resonance (San Diego, Calif. : 1997) 1–10 (2012).doi:10.1016/j.jmr.2012.11.022
- These references deal with NMR instrumentation
  - Hoult, D. I. The NMR Receiver : A Description and Analysis of Design. 12, 41–77 (1978). (VERY old, but very good, lots of electonics).
  - Laukien, D. D. & Tschopp, W. H. Superconducting NMR magnet design. Concepts in Magnetic Resonance 6, 255–273 (1994).
  - Cornell, D. a., Clewett, C. F. M. & Conradi, M. S. Versatile pulsed NMR system and experiments for students. Concepts in Magnetic Resonance 12, 257–268 (2000). (build your own NMR spectrometer).
- http://www.acornnmr.com/codeine/assignment_strategy.htm this is a (very old) webpage on the assignment strategy for small organic compounds using 1 and 2 dimensional NMR. (Note: HMQC contains the same information as HSQC).
- http://www.nmrfam.wisc.edu/links/biochem-800/lecture_notes/ This is the web site for my course (bchm 800). The pdf files: paradigm_I.pdf, paradigm_II.pdf, & paradigm_III.pdf have some classical (vector) NMR theory (esp. I and II), which is very pictorial in nature. There is also a lot of advanced stuff that I will not talk about. The presentation bchm_800.pdf has 380 slides. Most of it is probably unintelligible. I will use some sections of this. These have been incorporated into CBE_575_2013.pdf
- Understanding NMR Spectroscopy – James Keeler – an excellent introduction to modern NMR spectroscopy from a short course in Barcelona 2004. Keeler_understanding.zip

Nuclear Magnetic Resonance

What is it good for?

- **Structure and dynamics of molecules in solution**
  - **Biomolecular, organic, and inorganic**
- **Solid state**
  - **Atomic and bulk properties of materials**
- **Medical Imaging (MRI) – they dropped the word "nuclear"**
  - **detection, diagnosis, treatment planning and follow-up of many diseases.**
- **Other applications**
  - **Material transfer in porous media**
  - **Phase changes (hydration, crystallisation, gelling)**
  - **Diffusion**
  - **Displacement speeds**
  - **Petroleum industry**
    - **rock core analysis to help determine hydrocarbon reserves, estimate recoverable quantities, and gauge ease of recovery.**
  - **Magnetic resonance force microscopy (nm scales) –detected single electron**
  - **Optically detected NMR**
  - **Artic ice salinity (in earth's magnetic field)**
  - **Quantum computing (early)**

Zeeman Hamiltonian

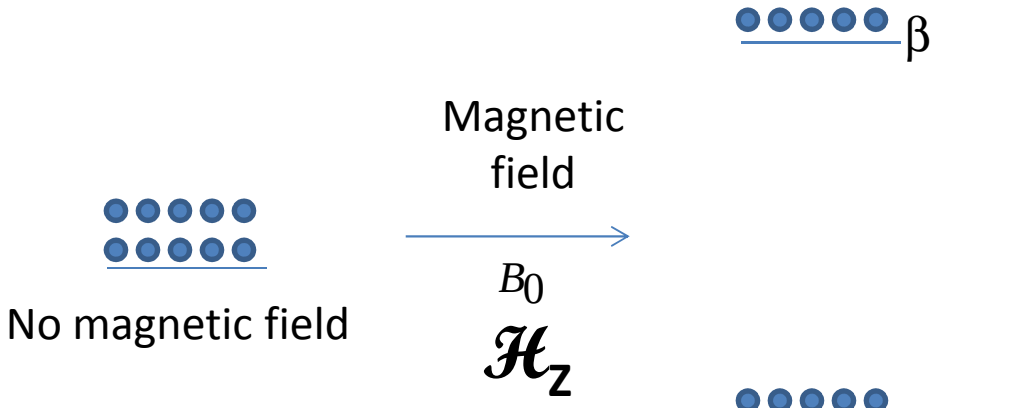

$$E = \gamma B_0 I_m$$

$$I_m = \pm\frac{1}{2} \equiv \text{nuclear spin}$$

$$\gamma = \text{gyromagnetic ratio}$$

$$n_\alpha = n_\beta$$

Zeeman/Relaxation Hamiltonian

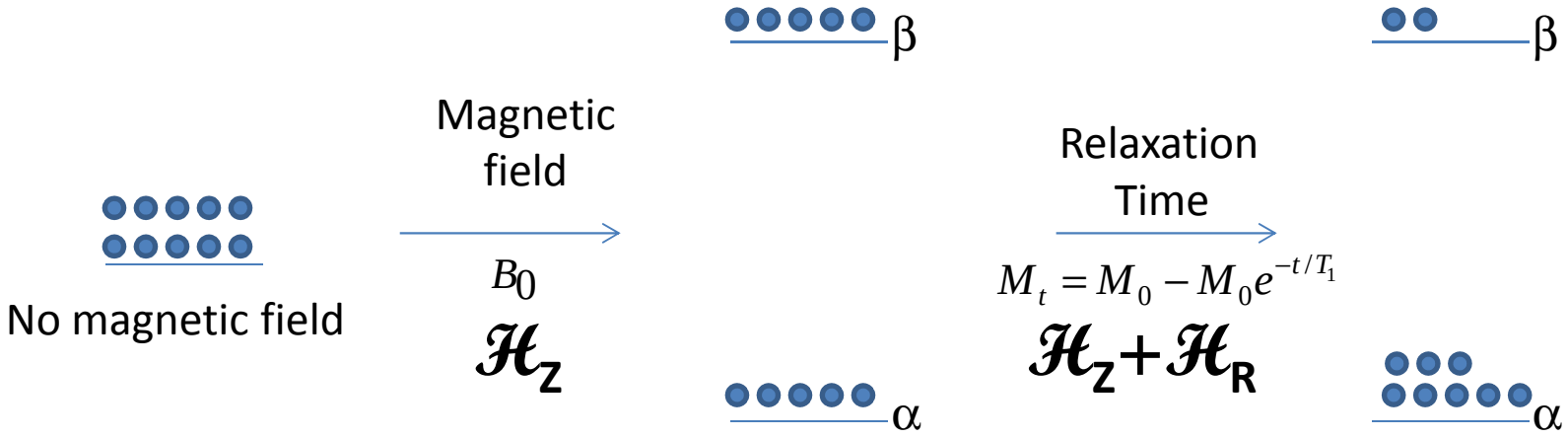

$$E = \gamma B_0 I_m$$

$$I_m = \pm\frac{1}{2} \equiv \text{nuclear spin}$$

$$\gamma = \text{gyromagnetic ratio}$$

$$n_\alpha = n_\beta$$

$$\frac{n_\beta}{n_\alpha} = e^{-\frac{\Delta E}{kT}}$$

- Thermal energy (kT) at 25 °C is about 600 calories/mole
- For ^{1}H nuclei @ 600 MHz (14.1 T): $\Delta E \sim 10^{-4} * kT$
  - The excess number of spins in the α state is only one part in about 10,000
  - ^{1}H second most sensitive nucleus after ^{3}H
  - An absorbed photon can cause transitions of the spins from the lower to the higher energy level or just as easily cause a stimulated emission of a spin from the upper energy state.

- In optical spectroscopy transition energies for blue light are ~6000 cal/mole
  - The occupation of high energy states in optical spectroscopy due to thermal energy is extremely rare (one part in 20,000) and therefore every absorbed photon causes an electron transition from the lower energy state to the higher energy state.
  - Optical spectroscopy is a very sensitive technique when compared to NMR spectroscopy.

- **At thermal equilibrium, individual nuclear magnetic moments precess about the Z axis of the external magnetic field at the Larmor frequency – $\omega_{(radians/s)}=2\pi\nu_{(Hz)}=\gamma B_0$**
- **magnetogyric ratio, γ, is a characteristic property of the nucleus**
- **B_0 is the strength of the magnetic field (Tesla).**

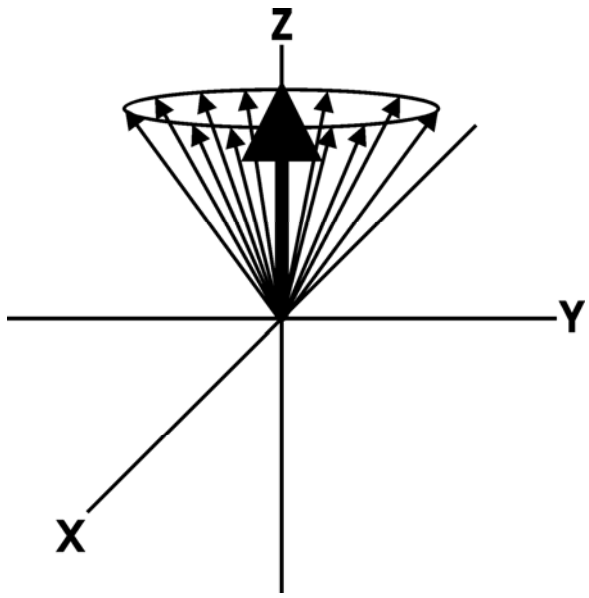

$$\omega = 2\pi\upsilon = \gamma B_0$$

	H				X	I = 1/2		X	I = 1/2 and I > 1/2									He
	Li	Be			X	I > 1/2						B	C	N	O	F	Ne	
	Na	Mg										Al	Si	P	S	Cl	Ar	
	K	Ca	Sc	Ti	V	Cr	Mn	Fe	Co	Ni	Cu	Zn	Ga	Ge	As	Se	Br	Kr
	Rb	Sr	Y	Zr	Nb	Mo	Tc	Ru	Rh	Pd	Ag	Cd	In	Sn	Sb	Te	I	Xe
	Cs	Ba	La	Hf	Ta	W	Re	Os	Ir	Pt	Au	Hg	Tl	Pb	Bi	Po	At	Rn
	Fr	Ra	Ac	Rf	Db	Sg	Bh	Hs	Mt									
				Ce	Pr	Nd	Pm	Sm	Eu	Gd	Tb	Dy	Ho	Er	Tm	Yb	Lu	
				Th	Pa	U	Np	Pu	Am	Cm	Bk	Cf	Es	Fm	Md	No	Lr	

Nuclear magnetic resonance frequencies (/MHz)

Nucleus (spin)	11.74 T	14.09 T	16.44 T	18.79 T	21.14 T
^{1}H (½)	500.0	600.0	700.0	800.0	900.0
^{19}F (½)	470.4	564.5	658.5	752.6	846.7
^{31}P (½)	202.4	242.9	283.4	323.8	364.3
^{13}C (½)	125.7	150.9	176.0	201.2	226.3
^{15}N (½)	50.7	60.8	70.9	81.1	91.2
^{2}H (1)	76.8	92.1	107.5	122.8	138.2

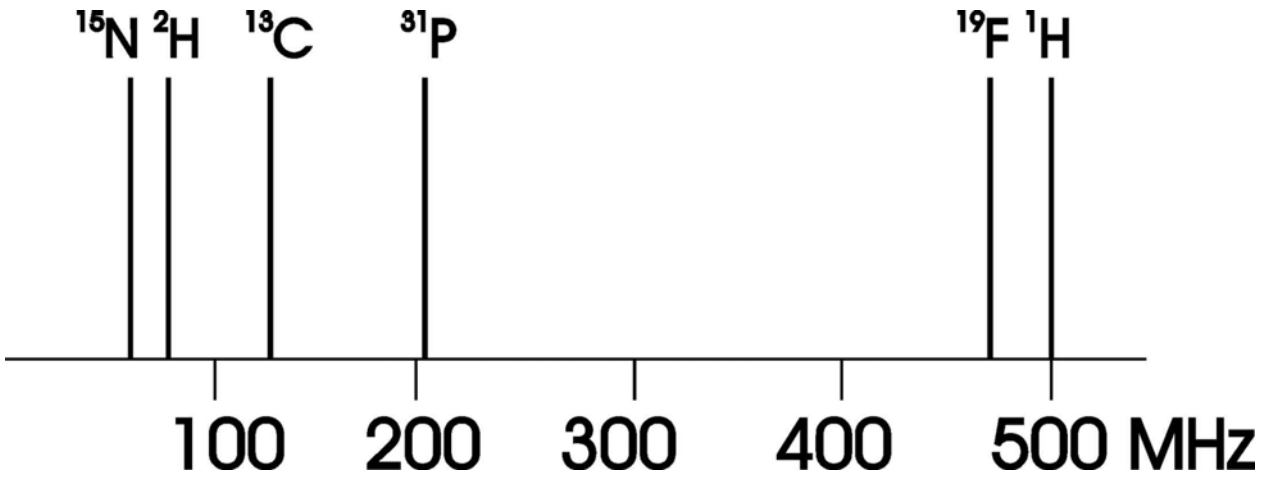

(@11.75 T)

Why higher field?

60 MHz

Sucrose

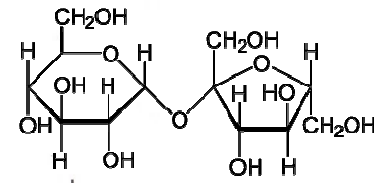

500 MHz

900 MHz

Why higher dimensions?

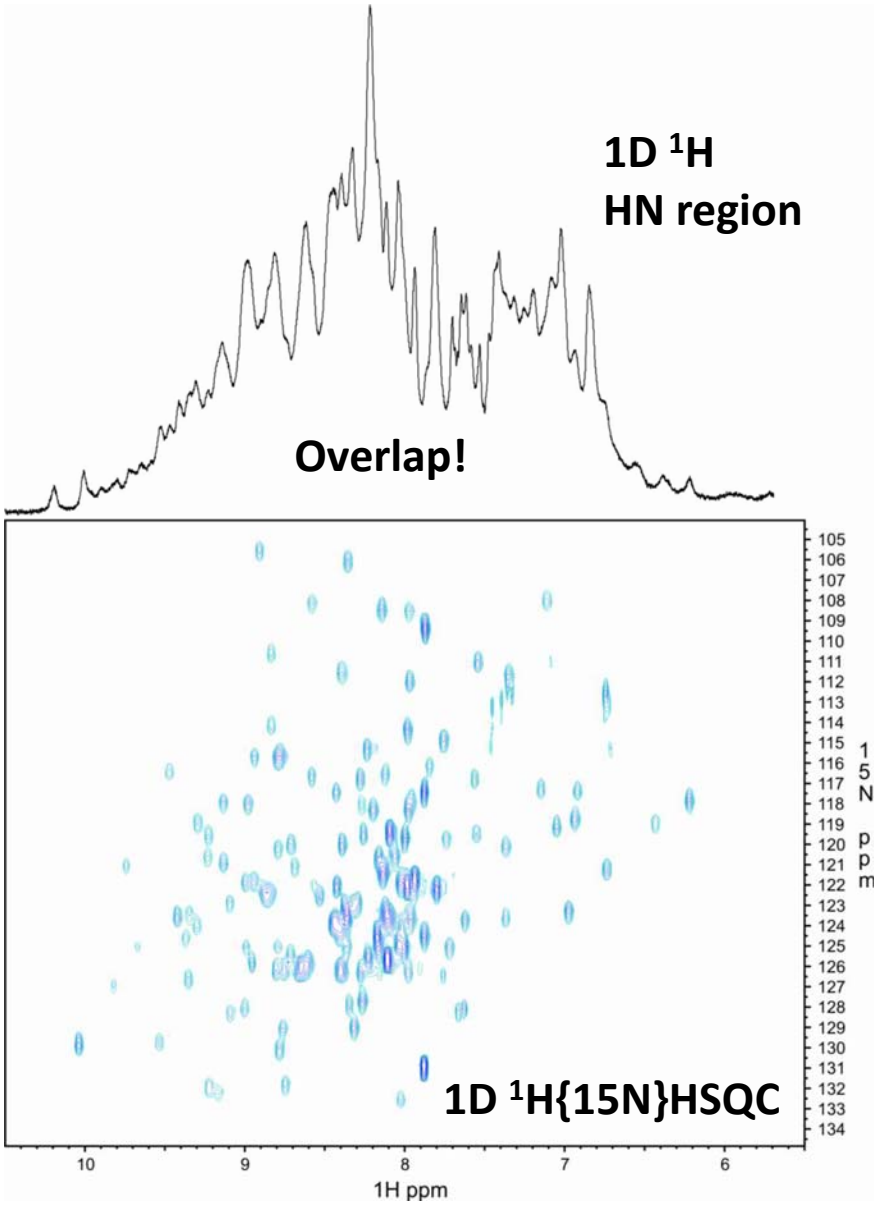

Continuous wave(CW) NMR –
Magnetic field is swept slowly across the spectrum
(Rarely done in modern times)

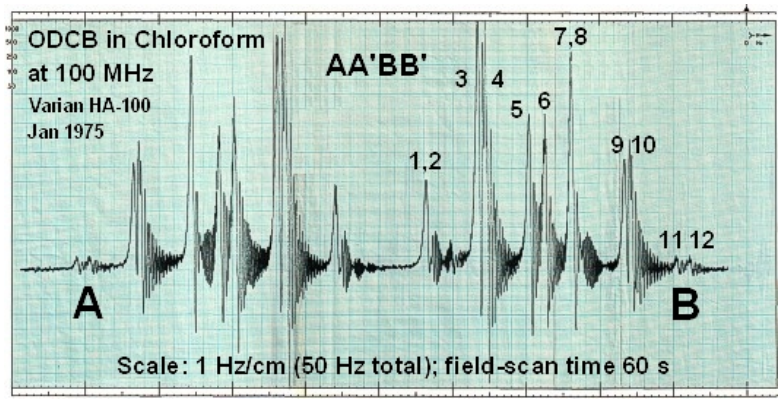

Pulsed NMR –

• Short pulse(s) (~μs) of radiofrequency electromagnetic energy is applied to spins that are initially at thermal equilibrium

• Frequency is "close" to the Larmour frequency $\omega(rad/s) = 2\pi\nu(Hz) = \gamma B_0$

• The "ringing" is detected and then Fourier transformed yielding the frequency spectrum

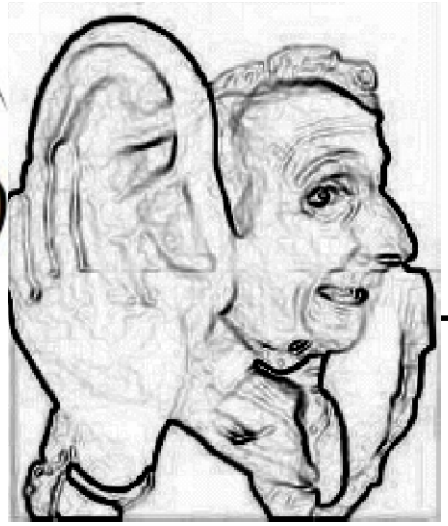

$$S(\nu) = \frac{1}{2\pi}\int_0^{\infty} F(t)e^{i2\pi\nu t}dt$$

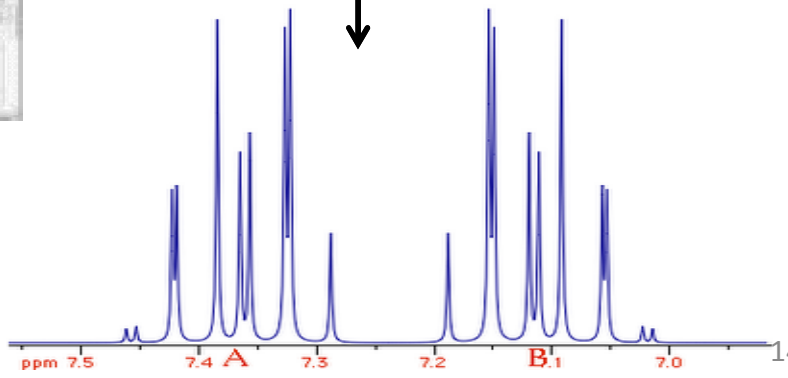

Relaxation between pulses

- **Pulsed NMR requires a delay between pulses and acquisition for the spins to return to thermal equilibrium**

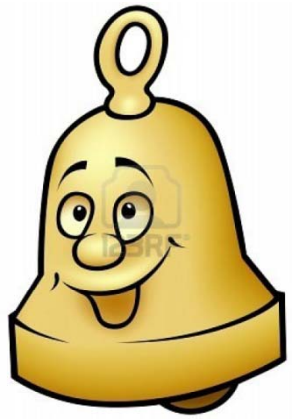

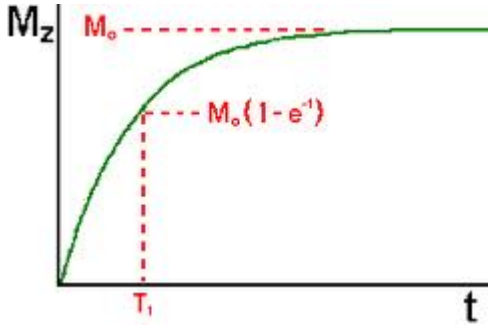

NMR spectrometer is a radio transmitter and receiver

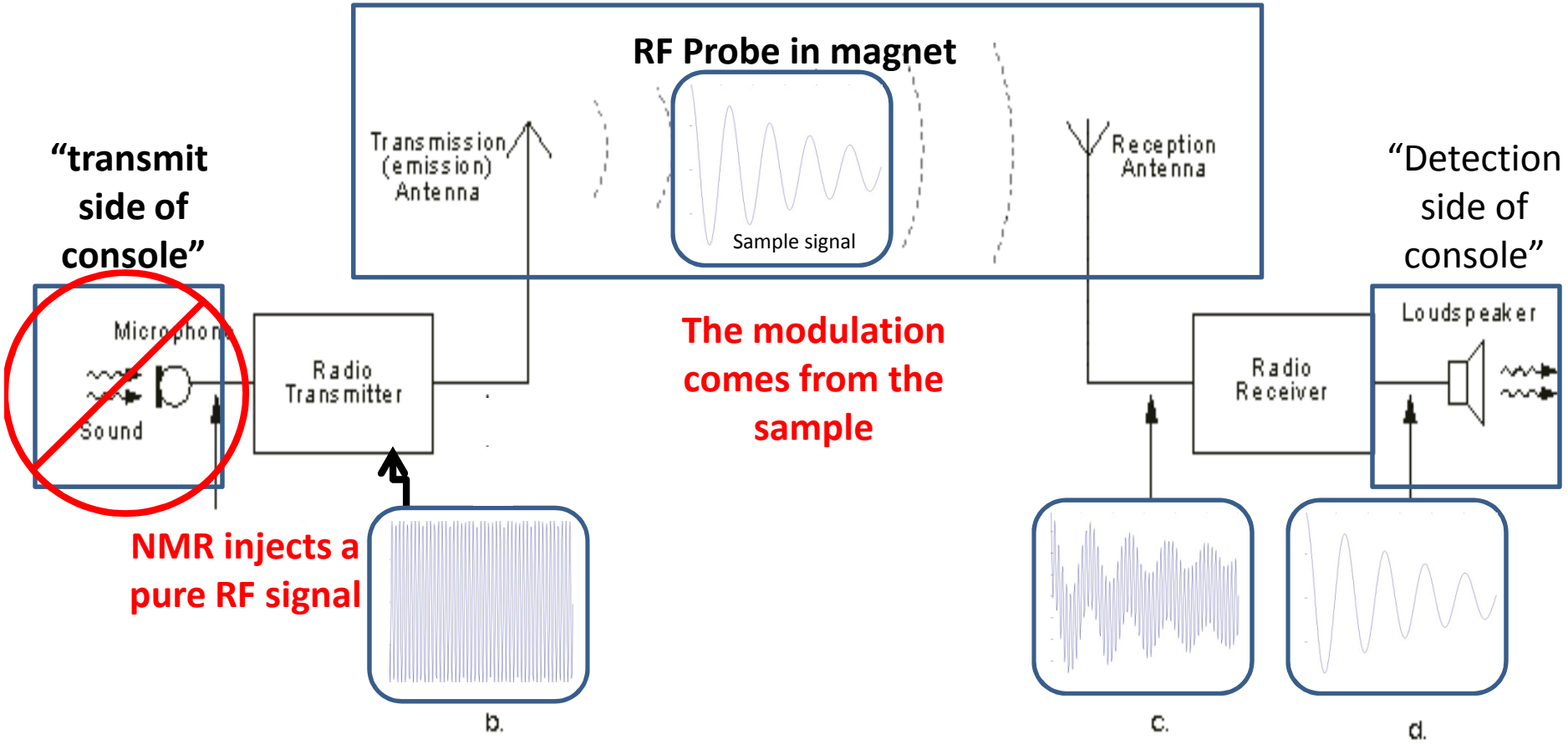

Pic.2.1. Radio Transmission Block-Diagram

Magnetic field

- **$$$$ most expensive component of NMR spectrometers >11.75 T (500MHz)**
  - **600 MHz (14.1T) ~$800,000 (console ~$200-250,000)**
  - **900 MHz (21.2T) ~$4M**
  - **1.2 GHz (23.5 T) ~$18M (not yet available; hopefully in ~5 years)**
- **Field strength 1 Tesla=10,000 gauss**
  - **10^{-9}–10^{-8} gauss – the magnetic field of the human brain**
  - **0.31–0.58 gauss – the Earth's magnetic field at its surface**
  - **25 gauss – the Earth's magnetic field in its core**
  - **50 gauss – a typical refrigerator magnet**
  - **2000 gauss – a small neodymium-iron-boron (NIB) magnet**
  - **600-70,000 gauss – a medical magnetic resonance imaging machine**
  - **23,500 gauss = 100Mhz magnet**
  - **235,000 gauss = 1GHz NMR spectrometer (highest available field for NMR) (0.3 meter wavelength)**
  - **97.4 tesla – record magnetic field NHMFL March 2012 (pulsed;non-destructive)**
  - **850 T – record highest magnetic field (destructive- exploding magnet)**
  - **10^{12}–10^{13} gauss – the surface of a neutron star (probably there are issues about doing NMR)**
  - **4×10^{13} gauss – the quantum electrodynamic threshold**
  - **10^{15} gauss – the magnetic field of some newly created magnetars**
  - **10^{17} gauss – the upper limit to neutron star magnetism; no known object in the universe can generate a stronger magnetic field (10^{-12} meter) (gamma ray 10^{-10} meter!)**

Superconducting magnets

- Miles of a superconducting wire (180 miles for 21.14 T (900 MHz))
- Superconducting joints between sections may have residual resistance ~10^{-13} Ohm
  - Causes magnet drift (typical specification 10 Hz/hr)
- Up to ~18T magnet is held at 4.2° K by liquid Helium
- >18T Joule-Thompson cooled to 2.2° K
- Energization
  - Cool magnet, introduce current, and then close a superconducting switch and disconnect leads
  - Keep it cold!!
  - Quench (a word best not repeated) – next slide
- The (Oxford) 21.14 T (900 MHz) magnet at NMRFAM has 17 MJ of stored energy
  - This equates to 4 kg of TNT. A stick of dynamite (0.19 kg) contains roughly 1 MJ of energy.

Test quench of NMRFAM 900 MHz (21.14 T)

21.14 T (900 MHz) Oxford magnet

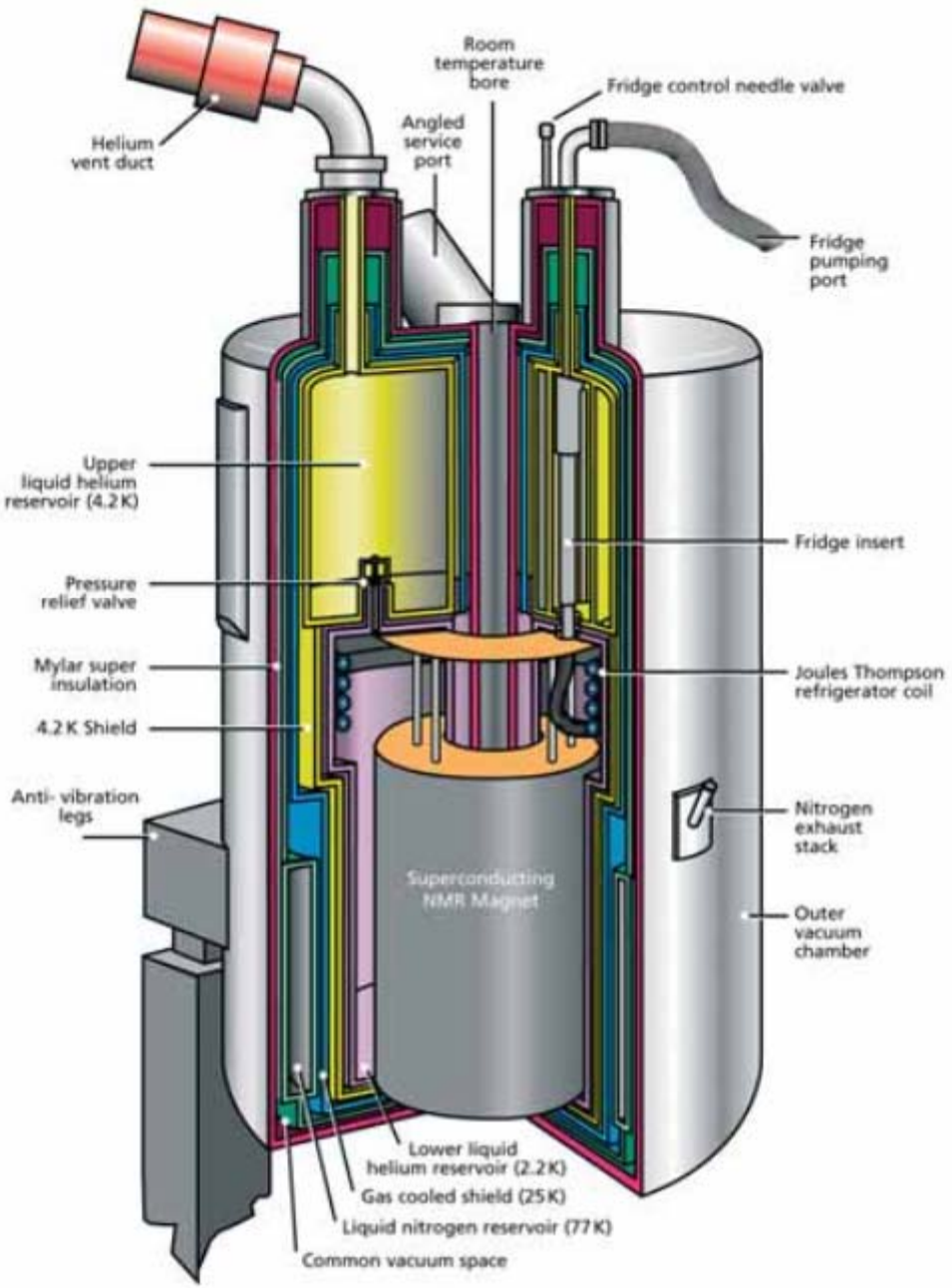

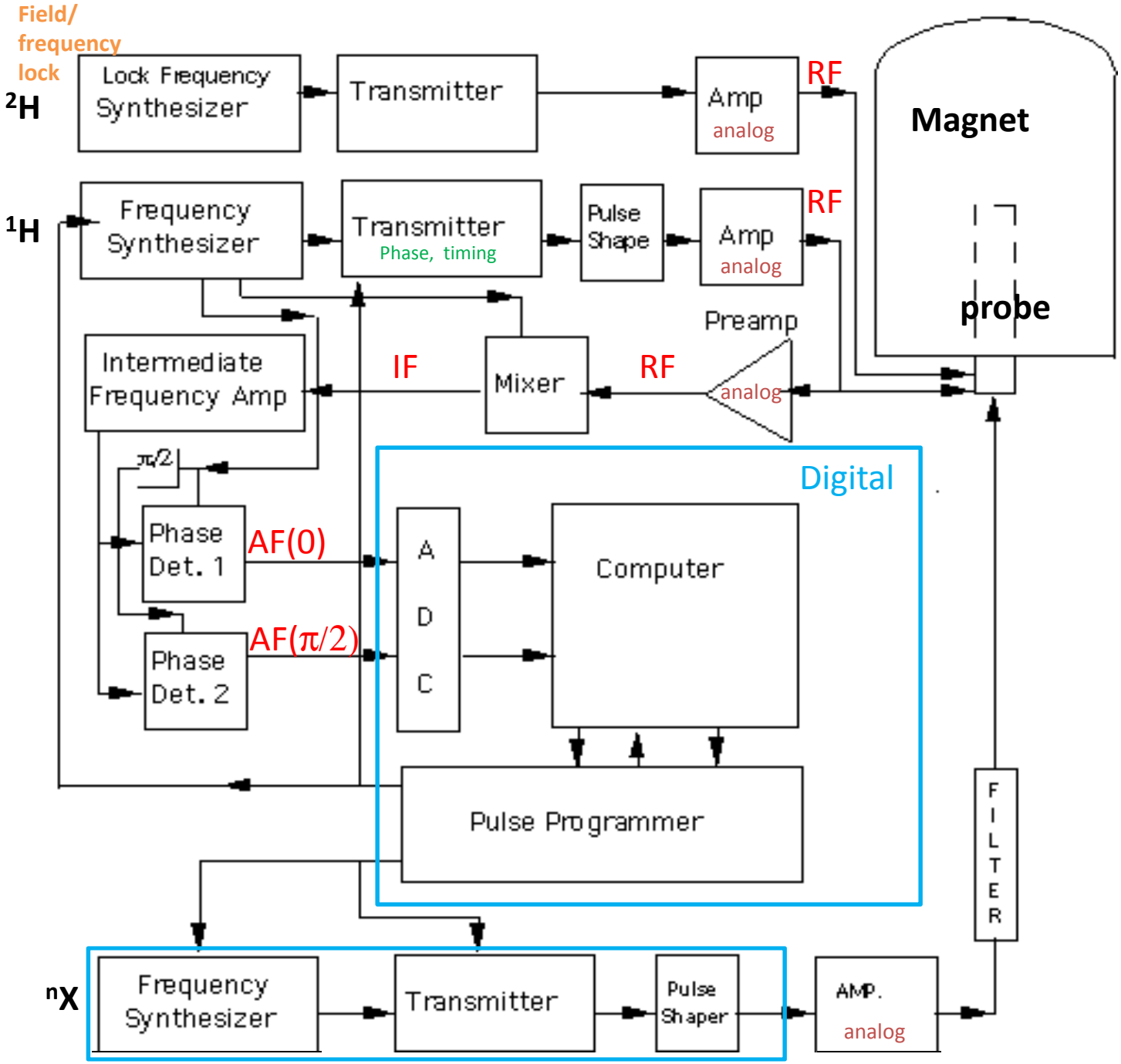
Field/
frequency
lock
^{2}H
Lock Frequency
Synthesizer
Transmitter
Amp
analog
RF
Magnet
^{1}H
Frequency
Synthesizer
Transmitter
Phase, timing
Pulse
Shape
Amp
analog
RF
probe
Preamp
Intermediate
Frequency Amp
IF
Mixer
RF
analog
π/2
Digital
Phase
Det. 1
AF(0)
A
D
C
Computer
Phase
Det. 2
AF(π/2)
Pulse Programmer
FILTER
^{n}X
Frequency
Synthesizer
Transmitter
Pulse
Shaper
AMP.
analog

NMR probe


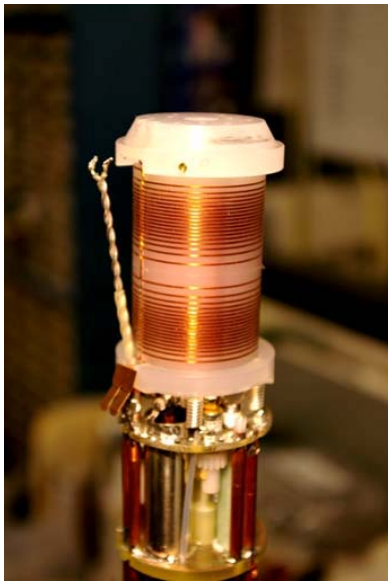
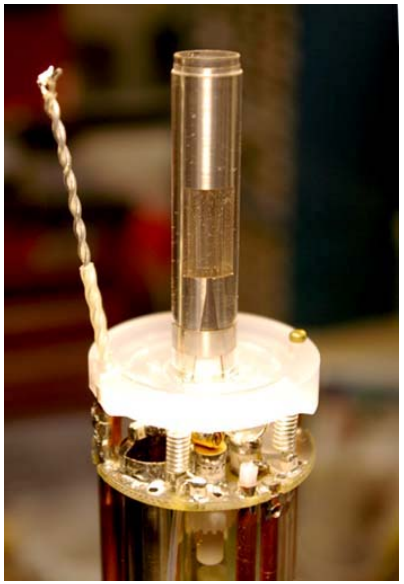
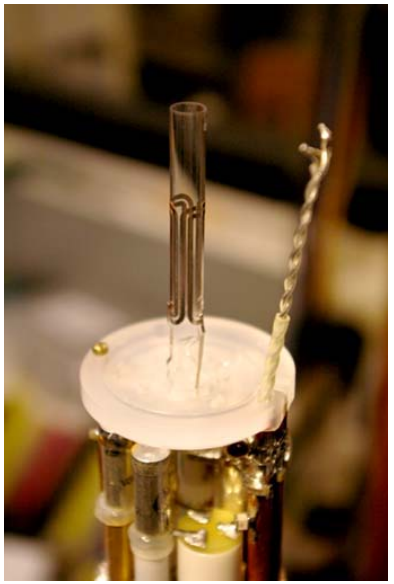


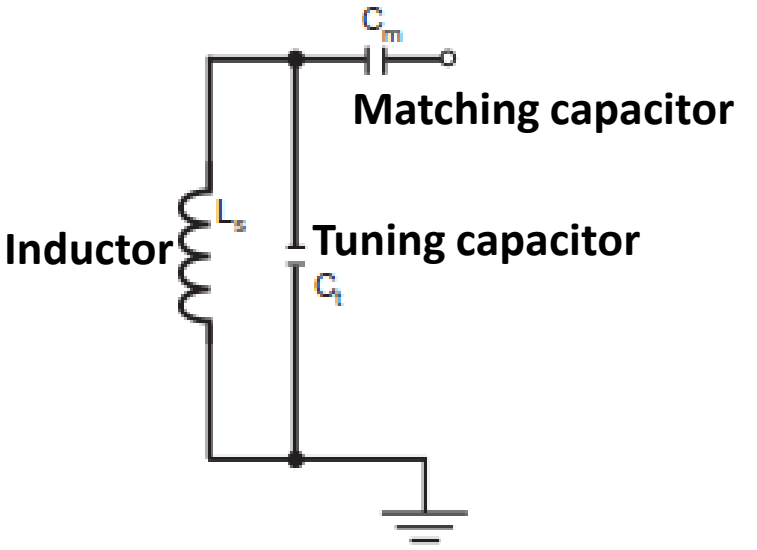

Singly tuned

~$25-50,000

Cryogenically cooled probes (and preamps)

Reduction of Johnson noise

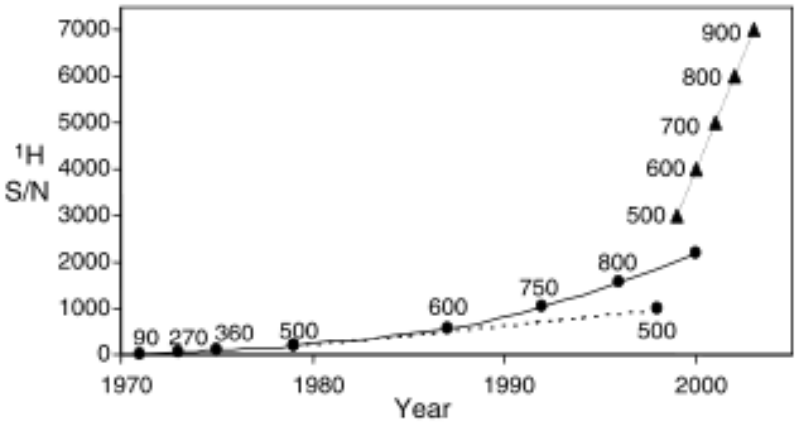

Fig. 1. The specified signal-to-noise ratio of 0.1% ethylbenzene (EB) in $CDCl_3$ for ^{1}H-observe probes plotted as a function of time. The black dots denote the sensitivity of a conventional probe at the launch of a magnet operating at a particular field, and the triangles mark the launches of cryogenic probes at different fields (all data from Bruker BioSpin). The magnetic field (indicated by the ^{1}H operating frequency MHz) is given above the marker. The dashed line indicates the increase in specified sensitivity during two decades for a conventional probe operating at 500 MHz.

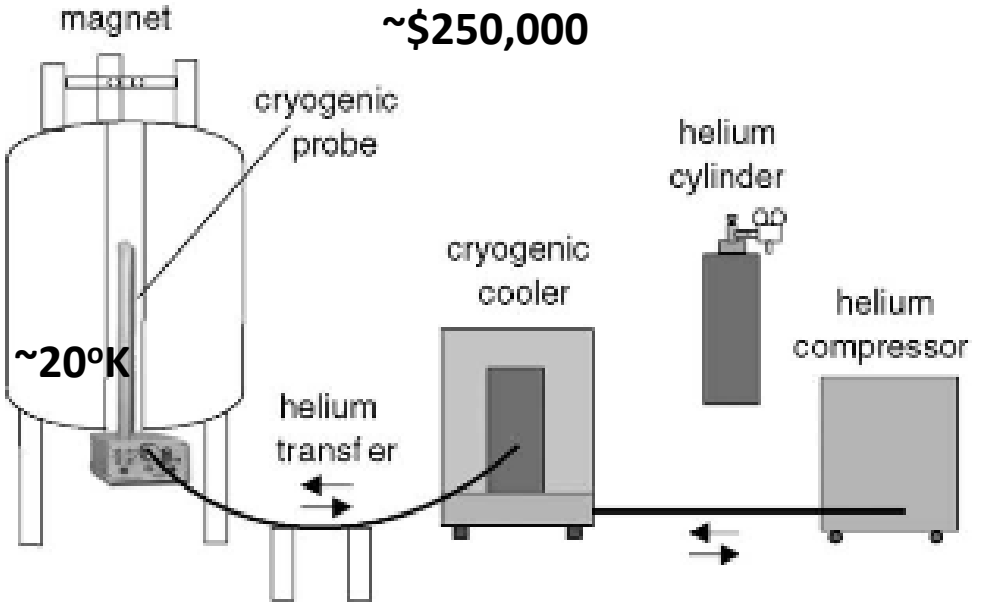

Fig. 2. Schematic presentation of the closed-loop cryogenic cooling system consisting of the cooling equipment, helium compressor and the cryogenic probe.

NMR Console

Transmitter

Brand A & B

Receiver

Brand B

Brand A

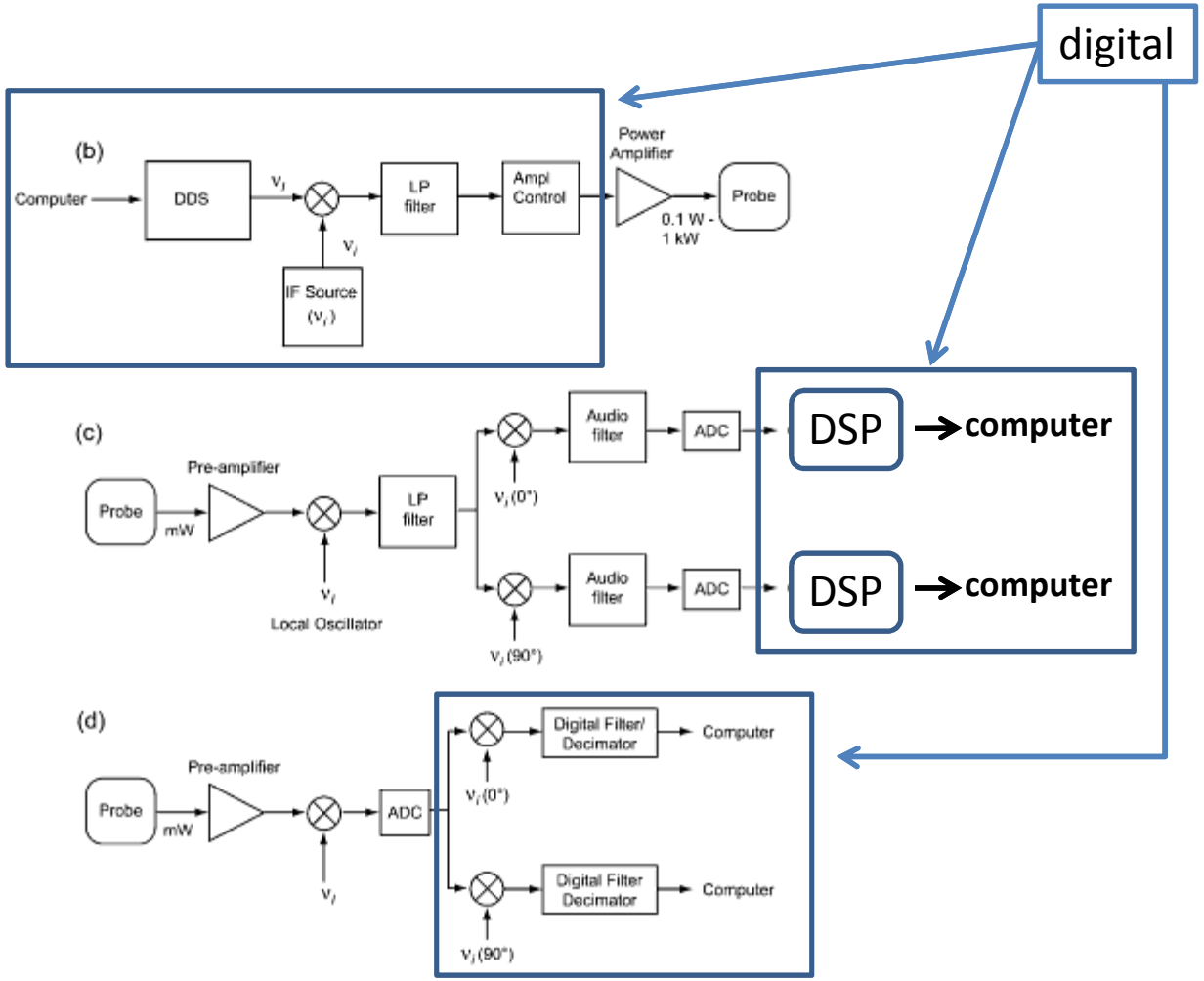

Figure 6 Block diagrams of analog (a) and digital (b) NMR transmitters. Block diagrams of analog (c) and digital (d) NMR receivers. Analog-to-digital converters are abbreviated as ADC.

B – Bruker

A – Agilent/Varian

Digitization of the Free induction decay (FID)

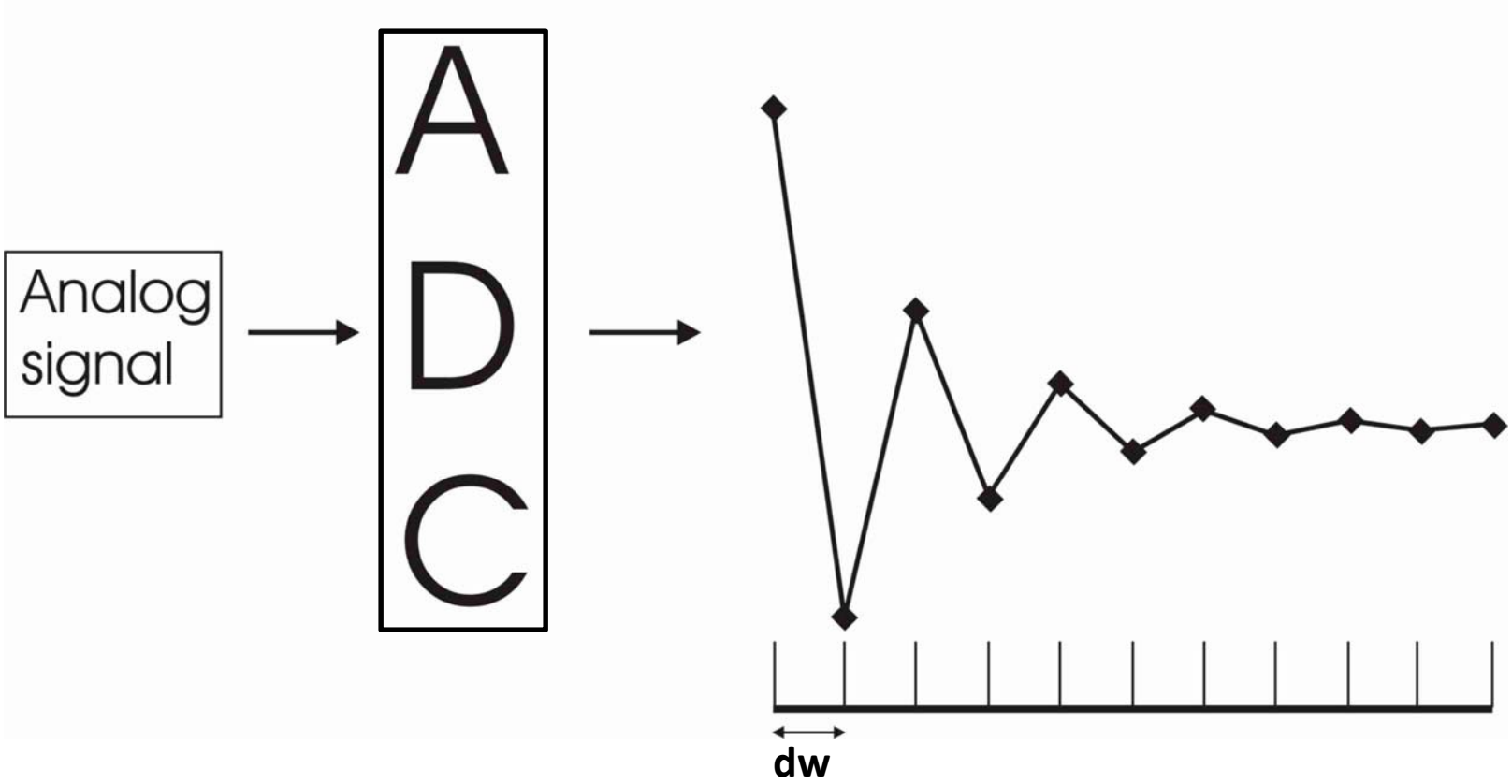

Nyquist sampling: dw=dwell time= 1/(full sweep width)

(This assumes complex data collection, i.e. 2 orthogonal axes (X,Y) sampled simultaneously)

Single Dectector

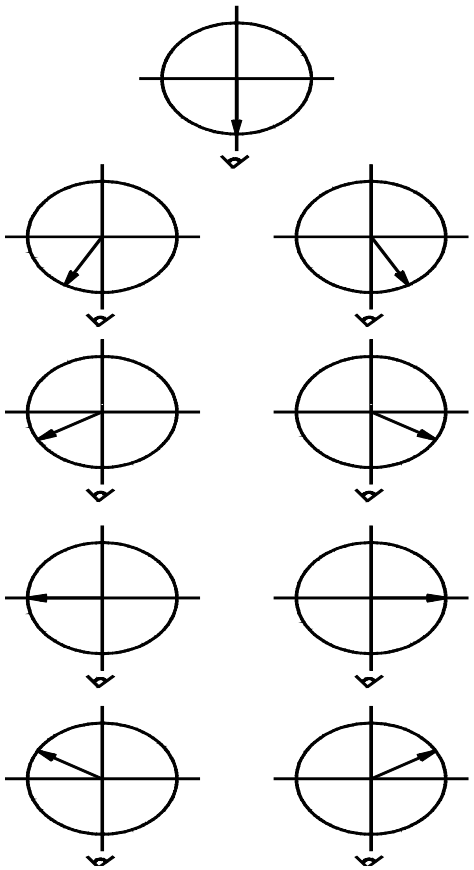

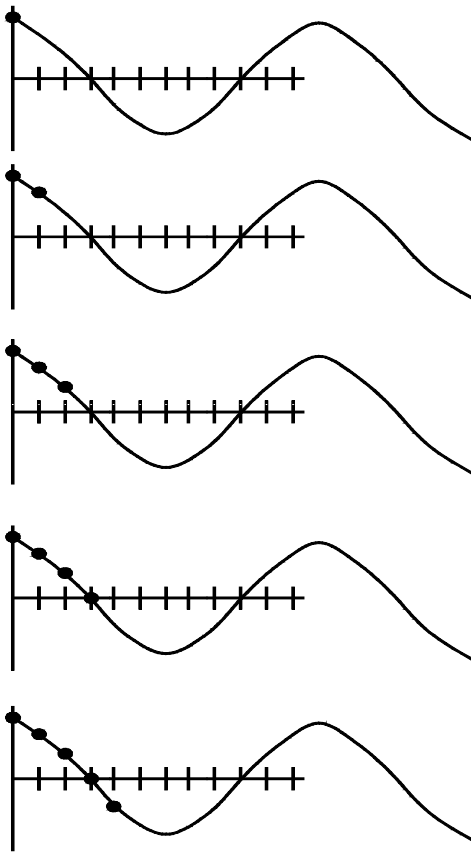

Single sideband detection

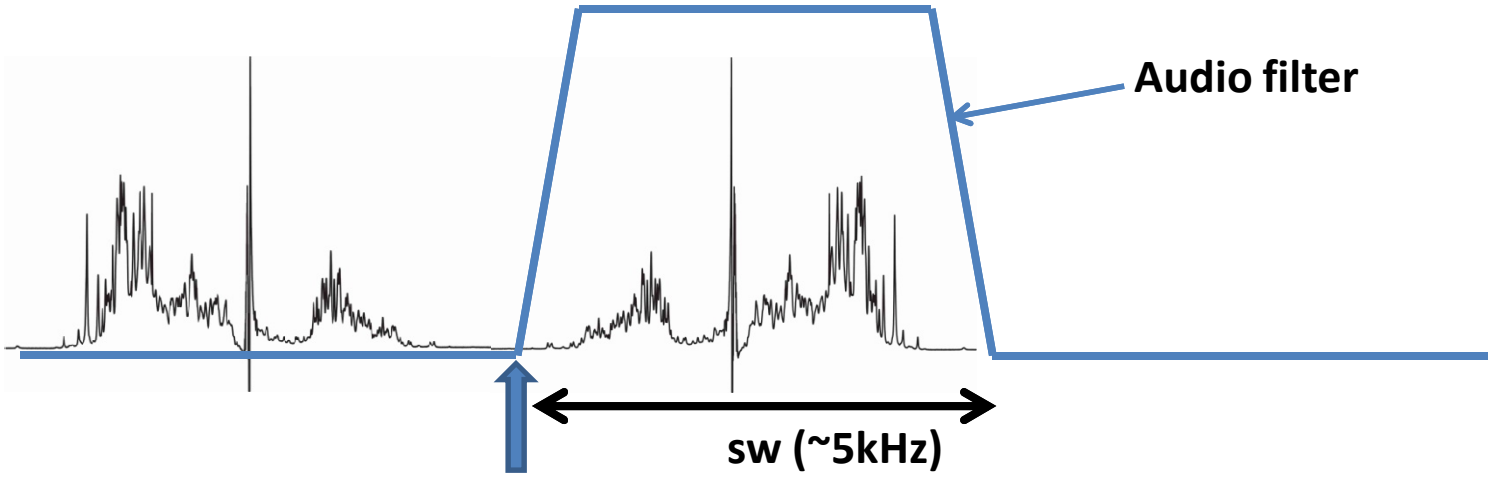

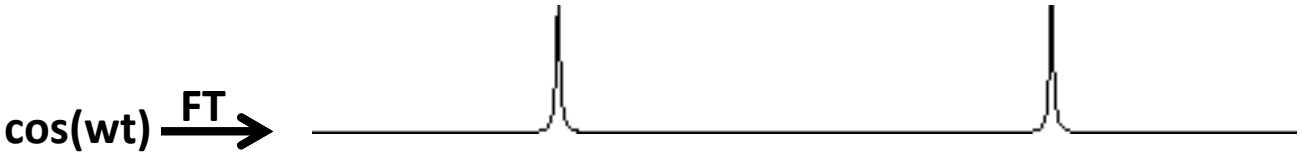

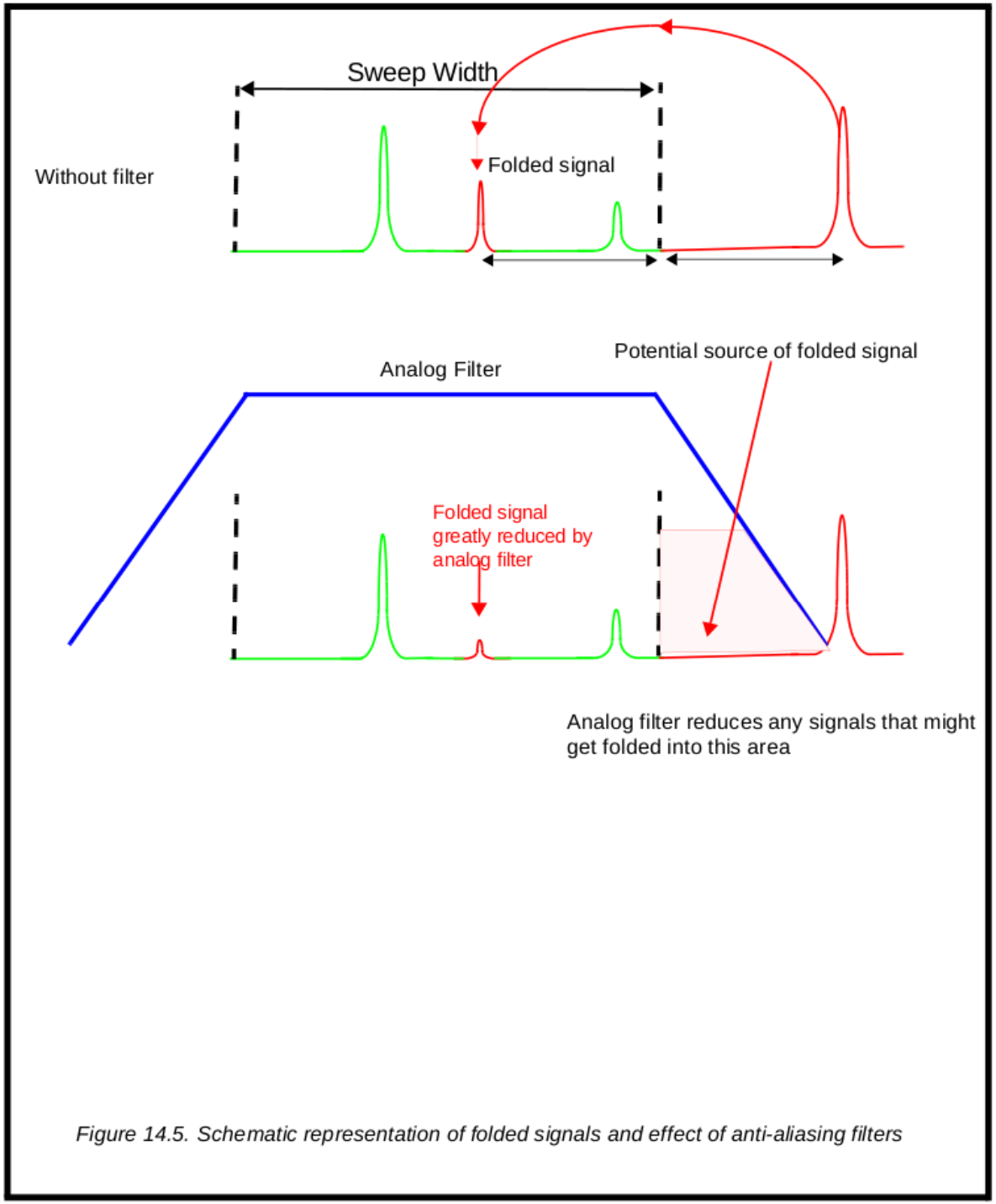

Figure 14.5. Schematic representation of folded signals and effect of anti-aliasing filters

Complex detection

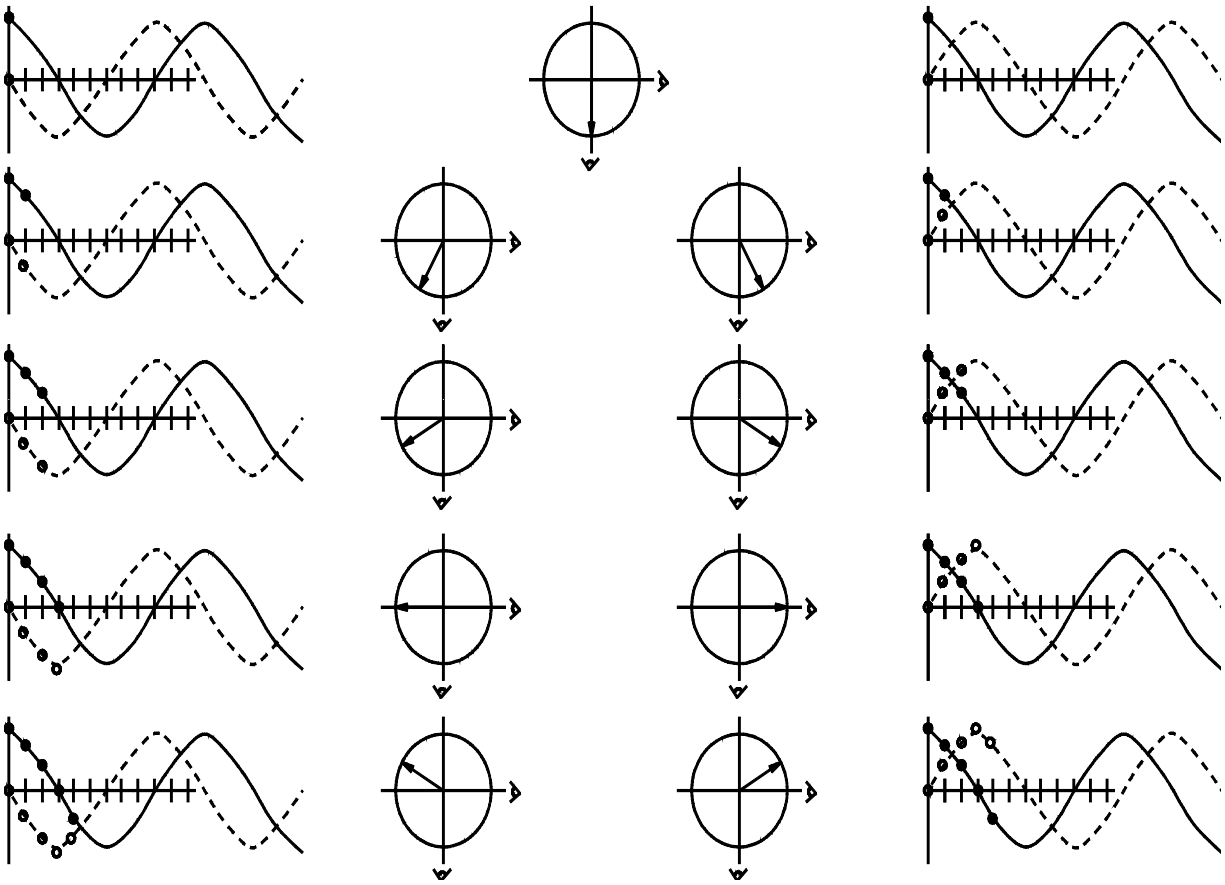

Quadrature detection (distinguish +/- frequencies)

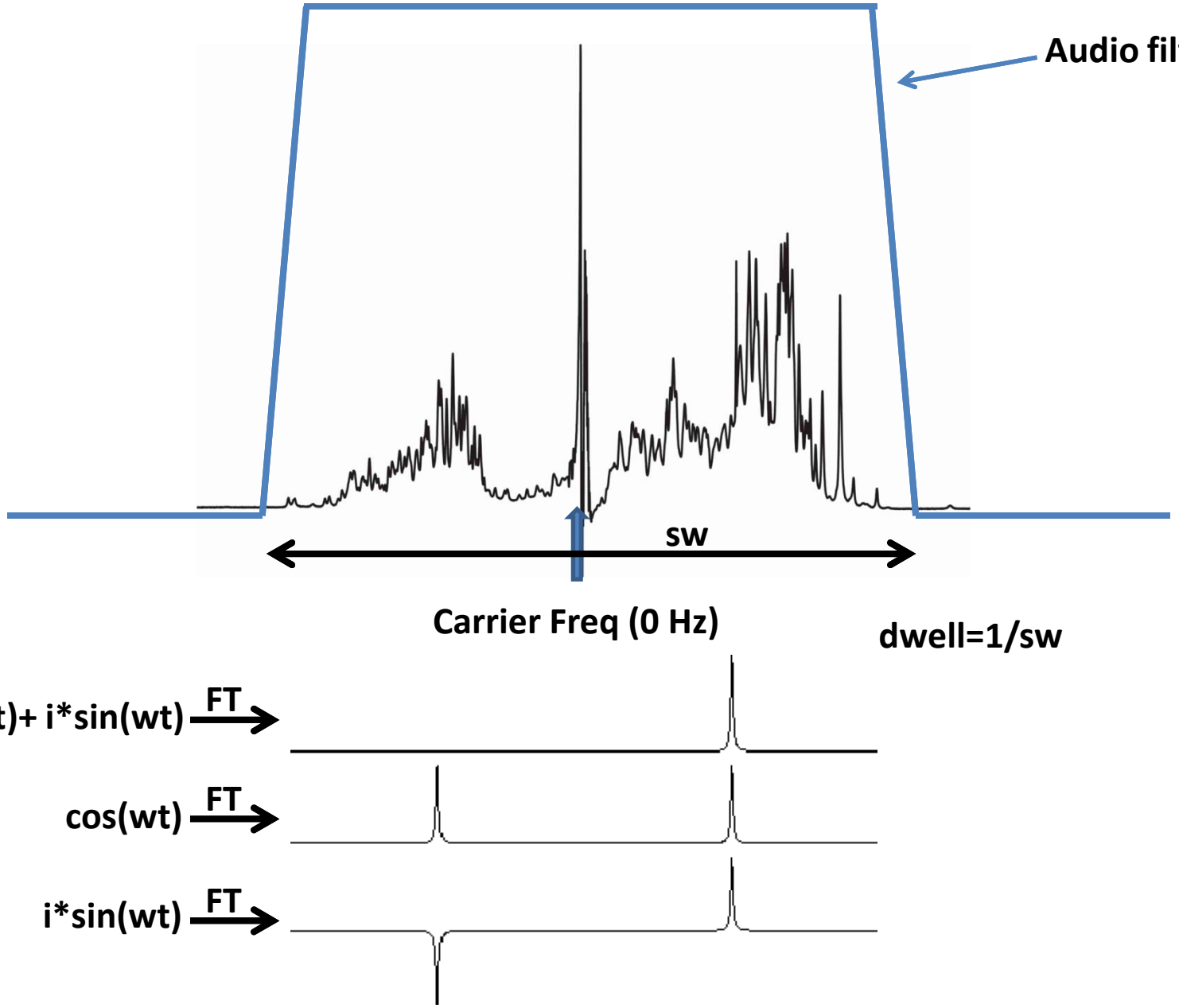

Quadrature images due to unbalanced X&Y channels

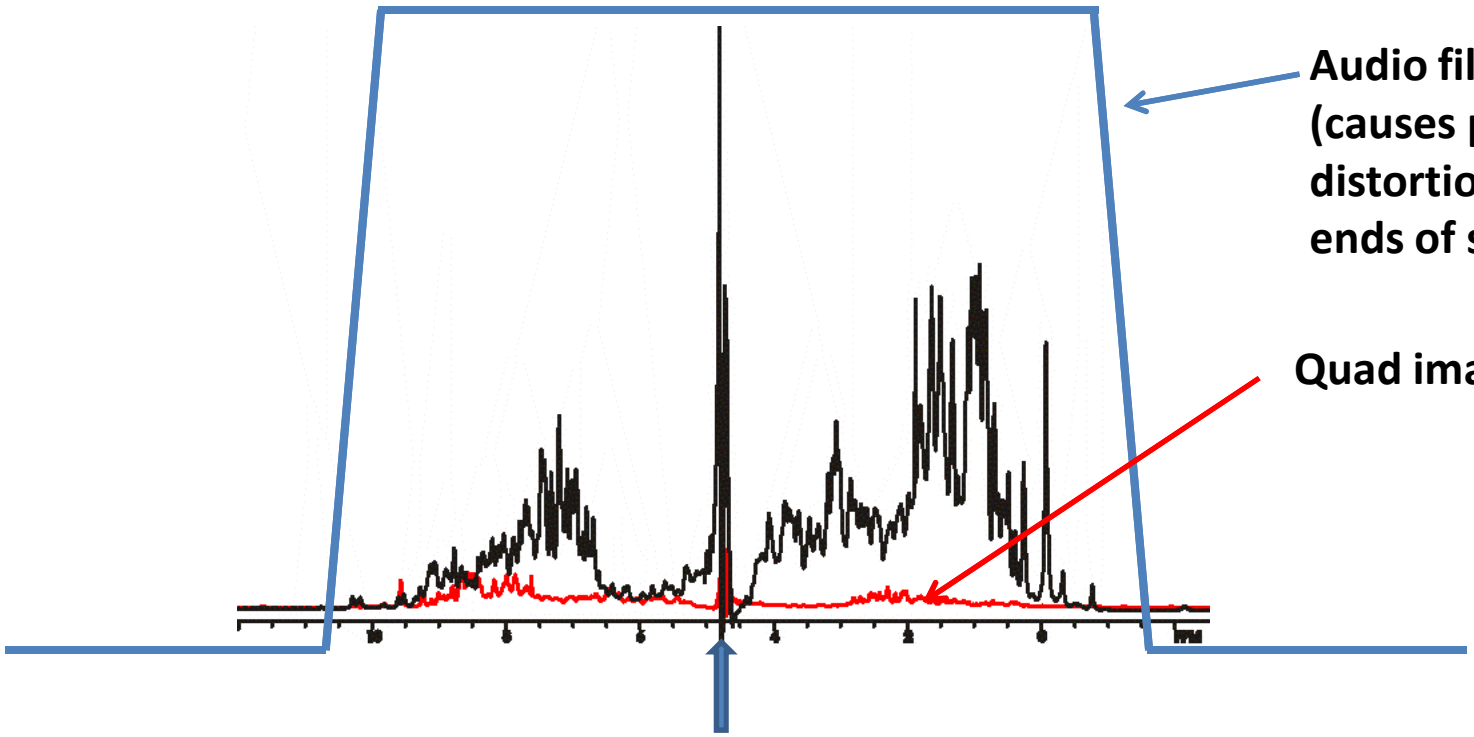

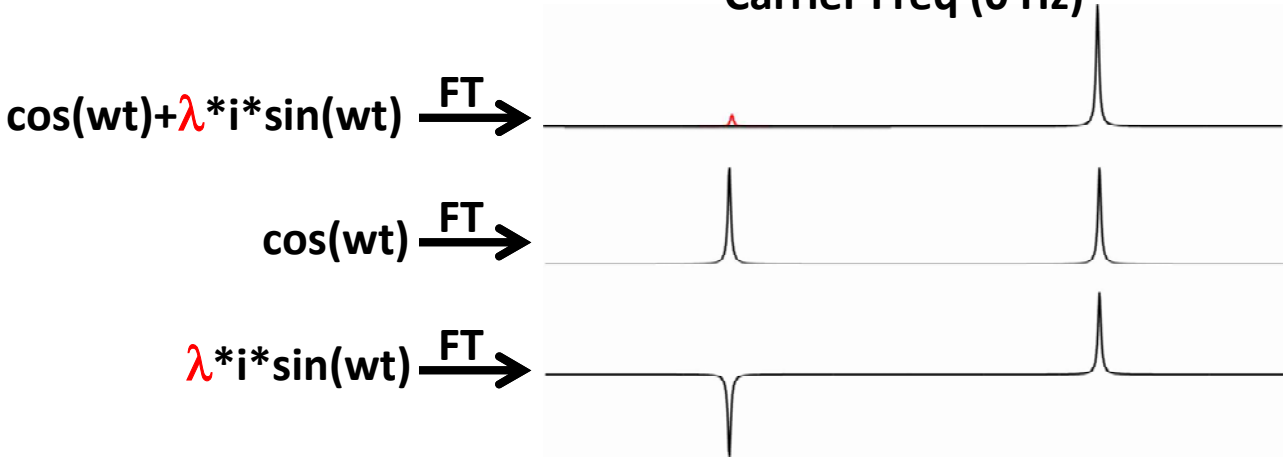

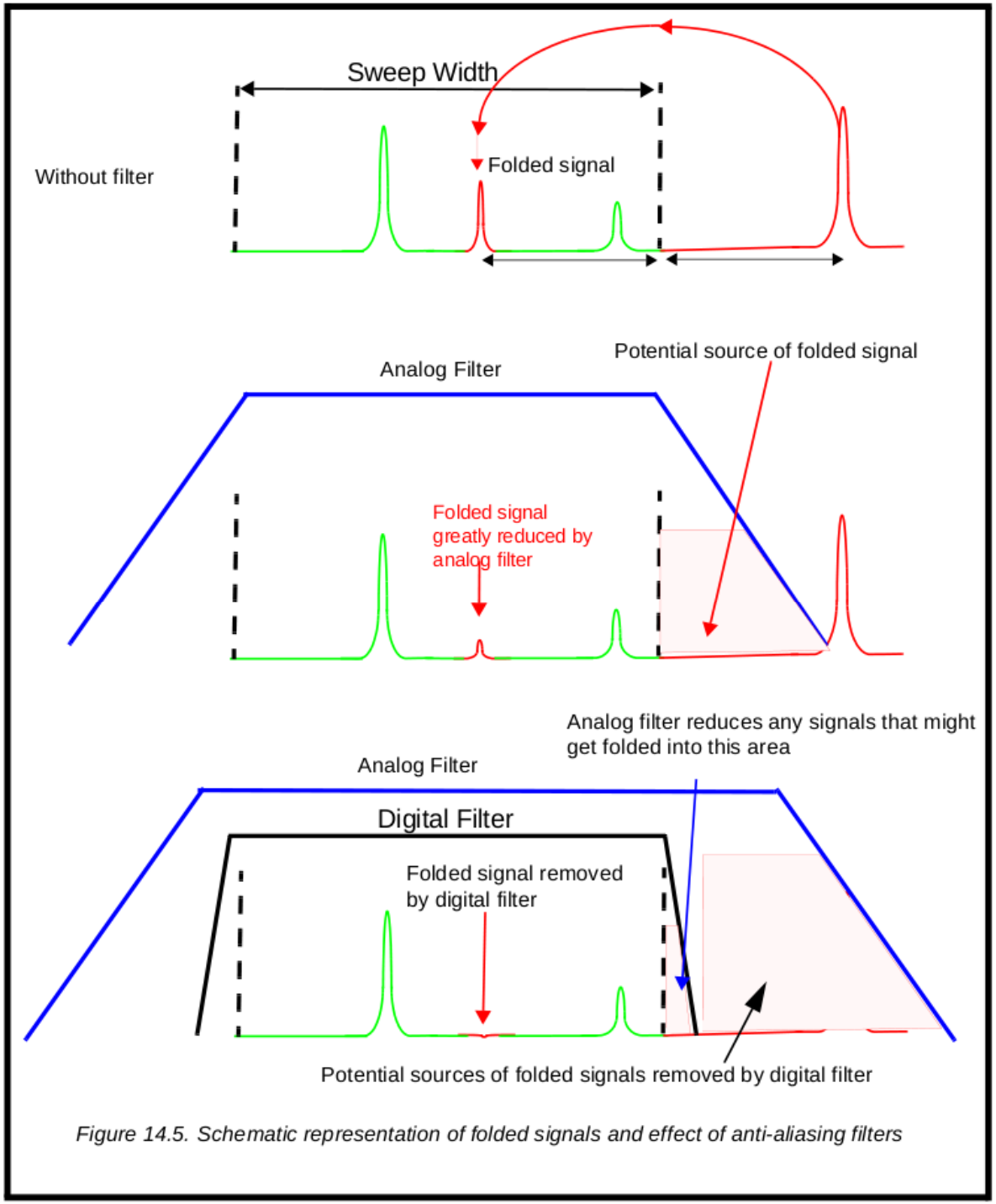

Figure 14.5. Schematic representation of folded signals and effect of anti-aliasing filters

Modern digital spectrometer – quad detection

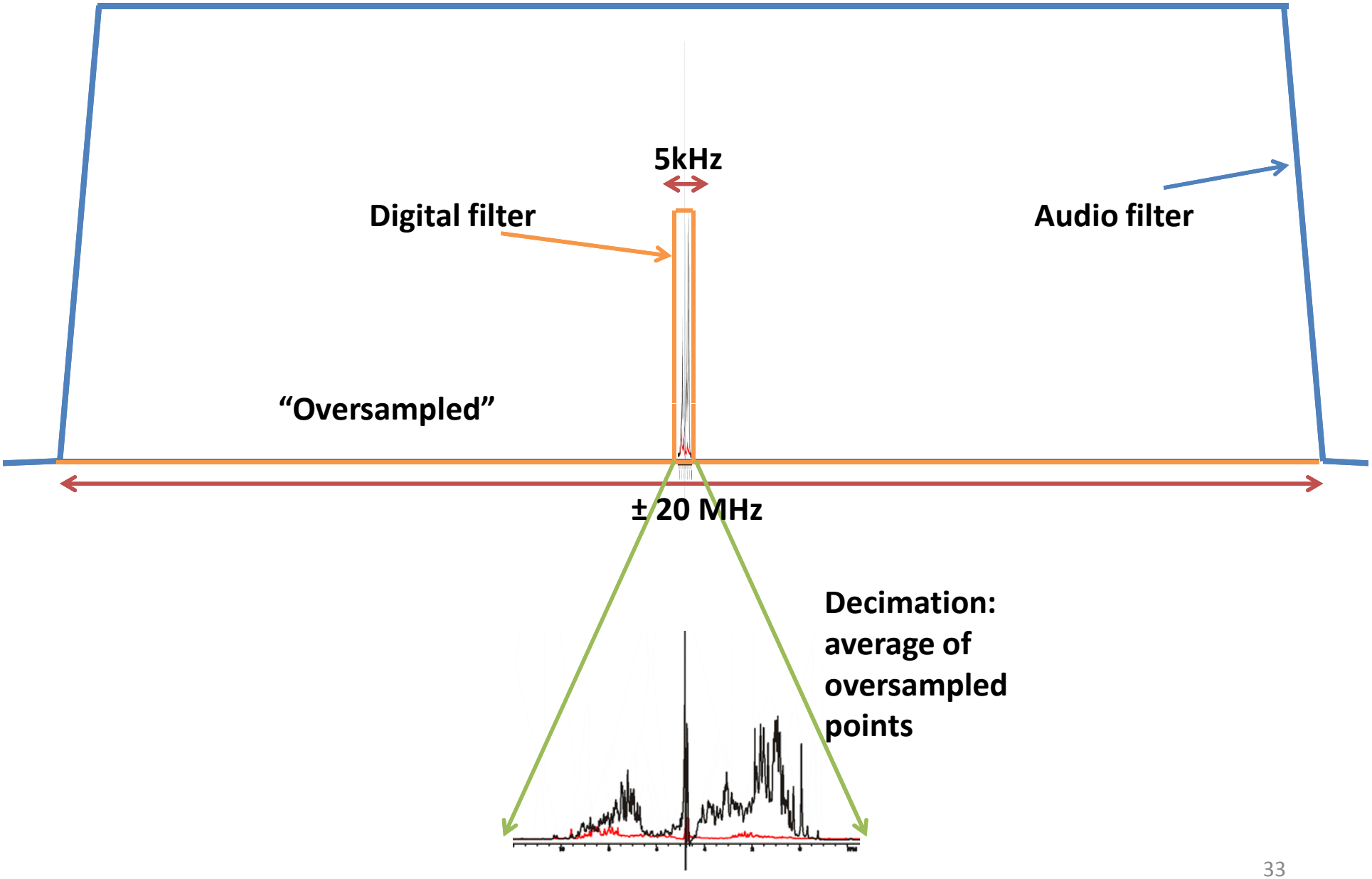

Bruker spectrometer – quad image removal (DQD)

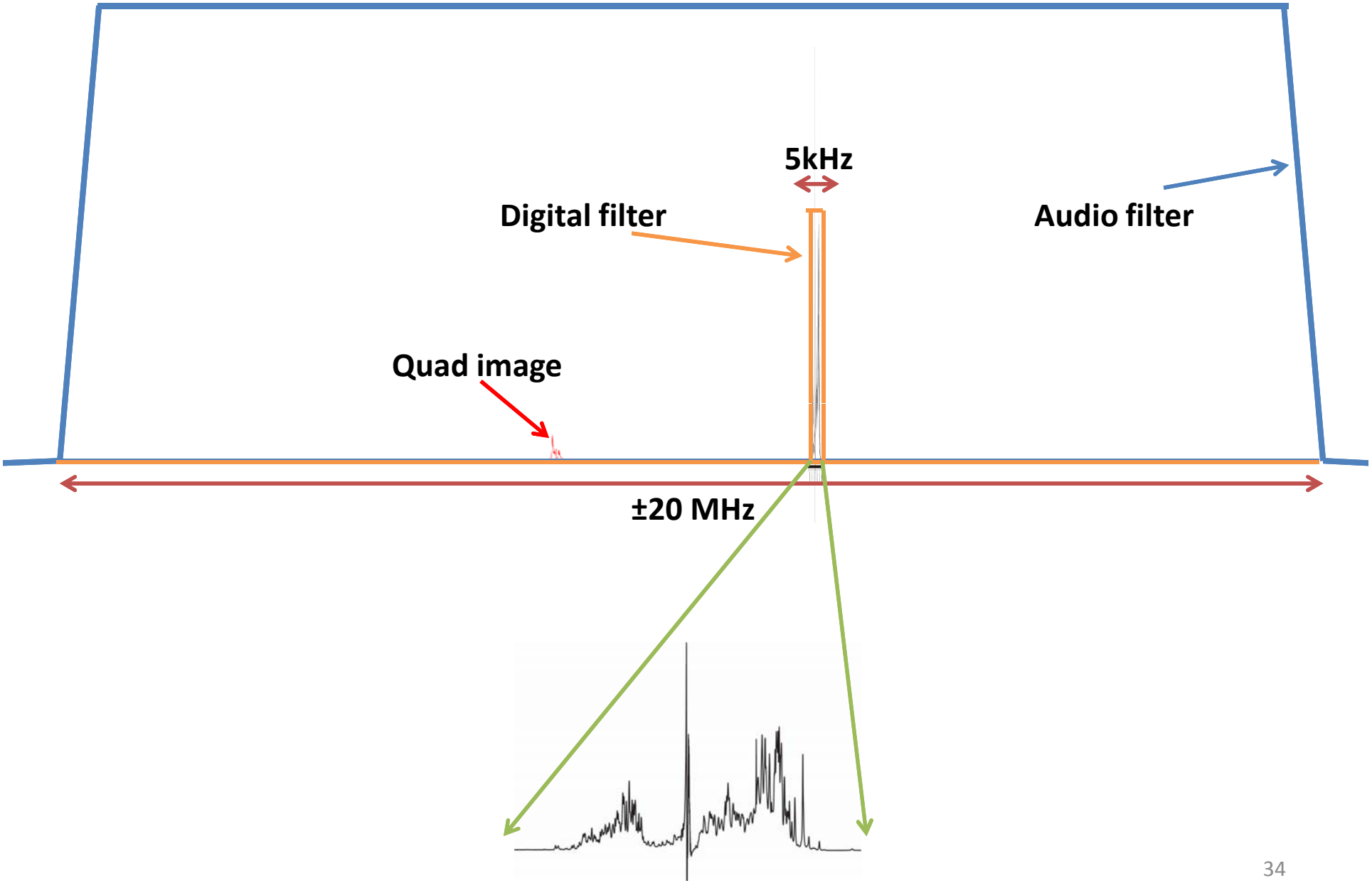

Not to be outdone, Agilent/Varian digitizes a single analog channel then uses artifact-free digital quadrature detection, eliminating quadrature images

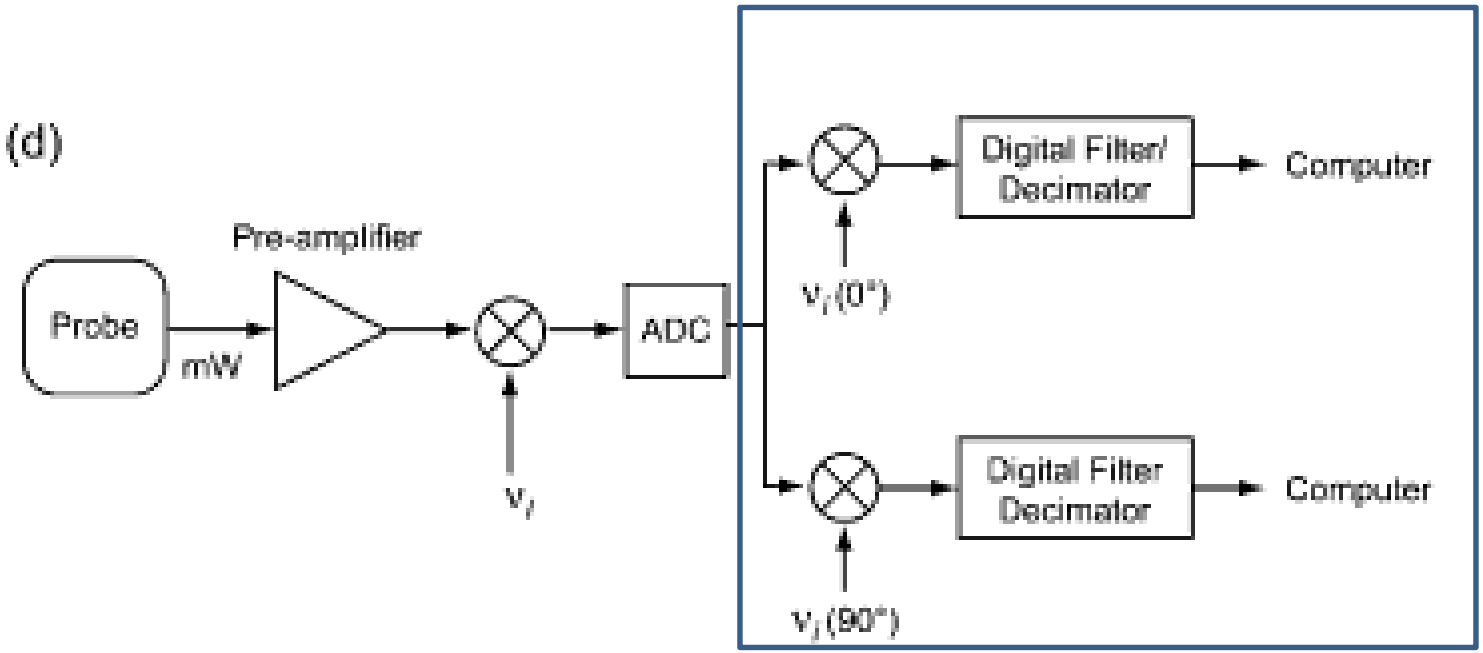

Rotations

Rotation of bulk magnetization with RF “pulse”

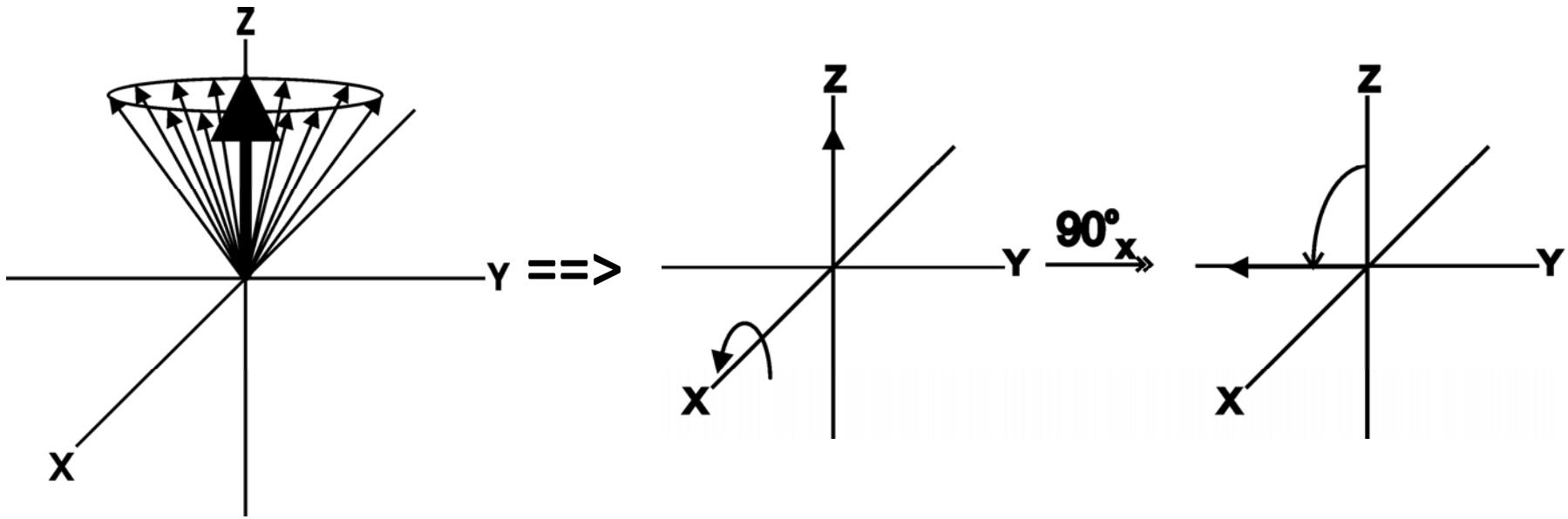

$$\omega = 2\pi\upsilon = \gamma B_0$$

RF pulse (amplifier turned on)

Free Induction Decay (FID)

Delay

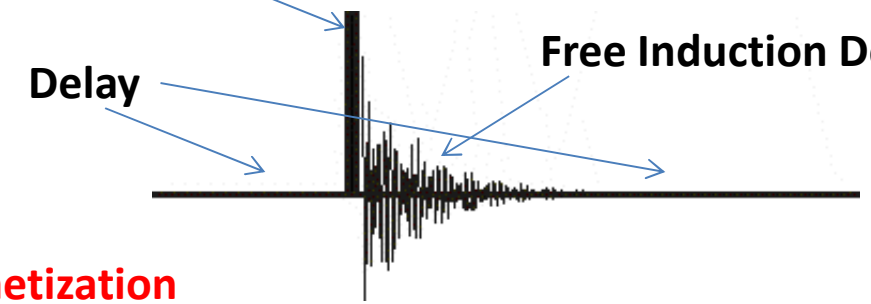

Sum of Z magnetization of multiple spins - Vector

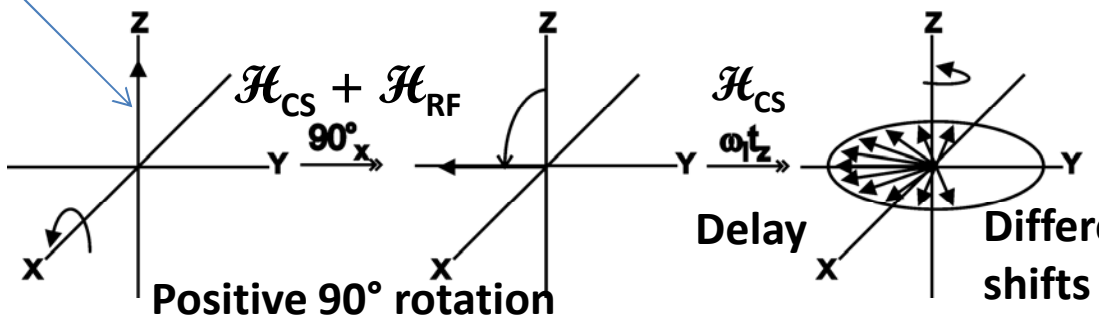

Positive 90° rotation about X to -Y

Delay

Different chemical shifts have different frequencies.

Magnetic field inhomogeneity also gives rise to different frequencies.

Different magnetic susceptibility causes field gradients.

Bubble velocities

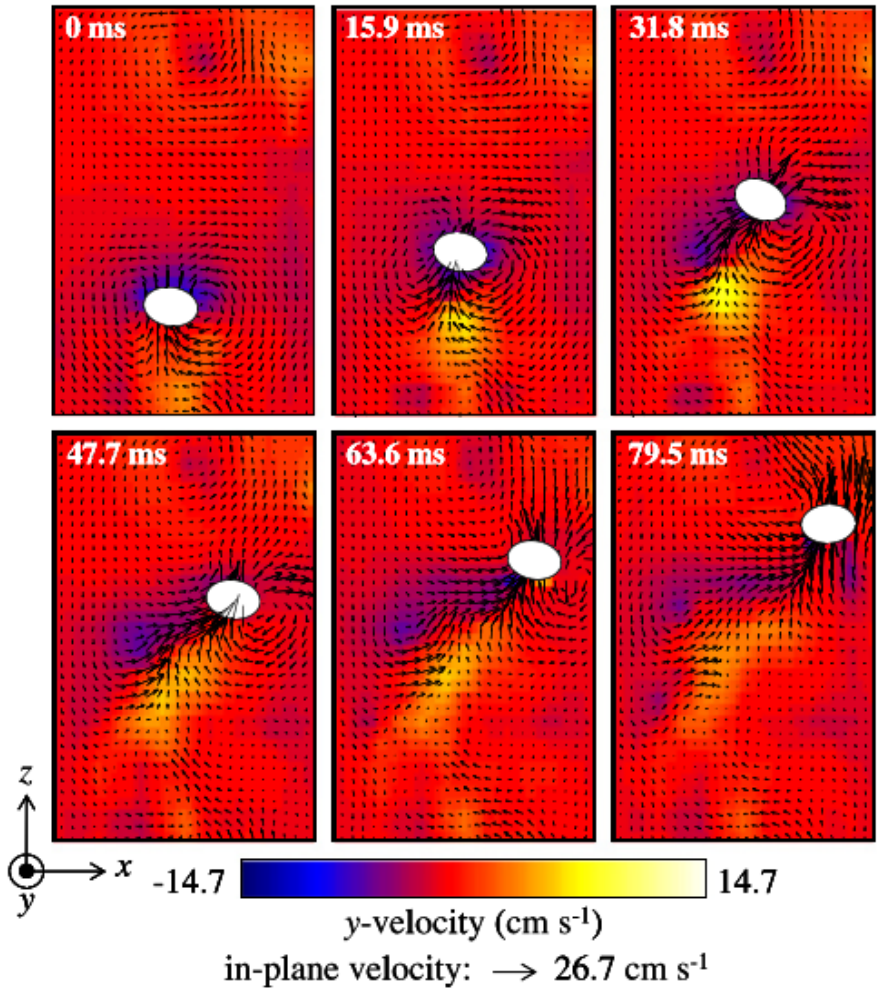

Fig. 10. Velocity maps about a single bubble rising freely through stagnant solution. The location of the bubble was identified from the signal intensity maps, and is highlighted by the filled white ellipses. The acquisition rate was 63 fps. The spatial resolution is 390 μm × 586 μm for a field of view of 20 mm × 30 mm.

A unit vector **I** decomposed into three orthogonal components (a*$\mathbf{I}_x$, b*$\mathbf{I}_y$, c*$\mathbf{I}_z$). The angles θ and ϕ are polar coordinates. This vector represents the sum of all of the spin isochromats in the sample.

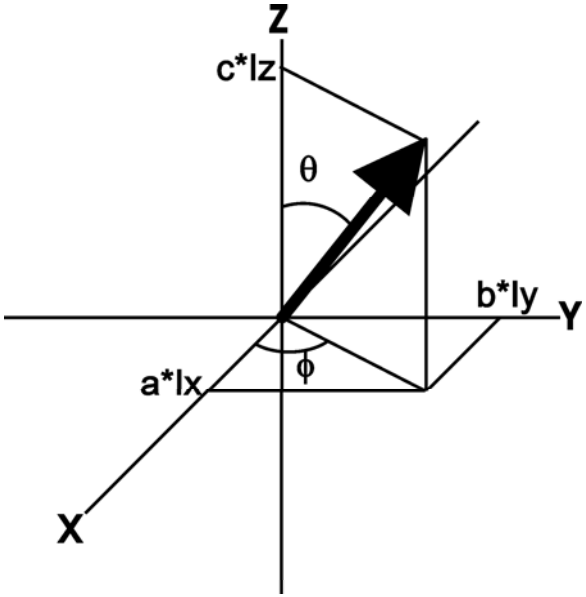

positive rotation about Y:

Z → X → -Z → -X → Z

positive rotation about X:

Z → -Y → -Z → Y → Z

positive rotation about Z:

X → Y → -X → -Y → X

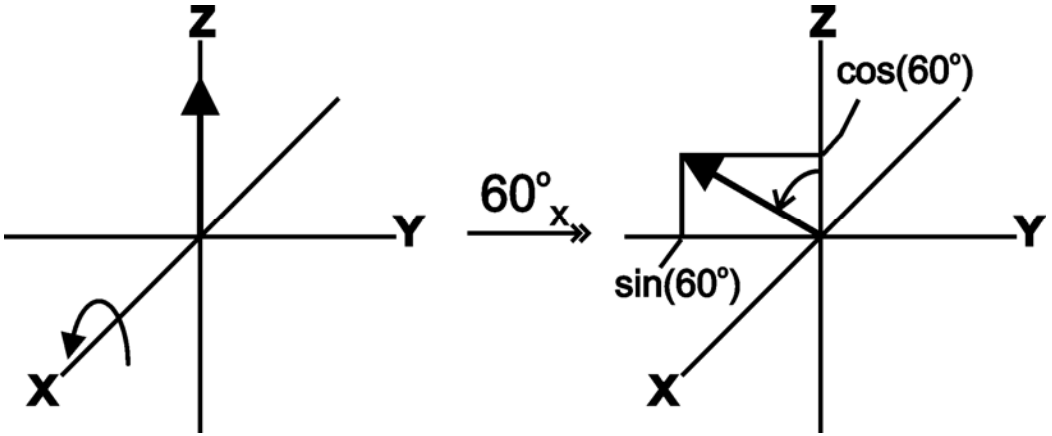

$$\mathbf{I}_z \xrightarrow{60^\circ \hat{\mathbf{I}}_x} \mathbf{I}_z \cos(60^\circ) - \mathbf{I}_y \sin(60^\circ)$$

Example rotations (positive)

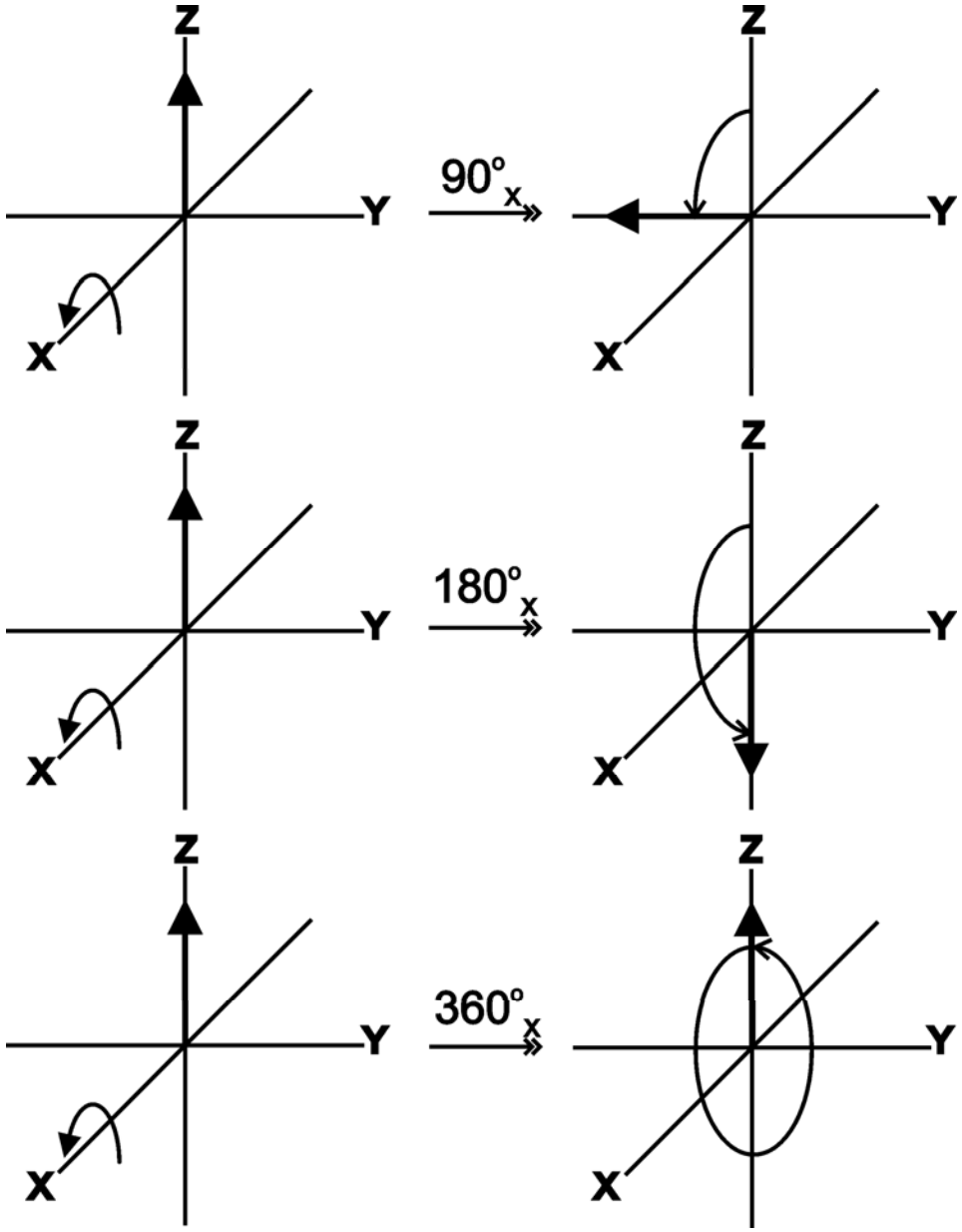

$$\mathbf{I}_z \xrightarrow{\frac{\pi}{2}\hat{\mathbf{I}}_x} -\mathbf{I}_y$$

$$\mathbf{I}_z \xrightarrow{\pi\hat{\mathbf{I}}_x} -\mathbf{I}_z$$

$$\mathbf{I}_z \xrightarrow{2\pi\hat{\mathbf{I}}_x} \mathbf{I}_z$$

Free precession around Z (chemical shift or field inhomogeneity)

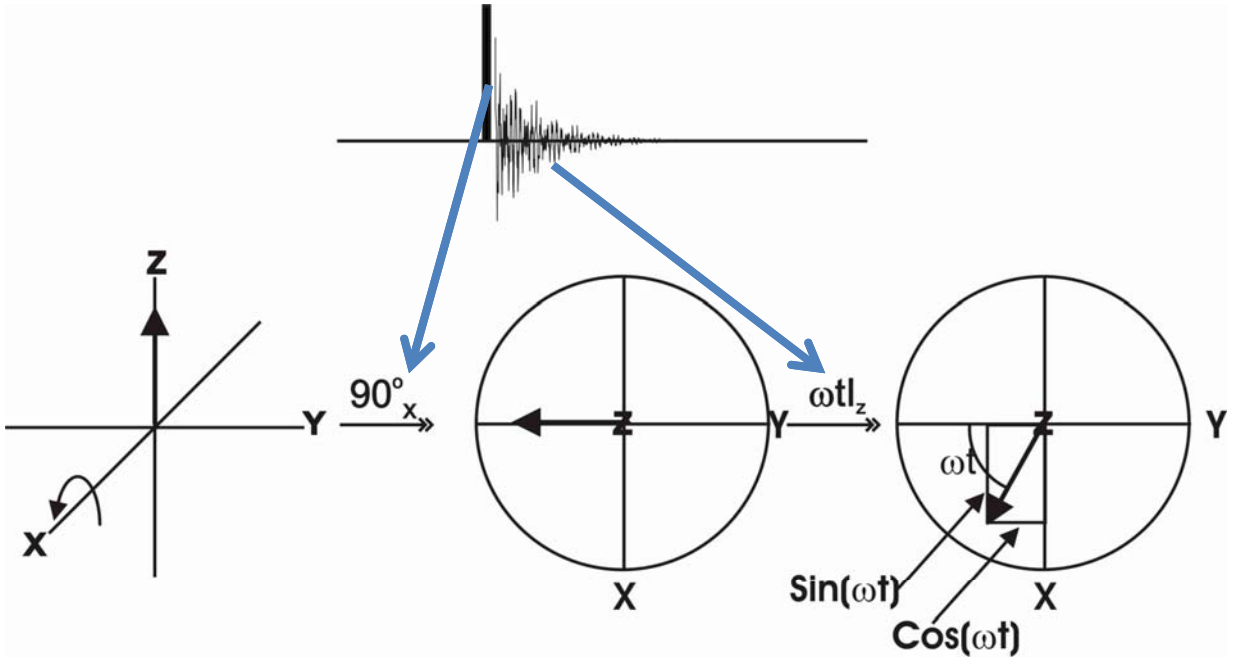

$$\mathbf{I_z} \xrightarrow{\frac{\pi}{2}\hat{\mathbf{I}}_x} -\mathbf{I_y} \xrightarrow{\omega_I t\hat{\mathbf{I}}_z} -\mathbf{I_y}\cos(\omega_I t) + \mathbf{I_x}\sin(\omega_I t)$$

Some other rotation examples

$$\mathbf{I_z} \xrightarrow{\theta\hat{\mathbf{I}}_x} \mathbf{I_z}\cos(\theta) - \mathbf{I_y}\sin(\theta)$$

$$\mathbf{I_z} \xrightarrow{\frac{\pi}{3}\hat{\mathbf{I}}_x} \mathbf{I_z}\cos\left(\frac{\pi}{3}\right) - \mathbf{I_y}\sin\left(\frac{\pi}{3}\right)$$

$$\mathbf{I_z} \xrightarrow{\frac{3\pi}{2}\hat{\mathbf{I}}_x} \mathbf{I_z}\cos\left(\frac{3\pi}{2}\right) - \mathbf{I_y}\sin\left(\frac{3\pi}{2}\right) = \mathbf{I_z} * 0 - \mathbf{I_y} * 1 \equiv \mathbf{I_y}$$

$$\mathbf{I_z} \xrightarrow{-\frac{\pi}{2}\hat{\mathbf{I}}_x} \mathbf{I_y}$$

In reality, the last rotation is physically impossible (unless you can change the sign of the nuclear gyromagnetic ratio), but it is often useful in computations.

$\xrightarrow{-\frac{\pi}{2}\hat{\mathbf{I}}_x}$ should be written as $\xrightarrow{\frac{\pi}{2}\hat{\mathbf{I}}_{-x}}$ (phase shift of transmitter)

The spin echo

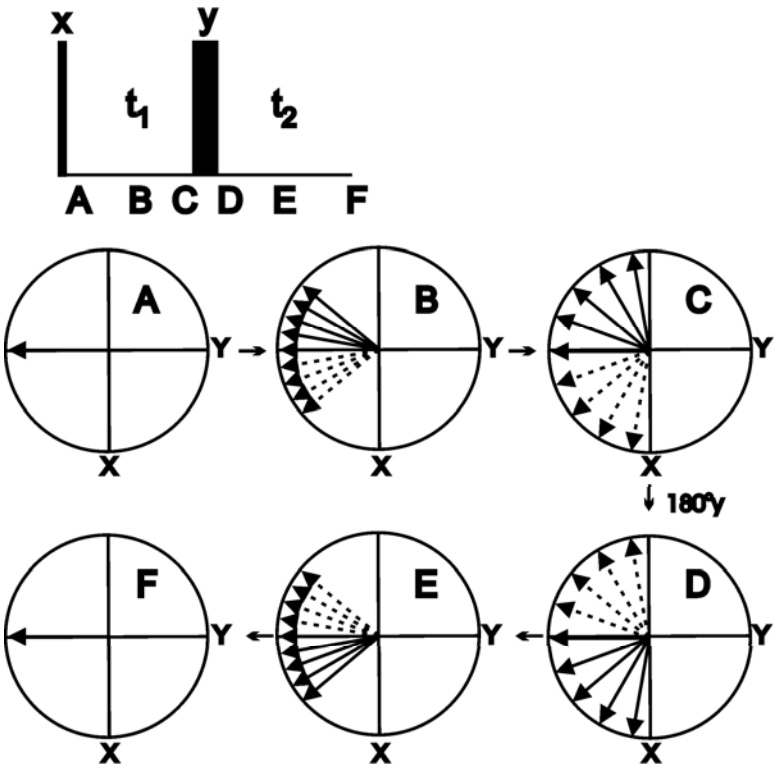

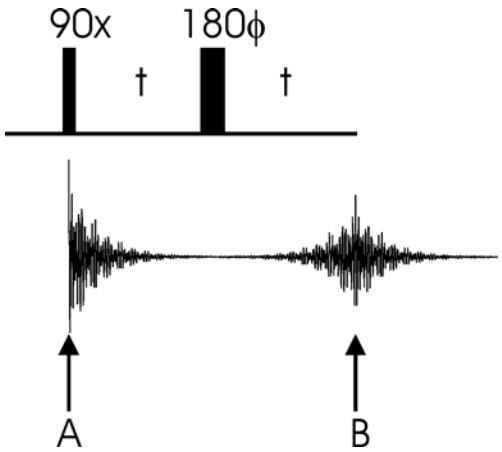

$$I_z \xrightarrow{\frac{\pi}{2}\hat{I}_x} -I_y$$

$$-I_y \xrightarrow{\omega t_1 \hat{I}_z} -I_y\cos(\omega t_1) + I_x \sin(\omega t_1)$$

$$\xrightarrow{\pi \hat{I}_y} -I_y\cos(\omega t_1) - I_x \sin(\omega t_1)$$

$$\xrightarrow{\omega t_1 \hat{I}_z} \left[-I_y\cos(\omega t_2) + I_x \sin(\omega t_2)\right]\cos(\omega t_1)$$

$$+\left[-I_x\cos(\omega t_2) - I_y \sin(\omega t_2)\right]\sin(\omega t_1)$$

$$\equiv -I_y\left[\cos(\omega t_1)\cos(\omega t_2) + \sin(\omega t_1)\sin(\omega t_2)\right]$$

$if\ t_1 = t_2$

$$\equiv -I_y\left[\cos^2(\omega t) + \sin^2(\omega t)\right] = -I_y$$

$\cos^2(\omega t) + \sin^2(\omega t) = 1$

There has to be a simpler way!

$$I_z \xrightarrow{\frac{\pi}{2}\hat{I}_x} -I_y$$

Pulsed field gradients

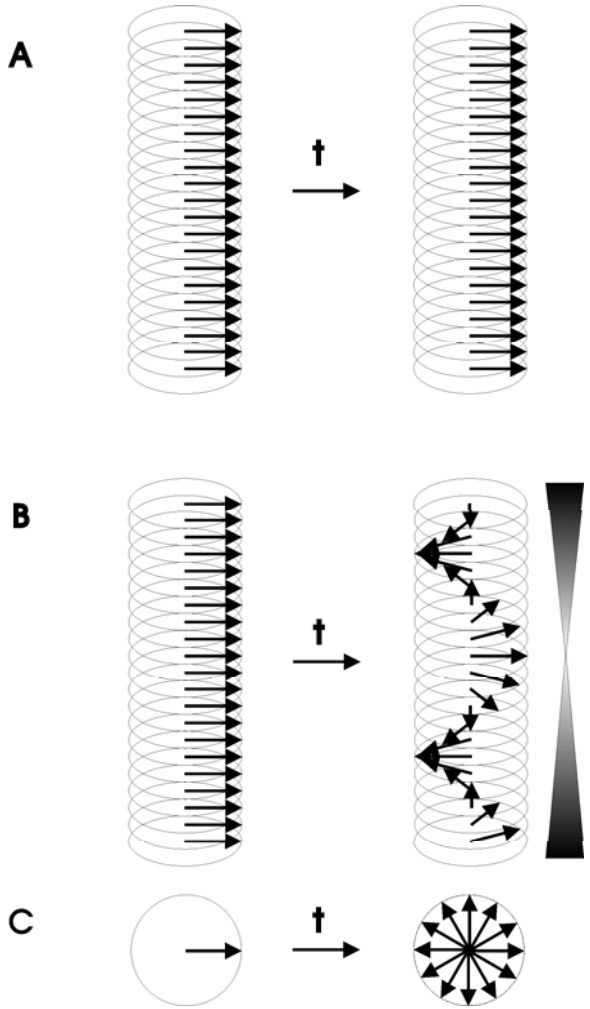

- **Schematic of the effect of a pulsed magnetic field gradient. The vertical slices represent the physical vertical extents of the sample in a NMR tube.**
  - **A). Time behavior of an ensemble of identical isolated spins having a rotating frame frequency of 0 Hz.**
  - **B). time behavior of the spin system in A subjected to a vertical linear magnetic field gradient.**
  - **C). Vertical projection of the spins in B.**

$$-I_y \xrightarrow{\gamma_I B_G(r) t \hat{I}_z} -I_y \cos(\gamma_I B_G(r) t) + I_x \sin(\gamma_I B_G(r) t)$$

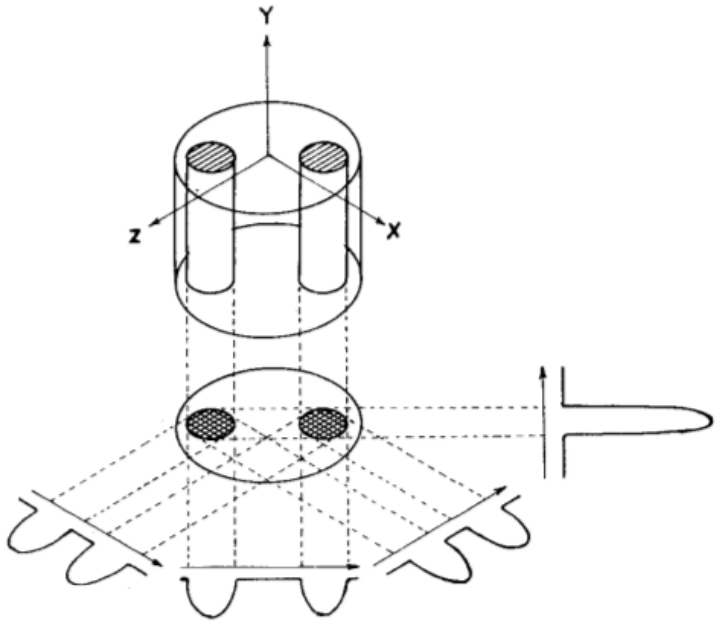

Fig. 1 Relationship between a three-dimensional object, its two-dimensional projection along the Y-axis, and four one-dimensional projections at 45° intervals in the XZ-plane. The arrows indicate the gradient directions.

Fig. 2 Proton nuclear magnetic resonance zeugmatogram of the object described in the text, using four relative orientations of object and gradients as diagrammed in Fig. 1.

MRI — a new way of seeing

In 1973, Paul Lauterbur described an imaging technique that removed the usual resolution limits due to the wavelength of the imaging field. He used two fields: one interacting with the object under investigation, the other restricting this interaction to a small region. Rotation of the fields relative to the object produces a series of one-dimensional projections of the interacting regions, from which two- or three-dimensional images of their spatial distribution can be reconstructed. Application of this technique as magnetic resonance imaging is now widespread.
Nature 242, 190 191 (1973)

1D image

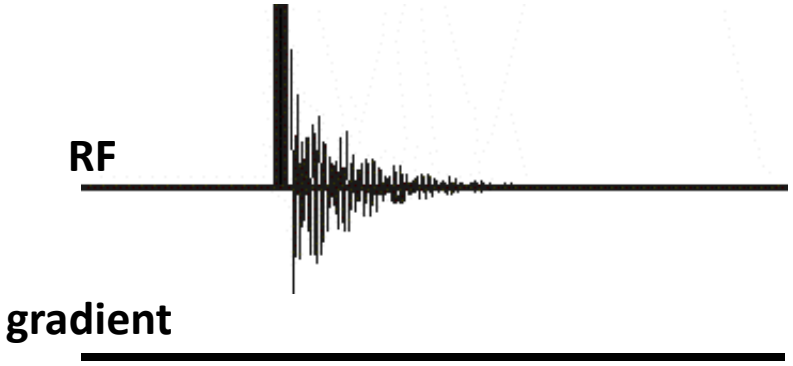

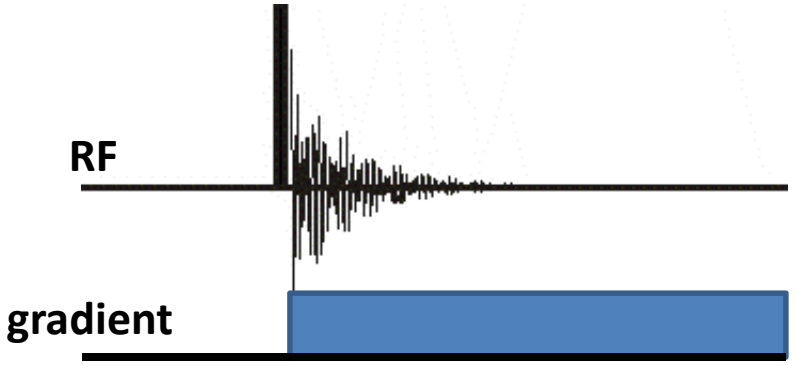

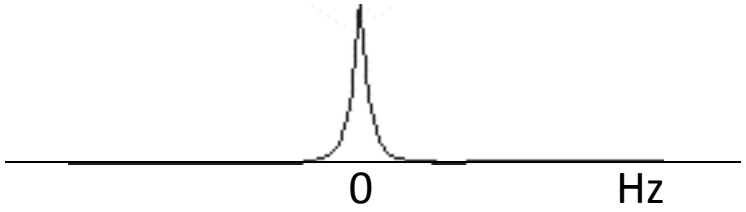

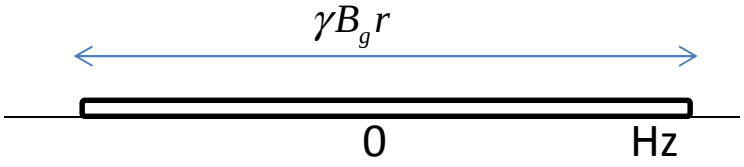

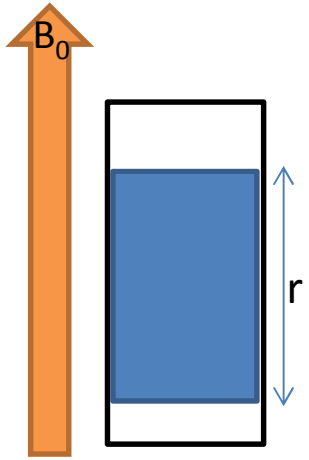

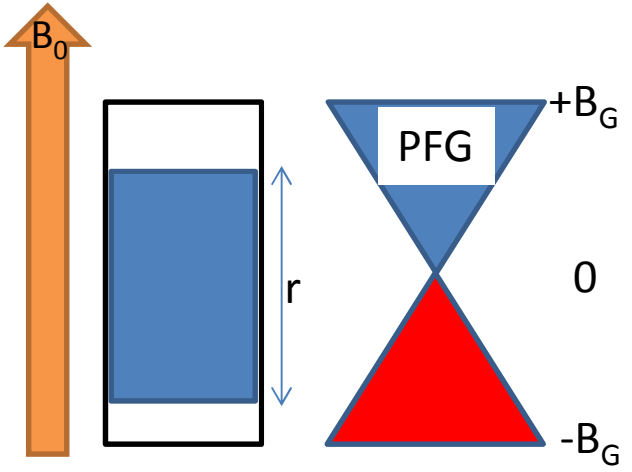

3D imaging

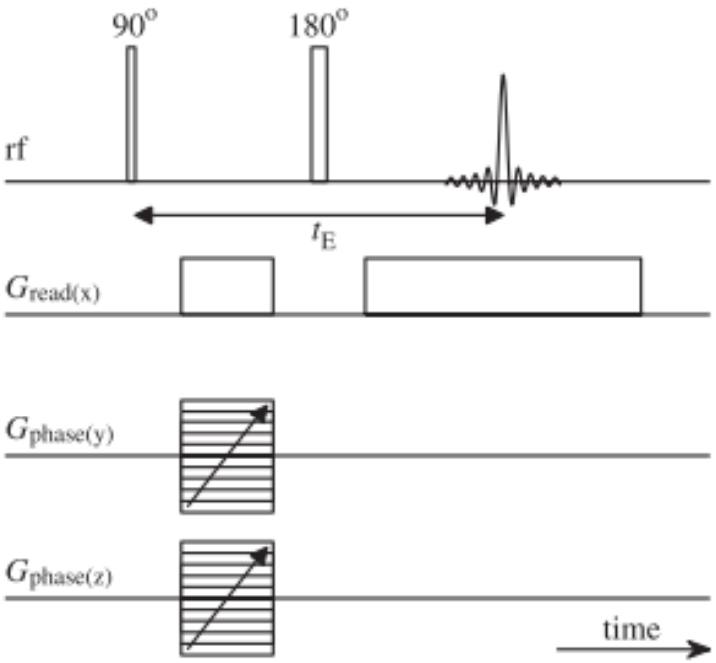

Figure 7. 3D spin warp imaging sequence utilizing one read gradient and two-phase encode dimensions. The spin echo is recorded at time t_E after the initial rf excitation pulse. The phase encode gradients are incremented in successive experiments.

Different flow imaging techniques

Table 1
Comparison of pulse sequences in their application to velocity imaging. Timescales and spatial resolutions are approximate and will be system-dependent. Approximate guides: spatial resolution – high (<50 μm), moderate (50–500 μm), low (>500 μm). T_2 – long (>0.5 s), moderate (20–500 ms), short (2–20 ms), very short (<2 ms). T_2^* – long (>50 ms), moderate (5–50 ms), short (0.5–5 ms), very short (<0.5 ms).

Pulse sequence	Time to acquire velocity image	Velocity measured	Comments
Single spin echo	1–100 min	Up to 5 m s^{-1}	Slow acquisition but applicable to most relaxation times. Suitable for short T_2 and short T_2^*. Acquisition time decreases as T_1 decreases. High spatial resolution possible. Too slow to capture transient behaviour.
EPI	20–100 ms	1–100 cm s^{-1}	Applicable to transient systems characterised by long T_2^* (τ_E 10–100 ms). Less sensitive to gradient imperfections than spiral sequences.
Spiral	3–25 ms	Up to 5 m s^{-1}	Can probe systems with shorter T_2^* than EPI (since τ_E 3–25 ms). Possibility of small tip angle excitation and rapid image frame rate. More complex image reconstruction than EPI.
RARE	2–10 s	Up to 10 cm s^{-1}	Higher spatial resolution achieved than with EPI and spiral. Appropriate for studying slowly changing systems. Requires long T_2 but can cope with quite short T_2^* (τ_E = 50–500 ms). Usually too slow to capture transient behaviour.
FLASH	>150 ms	50 cm s^{-1}	Best for short T_1 (<50 ms) to achieve rapid recycle, short T_2; moderately short T_2^*. Low SNR leads to low-moderate spatial resolution. Very robust. Usually too slow to capture transient behaviour.
SPI (SPRITE)	Seconds to hours (time-averaged)	0.5–50 m s^{-1}	Suitable for very short T_2^*. Too slow to capture transient behaviour.

Short T_2 means broad lines; time signal decays rapidly
Long T_1 means time averaging takes longer

1D flow imaging (time of flight)

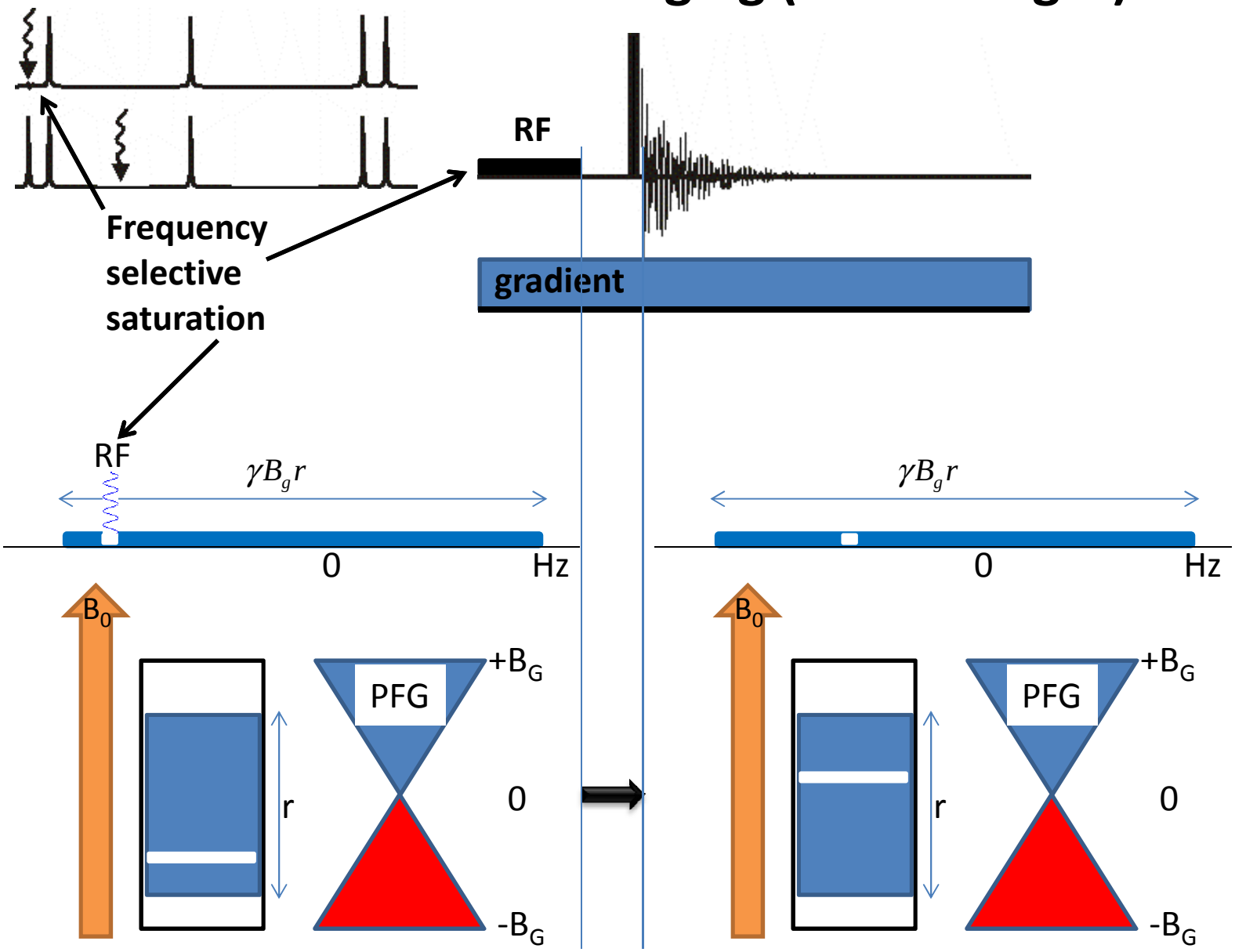

Presaturate slice **Flow Acquire image**

Time of flight imaging

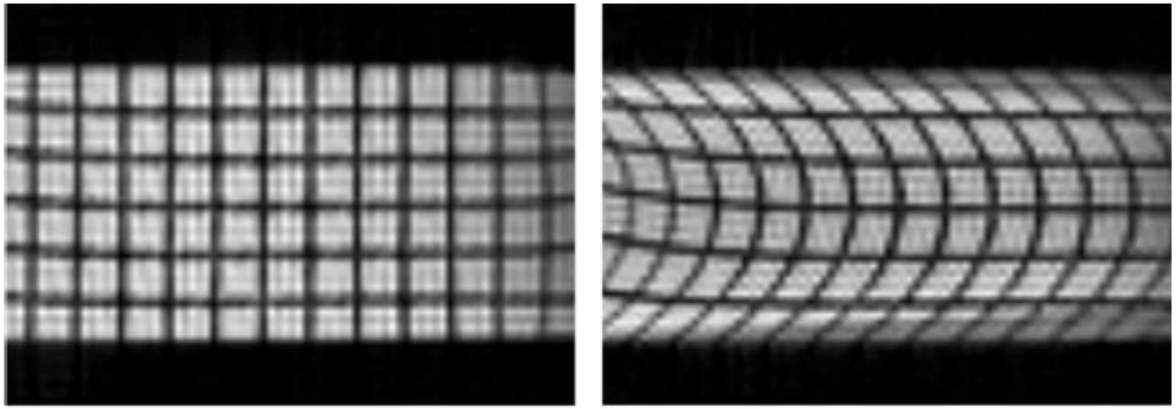

(a) (b)

Fig. 5. Example of a DANTE type velocity image. 199.7 MHz ^{1}H 2D image of a 2.0 mm thick longitudinal slice at (a) zero flowrate of water and (b) a flowrate of 486 cm^3 min^{-1}.

Gradient recalled echo

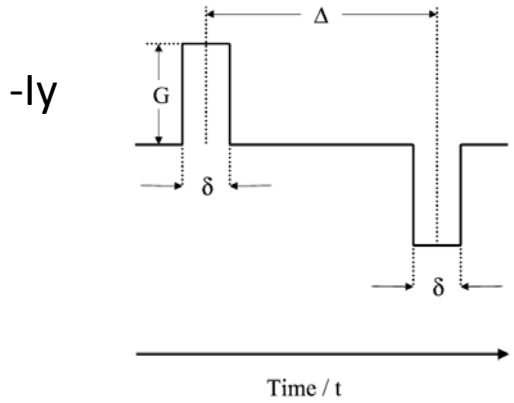

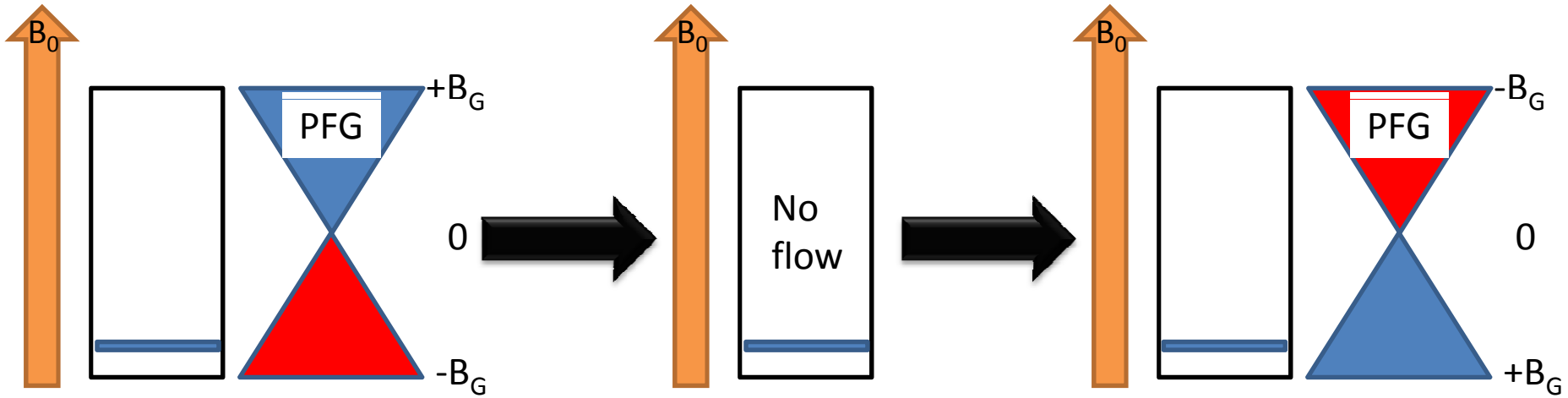

No change in position

$\gamma B_G(r)\delta$ →

$-\gamma B_G(r)\delta$ →

Refocusing field is same but negative

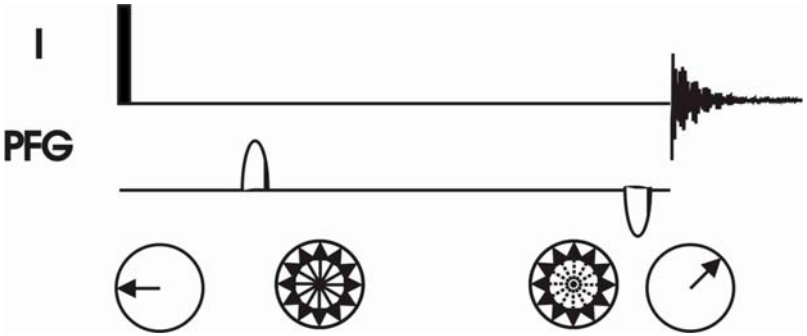

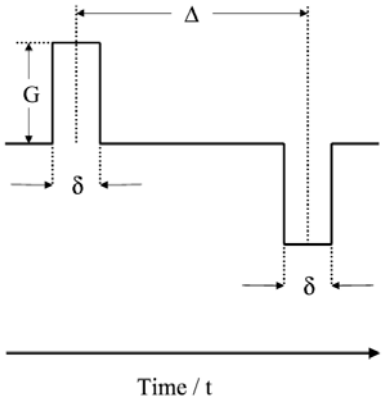

$$-I_y \xrightarrow[\text{defocusing}]{\gamma B_G(r_1)\delta} -I_y\cos\left(\gamma B_G(r_1)\delta\right)+I_x\sin\left(\gamma B_G(r_1)\delta\right)$$

$$\xrightarrow{\text{No position change}} B_G(r_1)=-B_G(r_2)$$

$$\xrightarrow[\text{refocusing}]{-\gamma B_G(r)\delta}\left[-I_y\cos\left(-\gamma B_G(r_2)\delta\right)+I_x\sin\left(-\gamma B_G(r_2)\delta\right)\right]\cos\left(\gamma B_G(r_1)\delta\right)+$$

$$\left[I_x\cos\left(-\gamma B_G(r_2)\delta\right)+I_y\sin\left(-\gamma B_G(r_2)\delta\right)\right]\sin\left(\gamma B_G(r_1)\delta\right)$$

Recall:

$\cos(-\theta)=\cos(\theta)$

$\sin(-\theta)=-\sin(\theta)$

$$\left[-I_y\cos\left(\gamma B_G(r_2)\delta\right)-I_x\sin\left(\gamma B_G(r_2)\delta\right)\right]\cos\left(\gamma B_G(r_1)\delta\right)+\left[I_x\cos\left(\gamma B_G(r_2)\delta\right)-I_y\sin\left(\gamma B_G(r_2)\delta\right)\right]\sin\left(\gamma B_G(r_1)\delta\right)$$

combining and since $B_G(r_1)=-B_G(r_2)=B_G(r)$

$$-I_y\left[\cos^2\left(\gamma B_G(r)\delta\right)+\sin^2\left(\gamma B_G(r)\delta\right)\right]+I_x\left[\cos\left(\gamma B_G(r)\delta\right)\sin\left(\gamma B_G(r)\delta\right)-\sin\left(\gamma B_G(r)\delta\right)\cos\left(\gamma B_G(r)\delta\right)\right]$$

resulting in

$-I_y$

1D Flow imaging (phase shift)

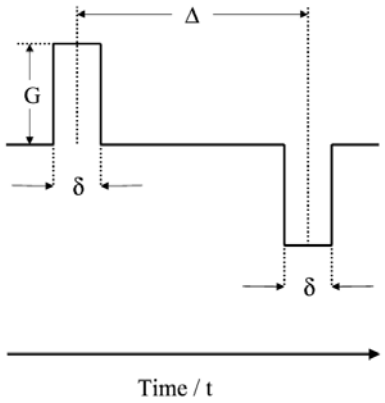

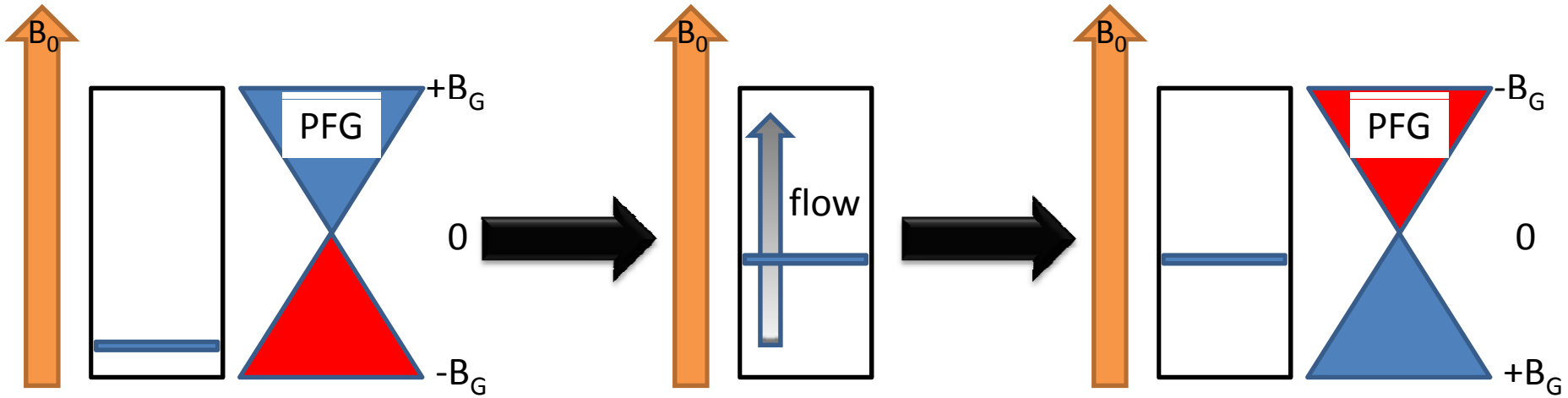

Position change due to flow

$\gamma B_G(r)t$ →

$-\gamma B_G(r')t$ →

Refocusing field is different

1D Flow imaging (phase shift)

-Iy

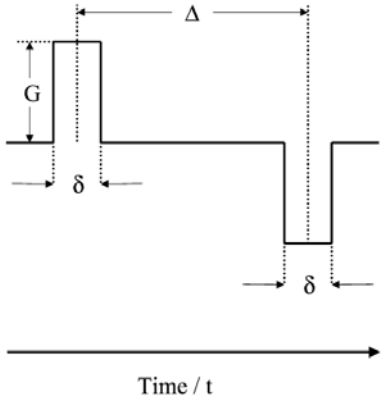

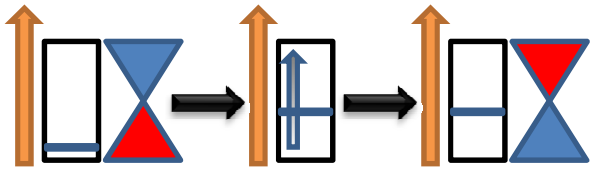

$$-I_y \xrightarrow[\text{defocusing}]{\gamma B_G(r_1)\delta} -I_y\cos\left(\gamma B_G(r_1)\delta\right)+I_x\sin\left(\gamma B_G(r_1)\delta\right)$$

$$\xrightarrow{\text{Position change}} B_G(r_1)\neq -B_G(r_2)$$

$$\xrightarrow[\text{refocusing}]{-\gamma B_G(r_2)\delta}\left[-I_y\cos\left(-\gamma B_G(r_2)\delta\right)+I_x\sin\left(-\gamma B_G(r_2)\delta\right)\right]\cos\left(\gamma B_G(r_1)\delta\right)+$$

$$\left[I_x\cos\left(-\gamma B_G(r_2)\delta\right)+I_y\sin\left(-\gamma B_G(r_2)\delta\right)\right]\sin\left(\gamma B_G(r_1)\delta\right)$$

Recall:

$\cos(-\theta)=\cos(\theta)$

$\sin(-\theta)=-\sin(\theta)$

$$\left[-I_y\cos\left(\gamma B_G(r_2)\delta\right)-I_x\sin\left(\gamma B_G(r_2)\delta\right)\right]\cos\left(\gamma B_G(r_1)\delta\right)+\left[I_x\cos\left(\gamma B_G(r_2)\delta\right)-I_y\sin\left(\gamma B_G(r_2)\delta\right)\right]\sin\left(\gamma B_G(r_1)\delta\right)$$

combining

$$-I_y\left[\cos\left(\gamma B_G(r_2)\delta\right)\cos\left(\gamma B_G(r_1)\delta\right)+\sin\left(\gamma B_G(r_2)\delta\right)\sin\left(\gamma B_G(r_1)\delta\right)\right]+$$

$$I_x\left[\cos\left(\gamma B_G(r_2)\delta\right)\sin\left(\gamma B_G(r_1)\delta\right)-\sin\left(\gamma B_G(r_2)\delta\right)\cos\left(\gamma B_G(r_1)\delta\right)\right]$$

1D Flow imaging (phase shift)

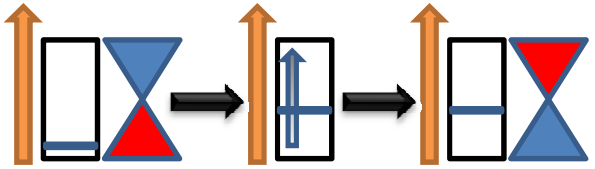

$$-I_y\left[\cos\left(\gamma B_G(r_2)\delta\right)\cos\left(\gamma B_G(r_1)\delta\right)+\sin\left(\gamma B_G(r_2)\delta\right)\sin\left(\gamma B_G(r_1)\delta\right)\right]+$$
$$I_x\left[\cos\left(\gamma B_G(r_2)\delta\right)\sin\left(\gamma B_G(r_1)\delta\right)-\sin\left(\gamma B_G(r_2)\delta\right)\cos\left(\gamma B_G(r_1)\delta\right)\right]$$

$$\cos(a)\cos(b)+\sin(a)\sin(b)=\cos(a-b)$$
$$\cos(a)\sin(b)-\sin(a)\cos(b)=-\sin(a-b)$$

$$-I_y\left[\cos\left(\gamma B_G(r_2)\delta-\gamma B_G(r_1)\delta\right)\right]=-I_y\left[\cos\left(\gamma\left[B_G(r_2)-B_G(r_1)\right]\delta\right)\right]$$
$$-I_x\left[\sin\left(\gamma B_G(r_2)\delta-\gamma B_G(r_1)\delta\right)\right]=-I_x\left[\sin\left(\gamma\left[B_G(r_2)-B_G(r_1)\right]\delta\right)\right]$$

The angle at the end of the refocusing is:

$$\gamma\left[B_G(r_2)-B_G(r_1)\right]\delta$$

$$\left[B_G(r_2)-B_G(r_1)\right]=\text{gradient\_strength}*\text{flow\_rate}*\Delta$$

Flow imaging (phase shift) example

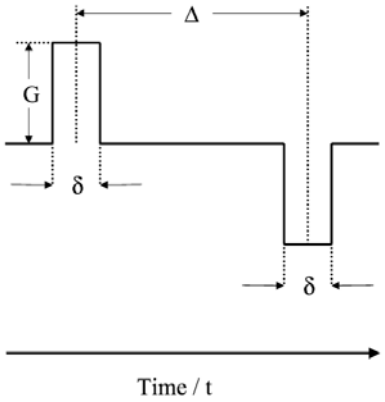

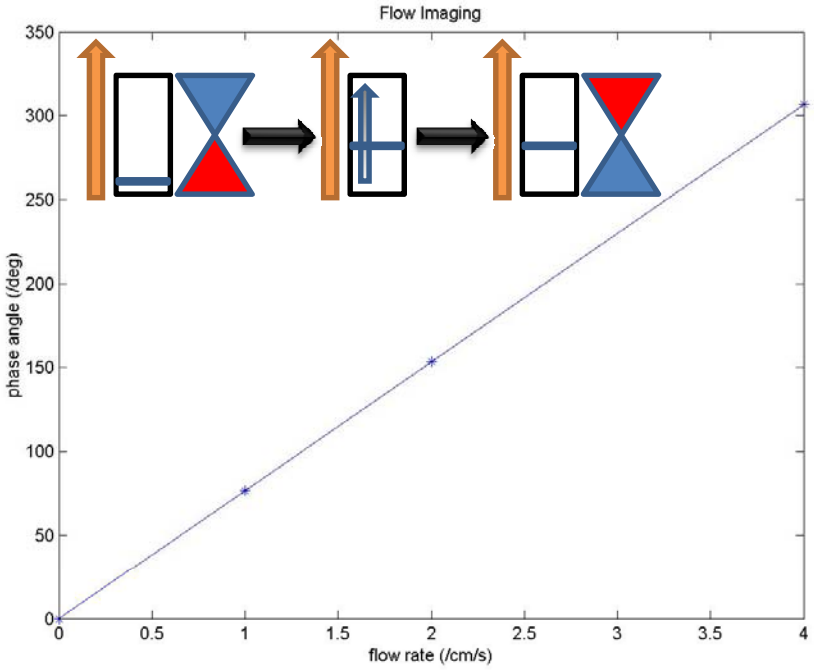

$\varphi = \gamma[B_G(r_2) - B_G(r_1)]\delta$

Flow rate =f

gradient strength=B_G=5 gauss/cm

δ=.001s

Δ=.01s

change in gradient due to flow= $[B_G(r_2) - B_G(r_1)]$=f * B_G * Δ

Flow rate = f =4cm/s

$[B_G(r_2) - B_G(r_1)]$ = 4cm/s * .01 s * 5 gauss/cm=.2 gauss

phase difference = φ = 26753 rad/s gauss * .2 gauss * .001 s = 5.35 rad=306.6

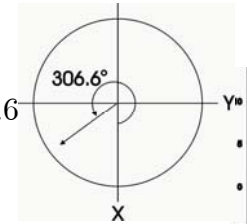

for f=2 cm/s:

$[B_G(r_2) - B_G(r_1)]$ = 2 * .01 * 5 = .1 gauss

φ = 26753 * .1 * .001 = 2.68 rad=153.3°

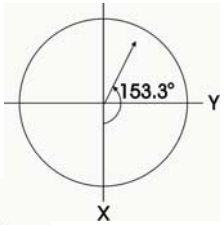

for f=1 cm/s:

$[B_G(r_2) - B_G(r_1)]$ = 1 * .01 * 5 = .05 gauss

φ = 26753 * .05 * .001 = 1.34 rad=76.6°

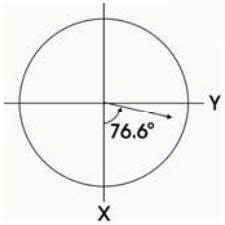

phase is linear with flow rate

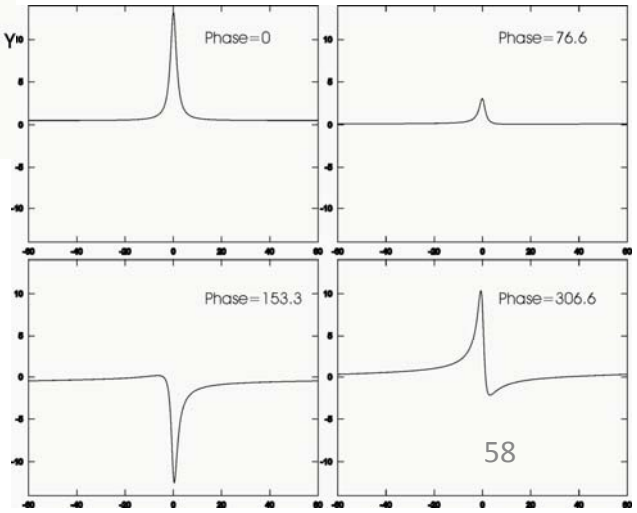

3D flow imaging

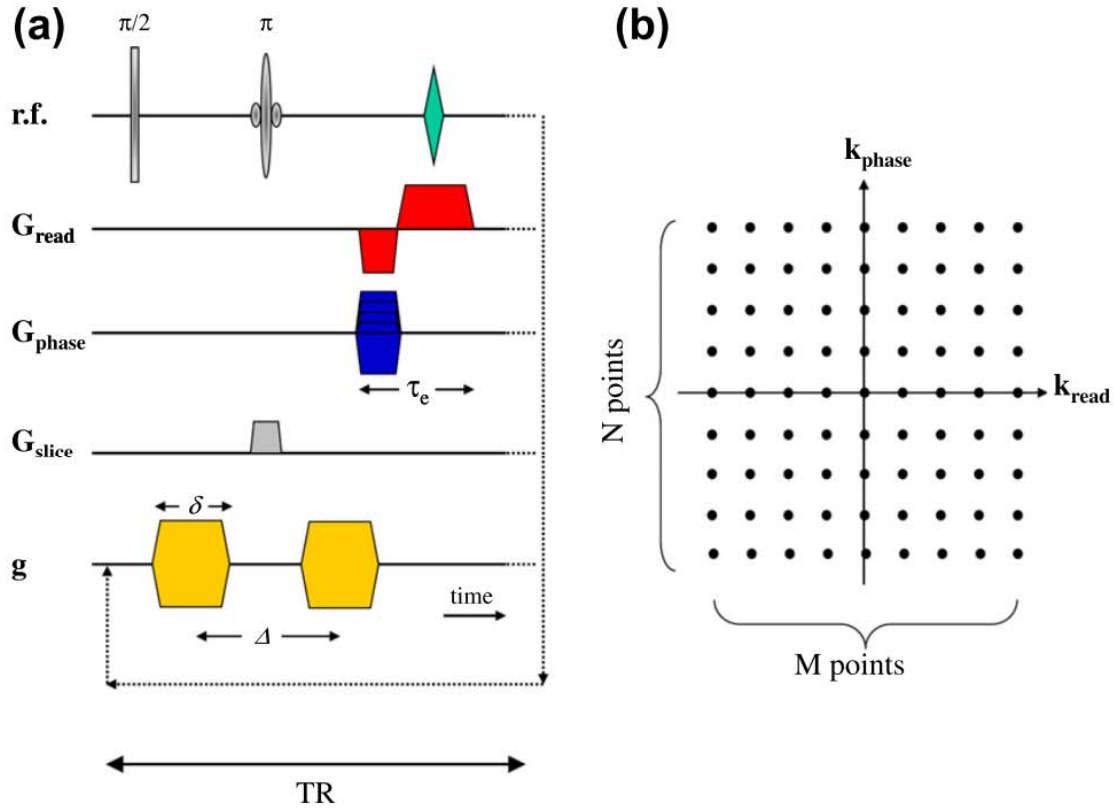

Fig. 1. (a) A schematic of a simple spin echo Flow MRI pulse sequence. Several timescales which must be considered when imaging transient flows are shown including the time for velocity measurement, Δ, the spatial encoding time, τ_e and the repetition time, TR. δ Is the timescale over which the flow encoding gradients are applied. (b) Schematic representation of the **k**-space raster.

Magnetic resonance in chemical process and reaction engineering

Bench-top NMR machines are now routinely used in the food industry for the quantification of fat and water, and NMR in oil-well bore holes is now a valuable tool to assess oil field properties for companies in the petroleum industries. More recently, a portable MRI machine, the NMR MOUSE [5], has successfully been used to determine the aging process in elastomers.

In particular, the study of transport, i.e. flow, diffusion and dispersion by magnetic resonance spectroscopy, relaxometry, diffusometry, and multi-dimensional multi-nuclear imaging is ever increasing.

- **Oil/water transport in rocks**
- **Transport and reaction in catalyst pellets**
- **Transport in bead packs/model porous media**
- **Controlled drug release in polymers**
- **Oil/water transport in rocks**
- **Transport and reaction in catalyst pellets**
- **Transport in bead packs/model porous media**
- **Controlled drug release in polymers**

Flow in a pipe with different Reynolds number

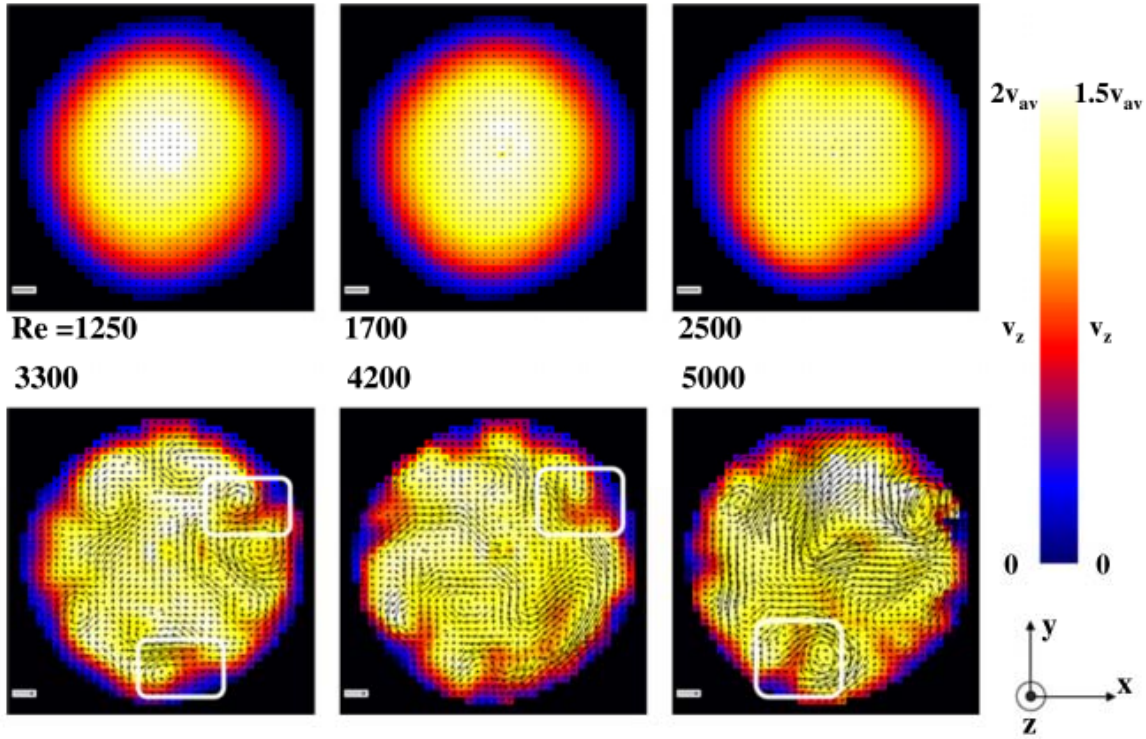

Fig. 4. Three orthogonal component velocity images of pipe flow (i.d. 29 mm) acquired at increasing Reynolds number of (a) 1250, (b) 1700, (c) 2500, (d) 3300, (e) 4200, and (f) 5000. The colour scale identifies the magnitude of the z-velocity, and ranges from zero to twice the average velocity for a–c and from zero to 1.5 times the average velocity for d–f. The flow velocity in the plane of the image (i.e. x–y) is shown by the vectors on each image. The vector scale bar on each image corresponds to 1 cm s^{-1}. (Sederman et al. [32] reproduced by permission of Elsevier.)

Reynolds number (Re) is a dimensionless number that gives a measure of the ratio of inertial forces to viscous forces

Trickle flow

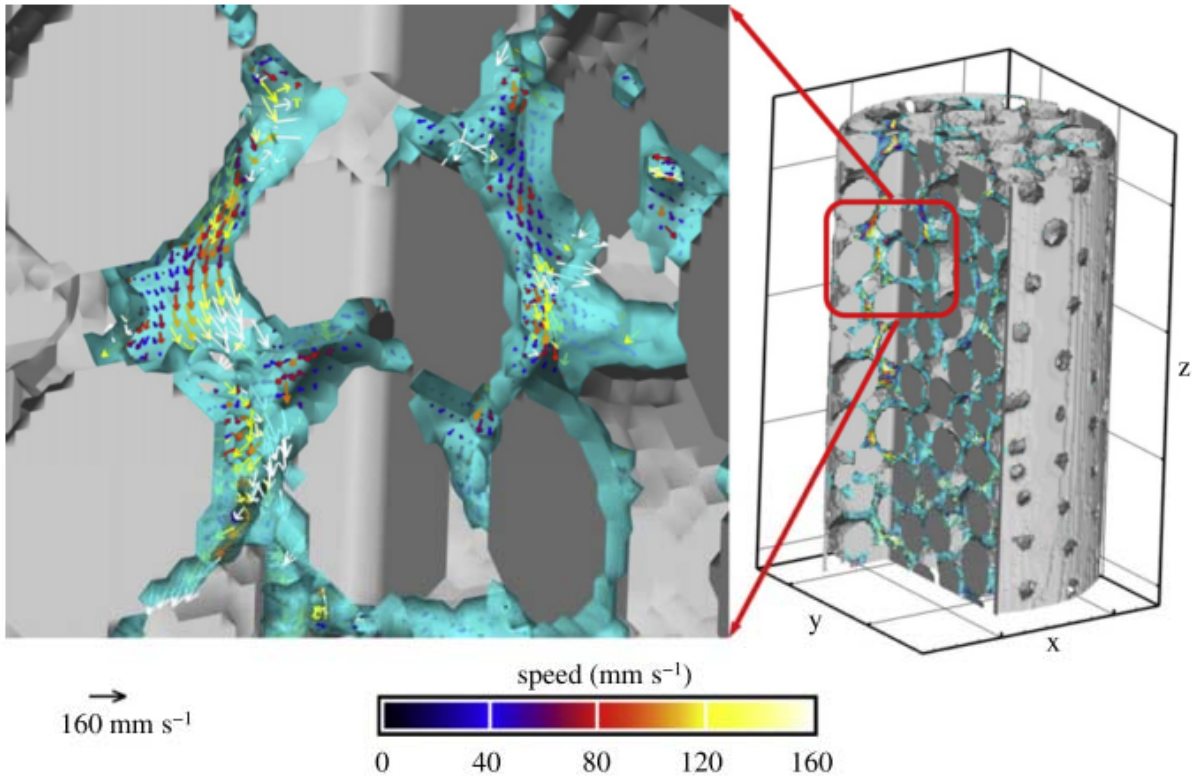

Fig. 6. 3D visualization of the v_x, v_y, v_z components of the liquid flow field during trickle flow. The gas and liquid superficial velocities are 52.4 mm s^{-1} and 2.3 mm s^{-1} respectively. The field-of-view was 34 mm × 34 mm × 68 mm, giving an isotropic voxel resolution of 266 μm. The bed was operated at atmospheric pressure. Packing elements are shown as grey; the gas is not shown (transparent). The liquid filled regions of the bed are identified as light blue. The flow vectors identify the direction and magnitude of the flow. For clarity, the magnitude is also colour-coded according to the colour scale shown. (For interpretation of the references to colour in this figure legend, the reader is referred to the web version of this article.)

Gas and liquid flow

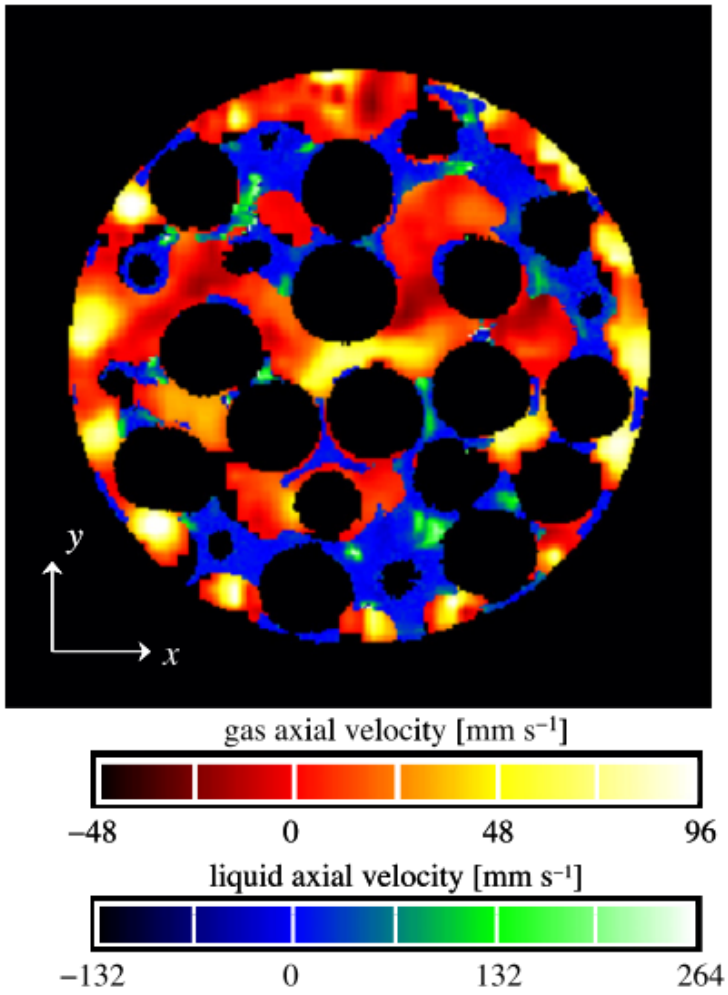

Fig. 7. Gas and liquid velocity map of SF_6 (red/yellow) and water (blue/green) during trickle flow. The gas and liquid superficial velocities were 8.7 mm s^{-1} and 2.3 mm s^{-1} respectively. The bed was operated at a pressure of 4.7 bara. (For interpretation of the references to colour in this figure legend, the reader is referred to the web version of this article.)

X,Y,Z velocities and stress tensors

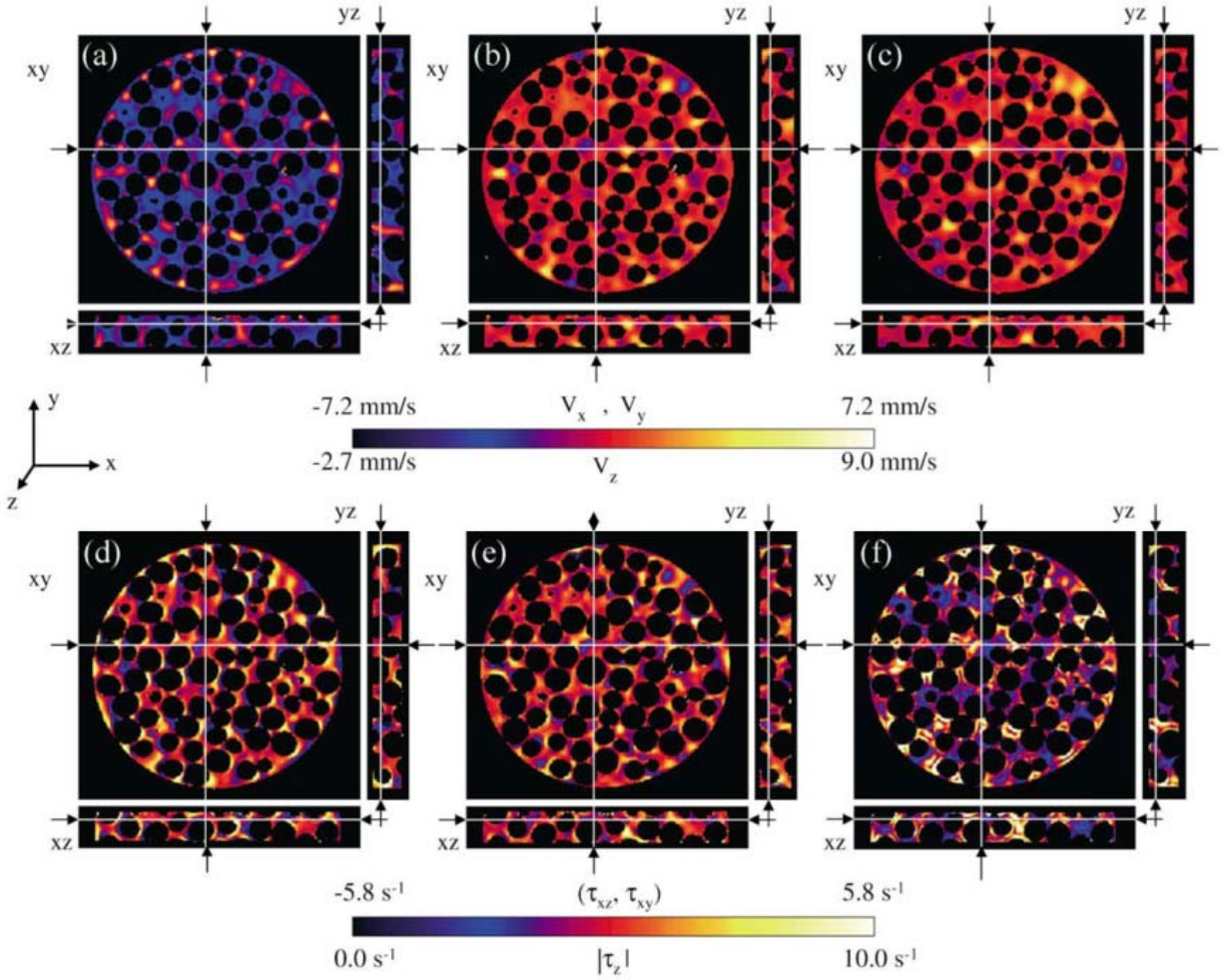

Fig. 11. Velocity fields within the packing of spheres. Fluid velocities in the (a) *z*- (b) *x*- and (c) *y*-directions are shown with slices taken in the *xy*, *yz* and *xz* planes for each of the velocity components. (d), (e) and (f) are the corresponding images of the liquid stress tensor, e_{ii}, derived from the data in (a), (b) and (c). Data are shown for (d) e_{xz}, (e) e_{xy} and (f) $|e_z|$ with slices taken in the *xy*, *yz* and *xz* planes for each of the shear components. All images were performed at a ^{1}H frequency of 199.7 MHz and the isotropic voxel resolution in all images is 195 μm for an isotropic data matrix size of 256^3. Reproduced with permission from Ref. [44].

1D Chemical shift imaging

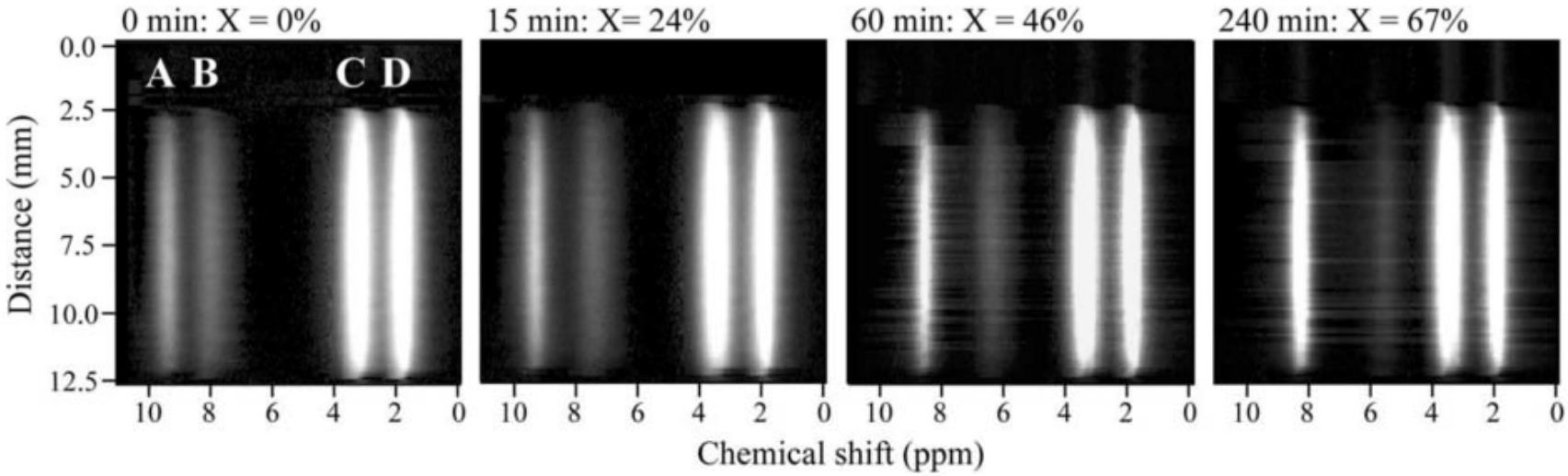

Fig. 21. 1D chemical shift imaging data sets showing the extent of conversion under batch reaction conditions. Four 'peaks' in the CSI data sets are evident: (A) and (B) are intra- and inter particle OH resonance, respectively; (C) is the ^{1}H resonance of the CH_3O group associated with the methanol and methyl acetate species; (D) is the ^{1}H resonance of the CH_3 group associated with the acetic acid and methyl acetate species. All images were performed at a ^{1}H frequency of 300.13 MHz. Reproduced with permission from Ref. [103].

2D slice from 3D chemical shift imaging

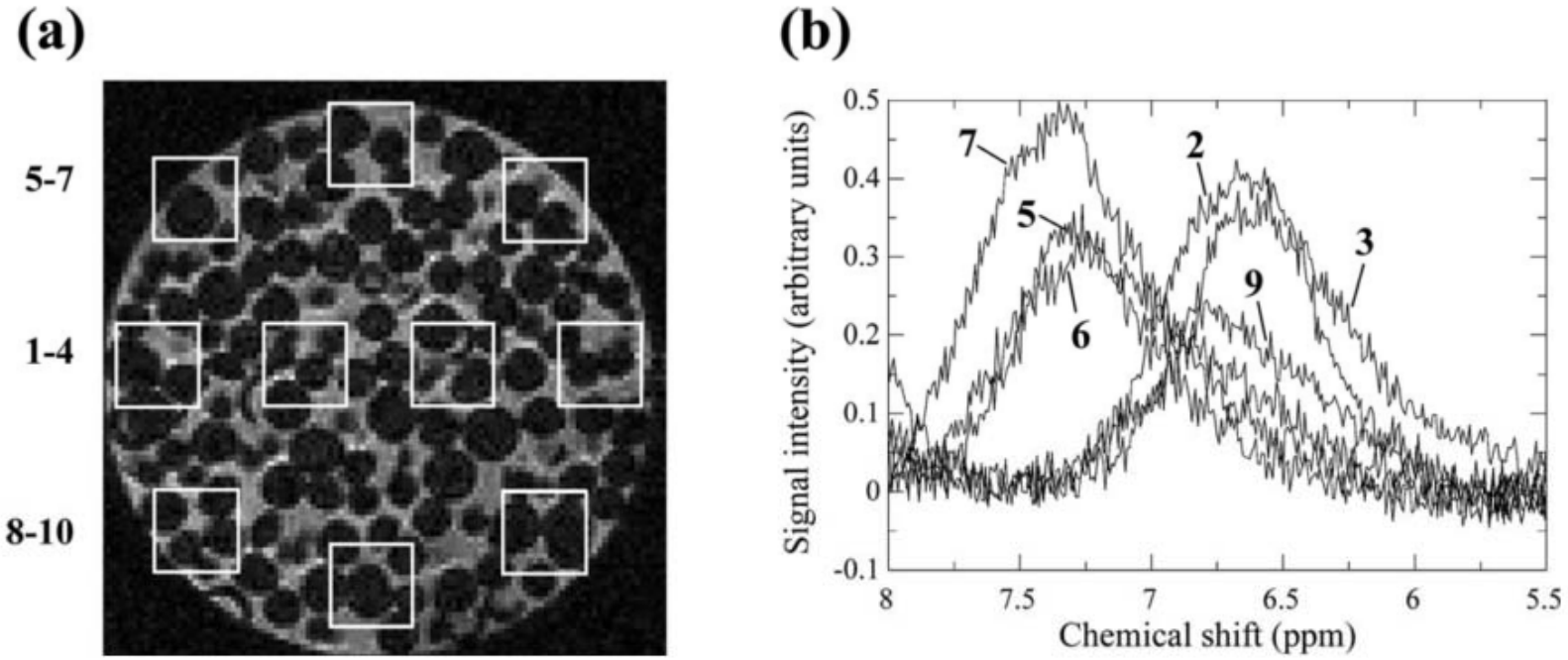

Fig. 22. Volume selective spectroscopy within the fixed bed reactor. (a) The location of the 10 volume elements within an image slice. (b) ^{1}H spectra for peak (B). The distribution in chemical shifts for the position of peak (B) clearly reflects the differences in chemical conversion within this particular transverse slice through the bed. All images were performed at a ^{1}H frequency of 300.13 MHz. Reproduced with permission from Ref. [103].

Drying

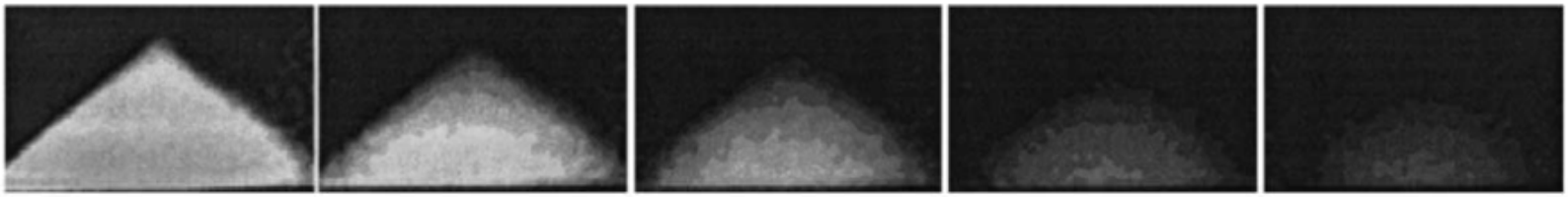

Fig. 33. Two-dimensional proton images of clay drying at times (a) $t = 0$, (b) 1.5, (c) 3.0, (d) 5.0 and, (e) 10.0 h. Environmental conditions, relative humidity = 0%, air flow rate = 1.7 m s^{-1}; air temperature 19 °C. Reproduced with permission from Ref. [157].

Filtration

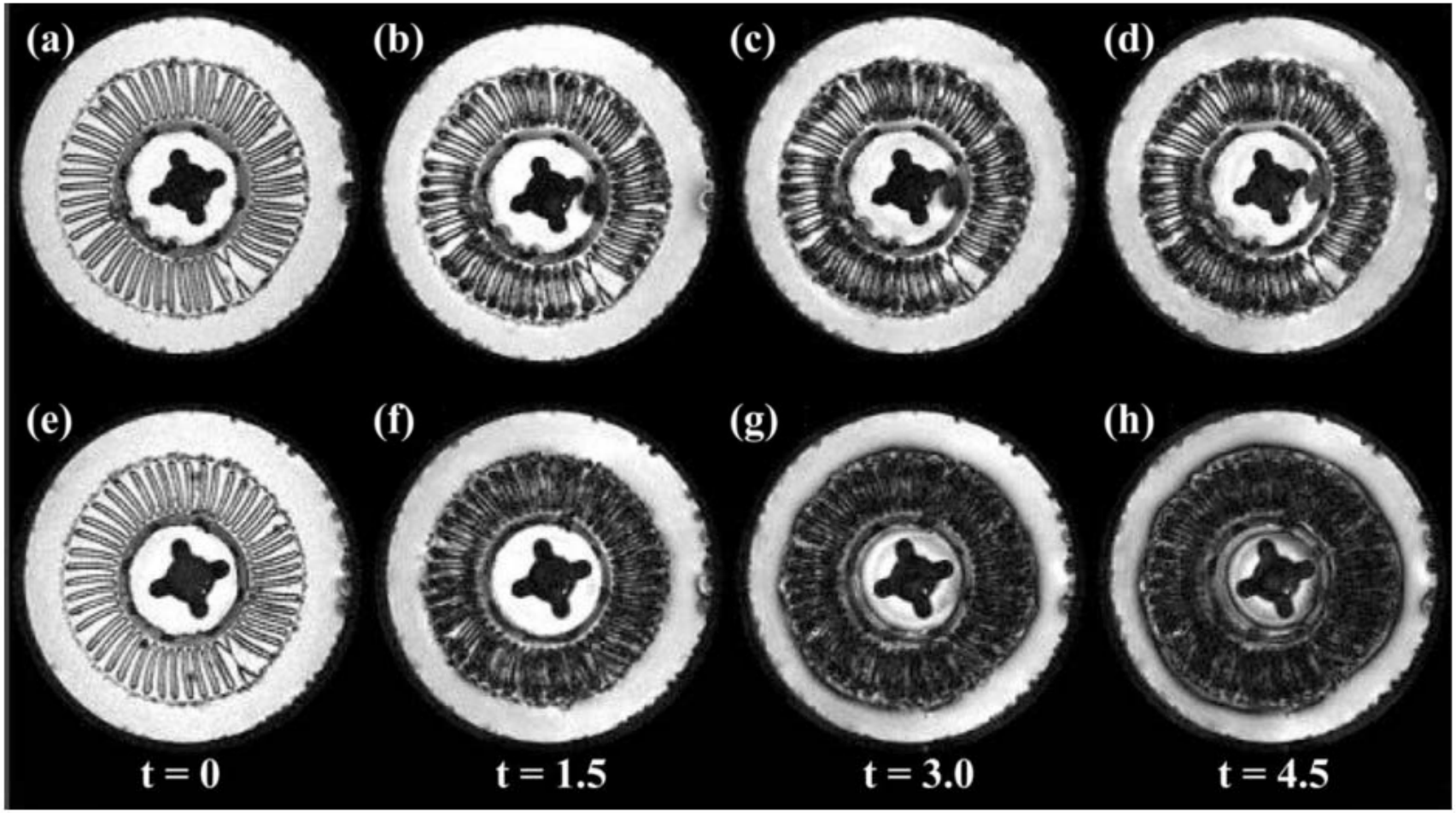

Fig. 34. Lightly blocked transverse section of the filter (frames a–d) vs. a heavily blocked transverse section (frames e–h). The accumulation of iron oxide particles at four successive time points is shown: $t = 0$, 1.5, 3.0 and 4.5 min after contaminated fluid flow. The heavily blocked transverse section shown was located 8.0 cm below the top of the filter, 4.0 mm below the hole in the central distribution pipe, and the lightly blocked section is located 25.0 mm below that section. Voxels containing no signal either due to the absence of fluid or the presence of iron (III) oxide are shown in black. All images were performed at a ^{1}H frequency of 85 MHz.

Diffusion & chemical shift imaging

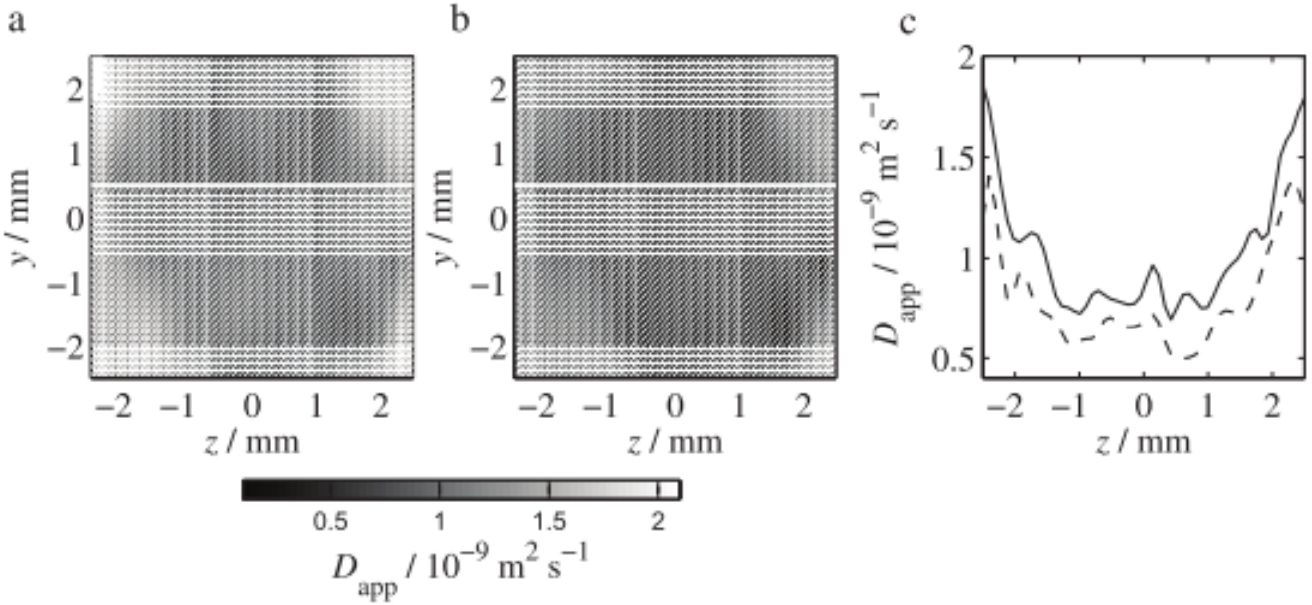

Figure 18. Chemically selective apparent diffusion coefficient maps for (a) 2-butanone and (b) 2-butanol in a single Ru/SiO_2 pellet. In (c), diffusion profiles for the 2-butanone (solid line) and 2-butanol (dotted line) are shown, corresponding to the white lines in (a) and (b).

Meat balls in soup! – thermal and spatial imaging

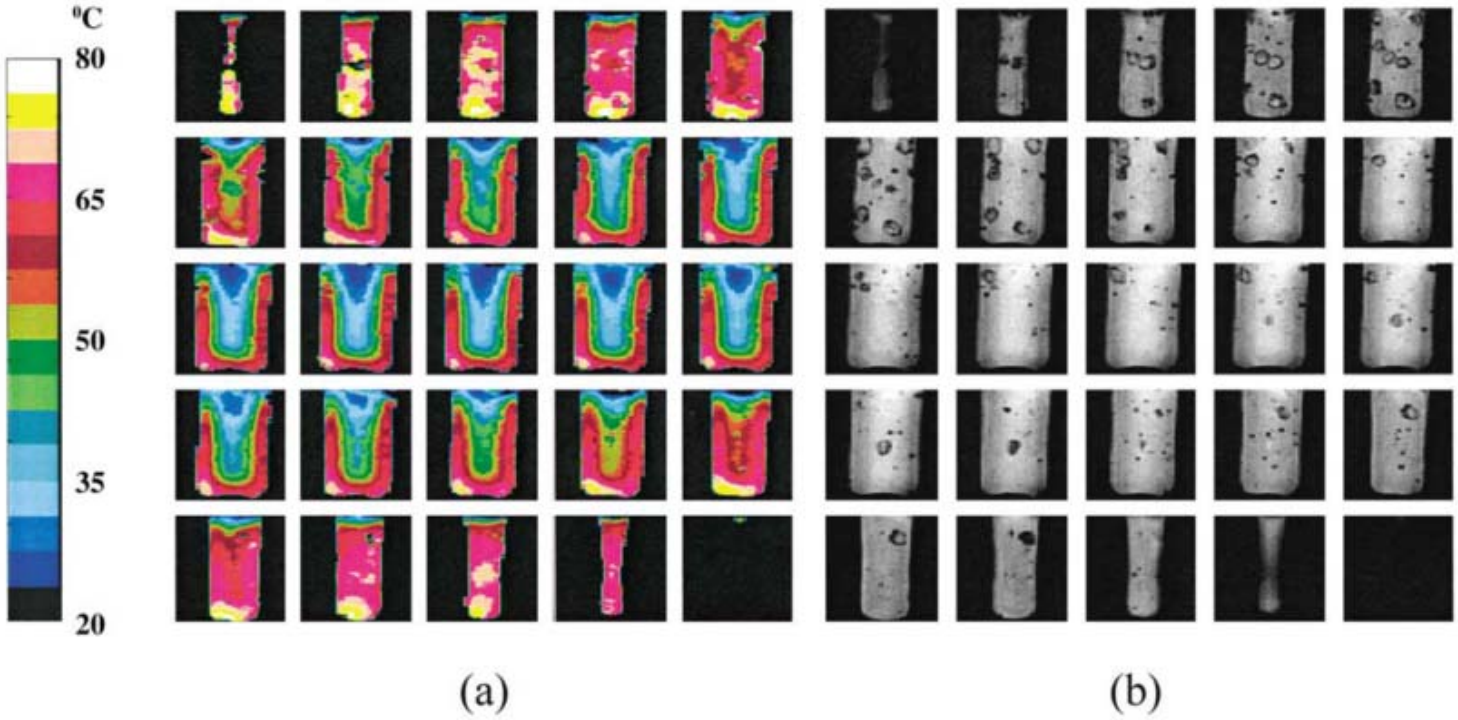

Fig. 38. 3D temperature (a) and spatial (b) heterogeneity images of a 500 cm^3 jar containing soup with meat balls that has been immersed into a water bath set (level coincident with that of soup) between 95 and 98 °C for 11 min displayed as a set of 2D sections. Resolution 0.78 mm (along cylindrical axis) × 3.13 mm × 3.13 mm. © 2001 Blackwell Publishing Ltd. Reproduced with permission from Ref. [185]

The chemical shift of water is temperature dependent (as well as pH dependent).
δ(H2O) = 7.83 – T / 96.9, where temperature is measured in Kelvins.
This equation is valid at pH 5.5. Dependence of δ(H2O) on pH is about 0.02 ppm per pH unit.

Two dimensional NMR

Two-dimensional NMR

Variable time (t1)

Detection (t2)

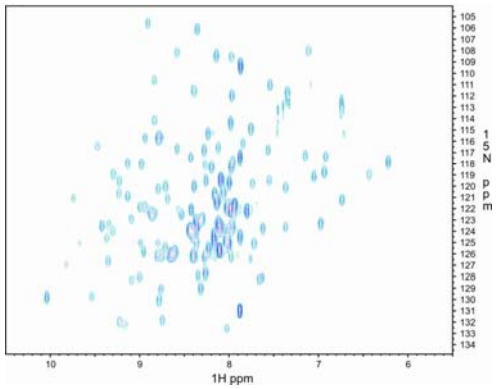

2-dimensional FT

$S(\omega_1,\omega_2)=FT\ (F(t_1,t_2))$

2 site chemical exchange at increasing exchange rates

$$A \underset{k_{-1}}{\overset{k_1}{\rightleftharpoons}} B$$

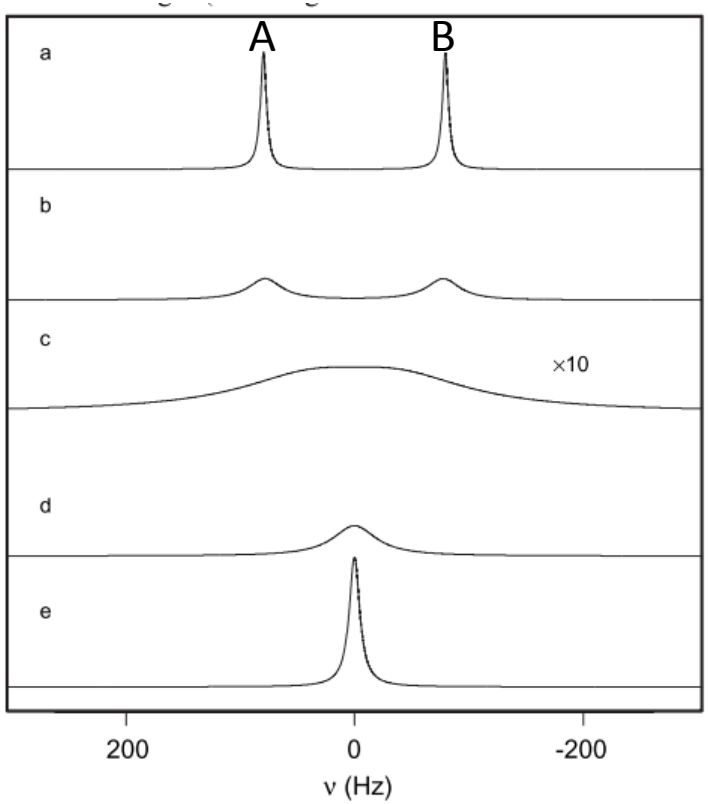

Figure 9. Chemical exchange for a two-site system. Shown are the Fourier transformations of FIDs calculated by using [160]. The calculations used Ω = 80 Hz and ρ = 10 s^{-1}. Calculations were performed for values of the exchange rate, k, equal to (a) 10 s^{-1}, (b) 100 s^{-1}, (c) 450 s^{-1}, (d) 1000 s^{-1} and (e) 5000 s^{-1}. The spectrum for (c) has been expanded vertically by a factor of 10 for clarity.

Palmer
Relaxation and Dynamic Processes

Light induced chemical exchange

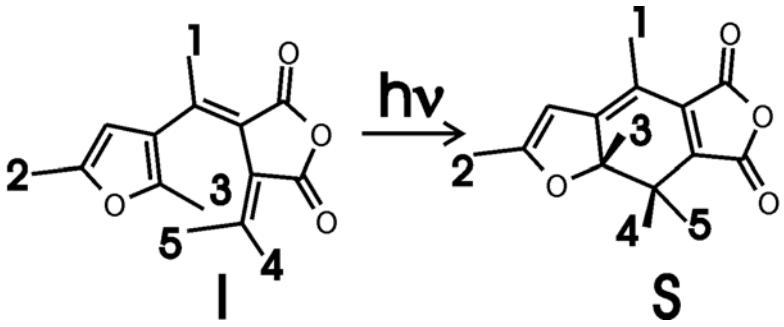

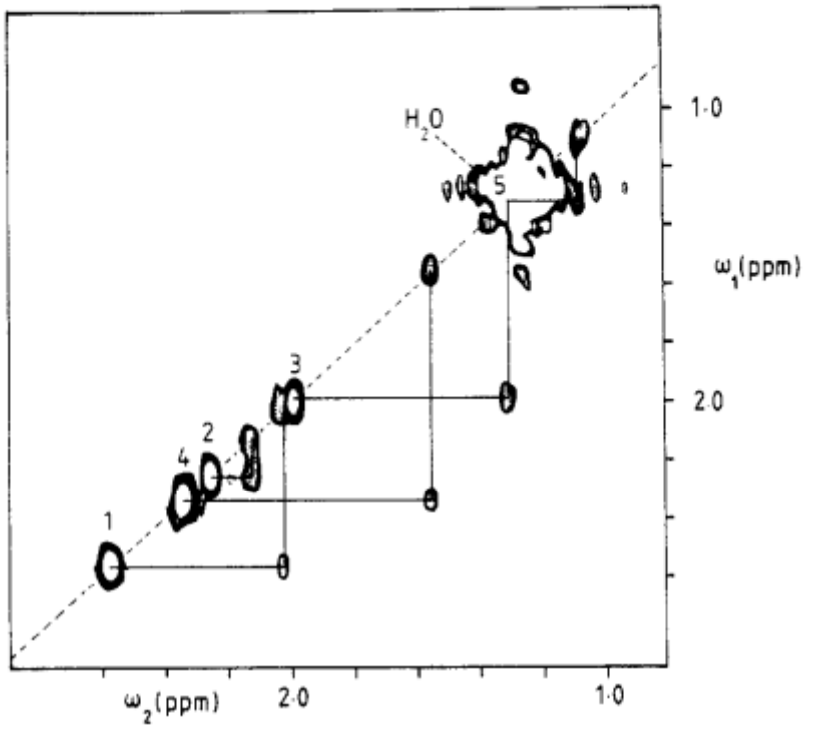

Figure 2. Two-dimensional ^1H NMR spectrum, 360-MHz, of the photoreaction of a 0.2 mM solution of **1** in $CDCl_3$ taken by the coherence transfer sequence of Figure 1a. The methyl group region is shown with numbering for the methyl groups in **1**. Laser pulses, 30 mJ, of 10-ns duration at 351 nm (XeF excimer laser) were used. FID's, 2K, were collected for 64 t_1 values ranging from 10 μs to 40 ms corresponding to a spectral width of 800 Hz; 32 FID's were accumulated for each t_1 value. Before Fourier transformation the data were weighted by a sine bell function in both dimensions; an absolute value mode presentation is shown.

Kemmink et. al. JACS 108 5631-533 (1986)

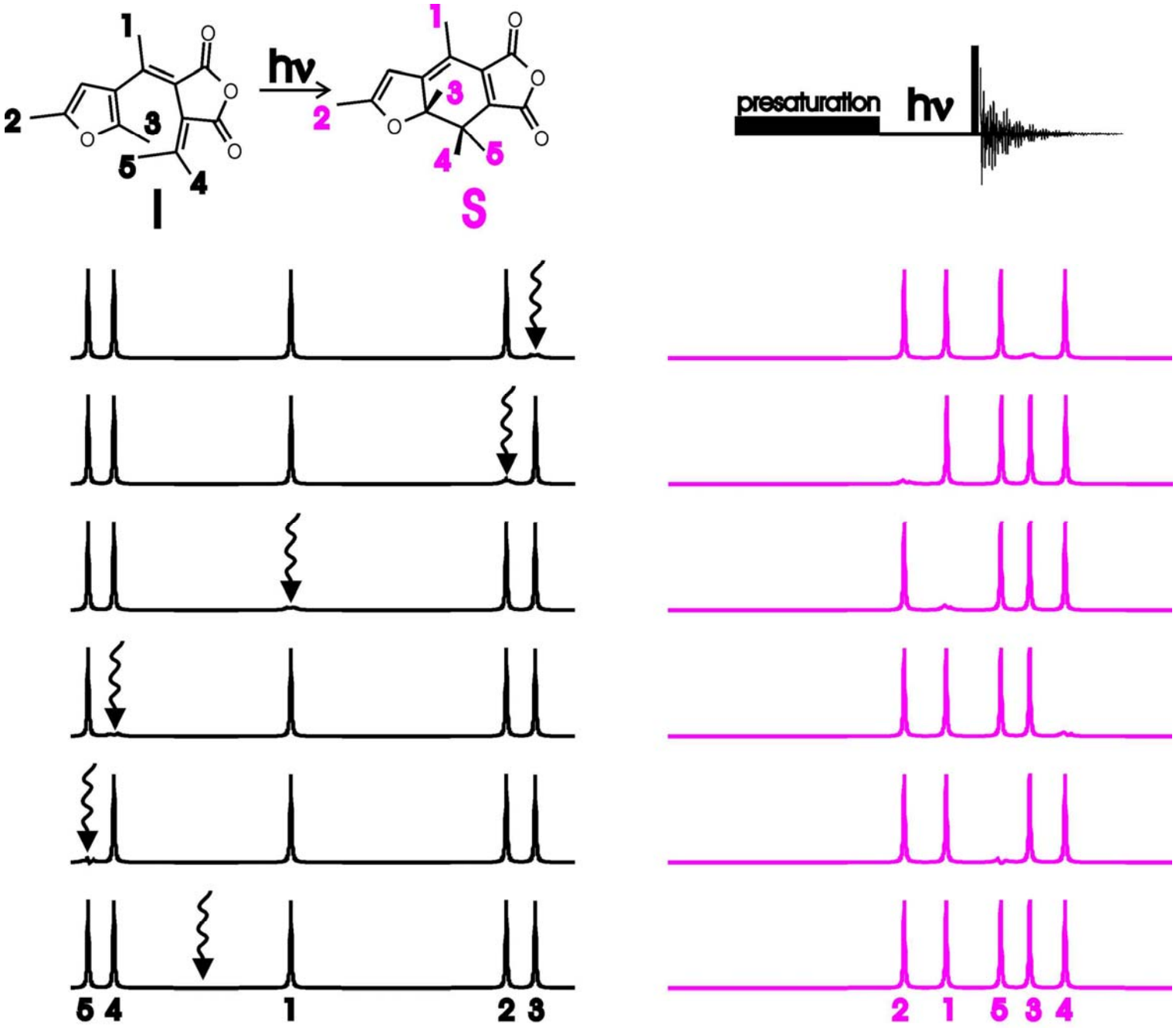
1
2
3
5
4
I
hv
1
2
3
4
5
S
presaturation
hv
5 4
1
2 3
2 1 5 3 4

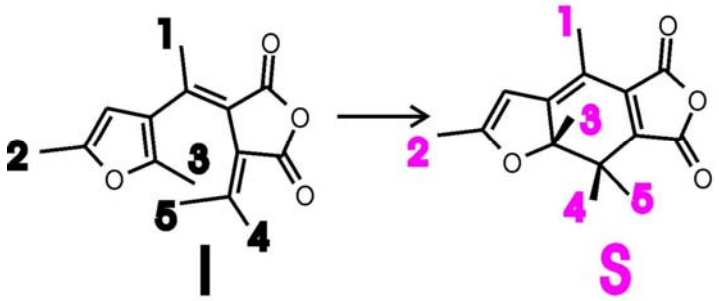
1
2
3
5
4
I
1
2
3
4
5
S


hν

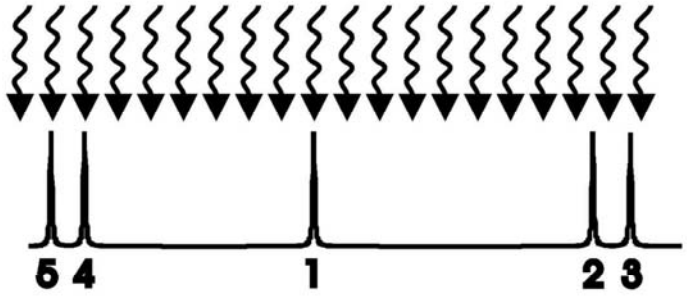
5 4
1
2 3

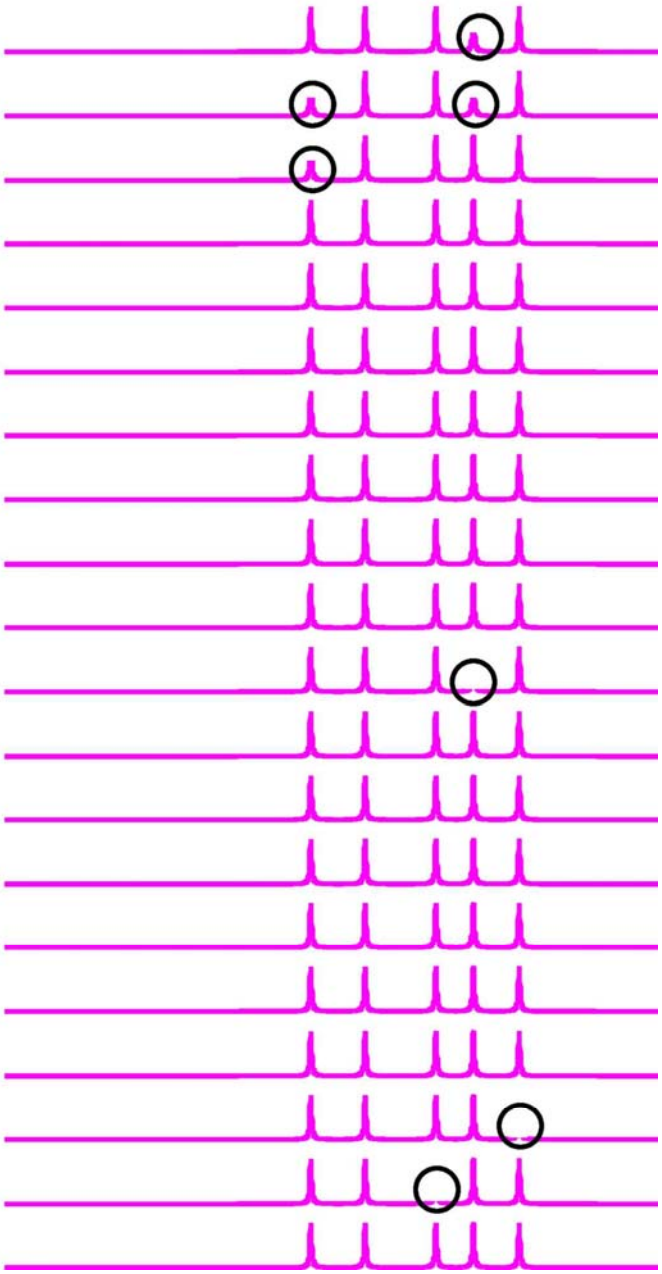

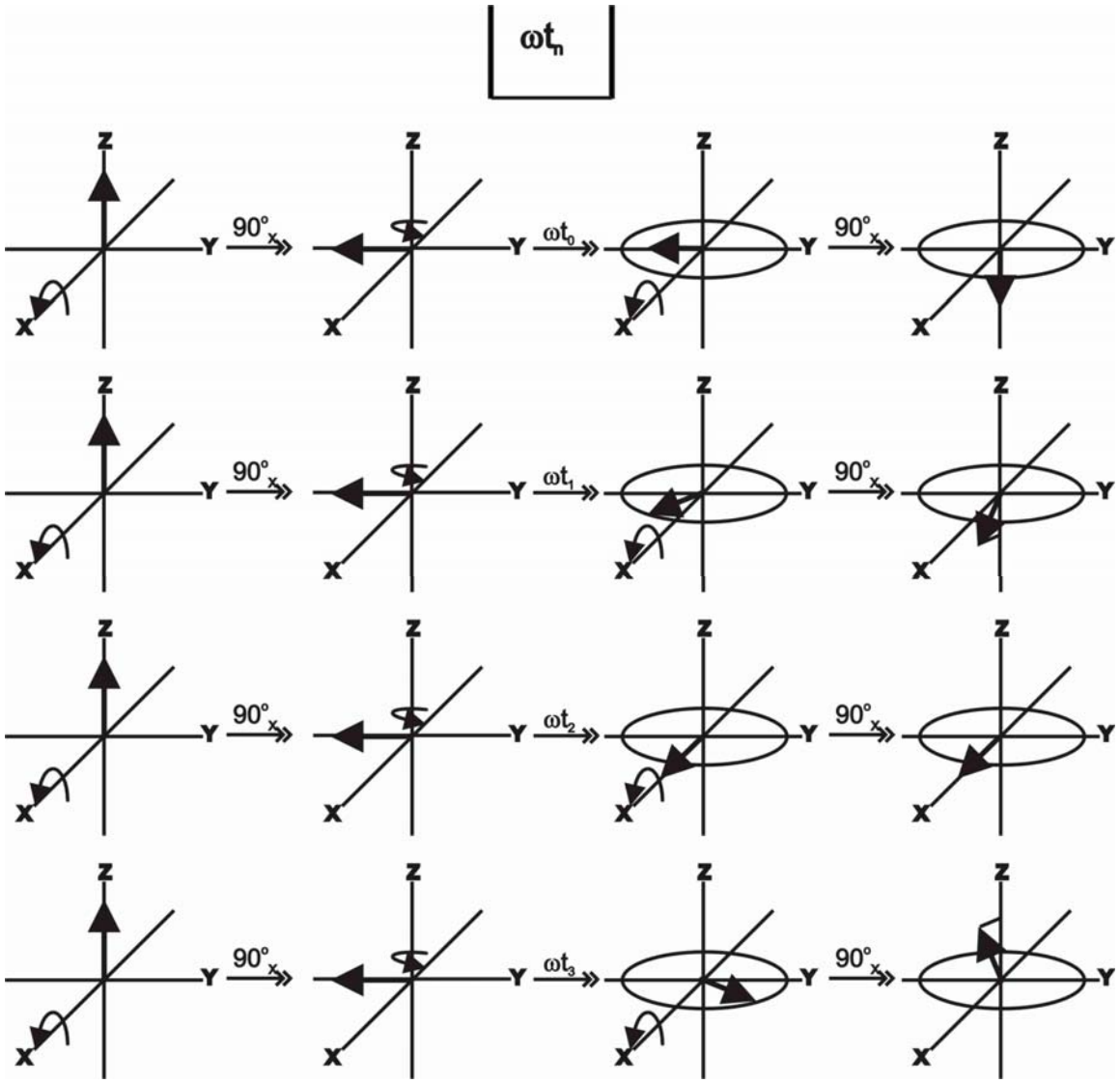
ωt_n
Z
Y
X
90°x
ωt0
ωt1
ωt2
ωt3

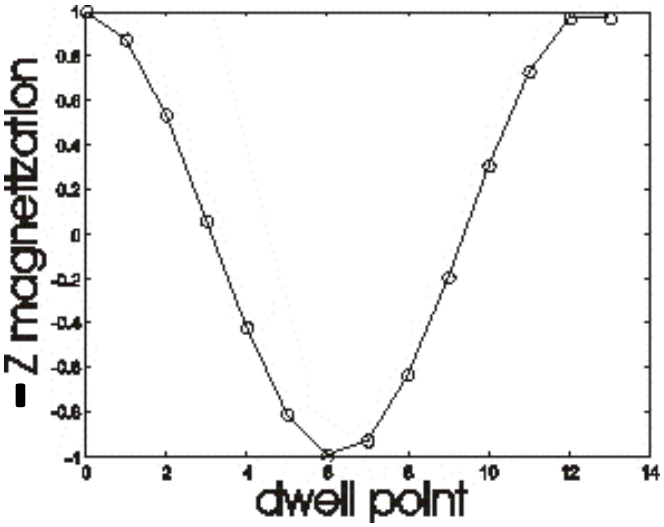
-Z magnetization
dwell point
1
0.8
0.6
0.4
0.2
0
-0.2
-0.4
-0.6
-0.8
-1
0
2
4
6
8
10
12
14

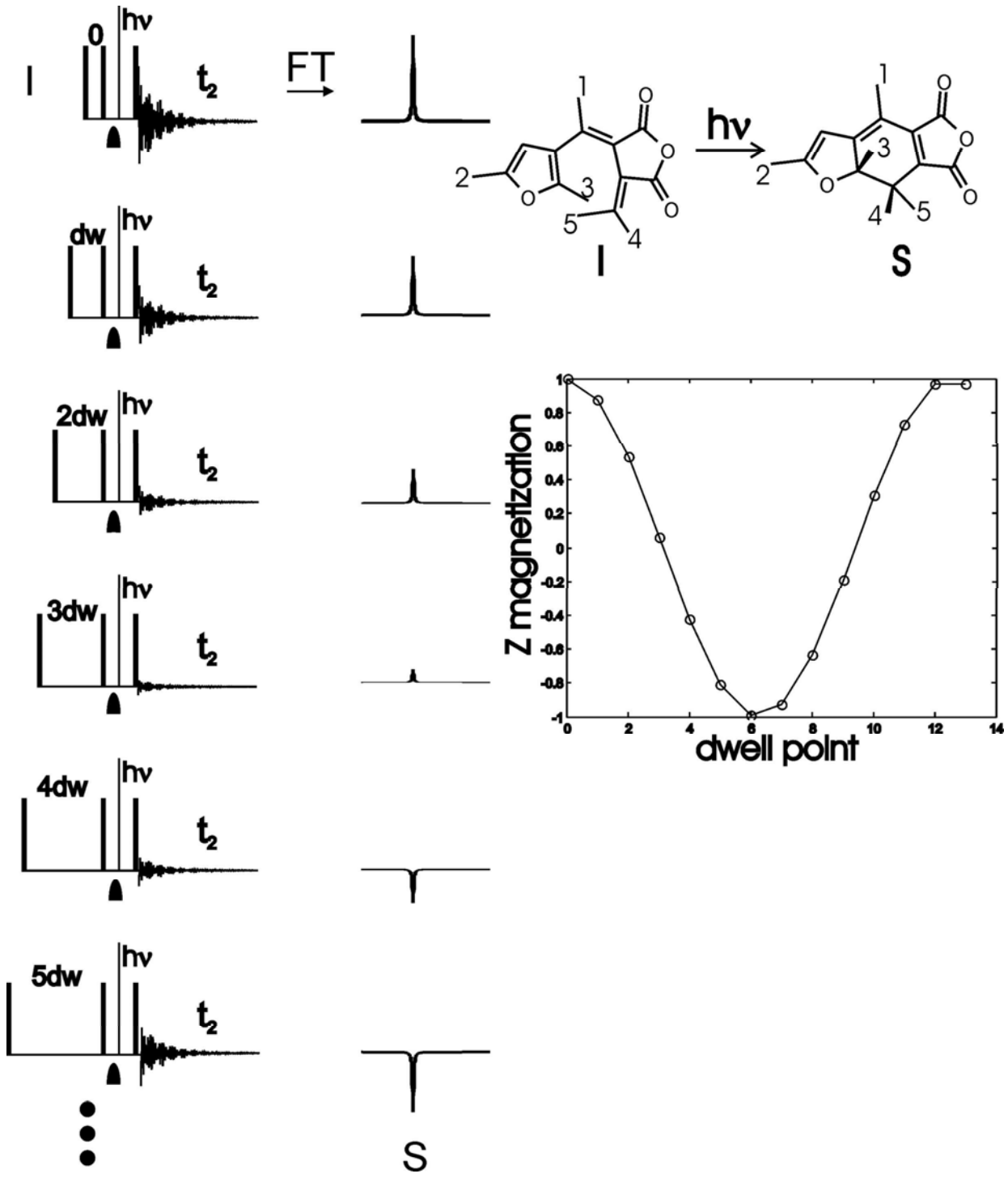
I
0
hν
t2
FT
dw
2dw
3dw
4dw
5dw
S
hν
I
S
Z magnetization
dwell point

2D exchange spectroscopy (EXSY)

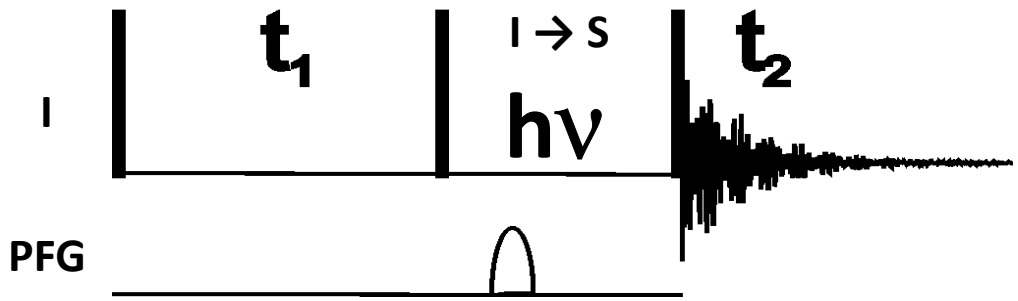

$$I_z \xrightarrow{\frac{\pi}{2}\hat{I}_x} -I_y$$

$$\xrightarrow{\omega_I t_1 \hat{I}_z} -I_y\cos(\omega_I t_1) + I_x \sin(\omega_I t_1)$$

$$\xrightarrow{\frac{\pi}{2}\hat{I}_x} -I_z\cos(\omega_I t_1) + I_x \sin(\omega_I t_1)$$

$$\xrightarrow{\gamma B_G t \hat{I}_z} -I_z\cos(\omega_I t_1) + \left\{ I_x \sin(\omega_I t_1)\cos\left(\gamma B_G t \hat{I}_z\right) - I_y \sin\left(\gamma B_G t \hat{I}_z\right)\right\}$$

$$\xrightarrow{h\nu(light)} -(1-\lambda) I_z\cos(\omega_I t_1) - \lambda S_z \cos(\omega_I t_1)$$

$$\xrightarrow{\frac{\pi}{2}\hat{I}_x} (1-\lambda) I_y\cos(\omega_I t_1) + \lambda S_y \cos(\omega_I t_1)$$

$$\xrightarrow{\omega_I t_2 \hat{I}_z} (1-\lambda)\left[I_y\cos(\omega_I t_2) - I_x \sin(\omega_I t_2)\right]\cos(\omega_I t_1)$$

$$+ \lambda S_y \left[S_y\cos(\omega_S t_2) - S_x \sin(\omega_S t_2)\right]\cos(\omega_I t_1)$$

Transverse magnetization dephased by PFG

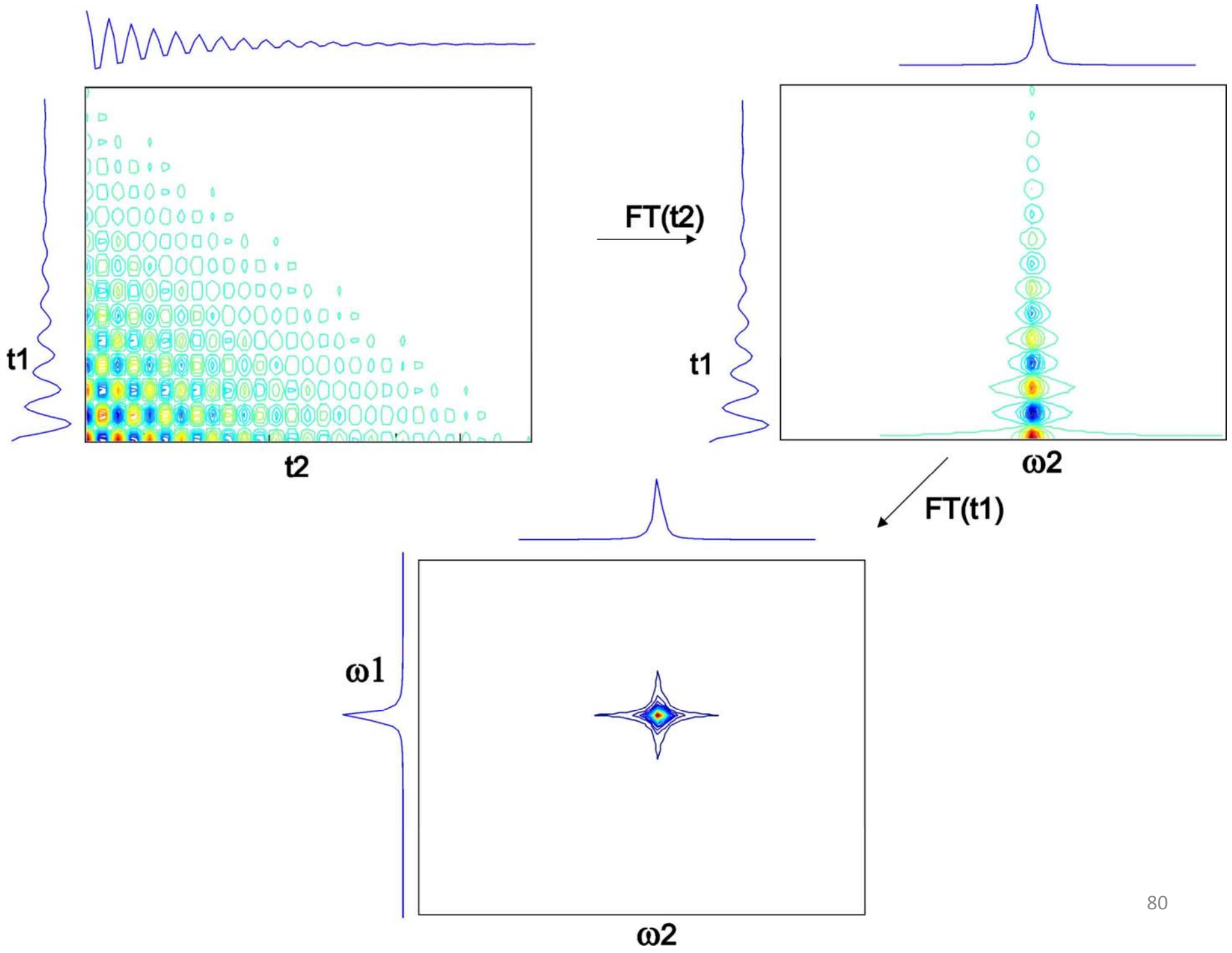
t1
t2
FT(t2)
t1
ω2
FT(t1)
ω1
ω2

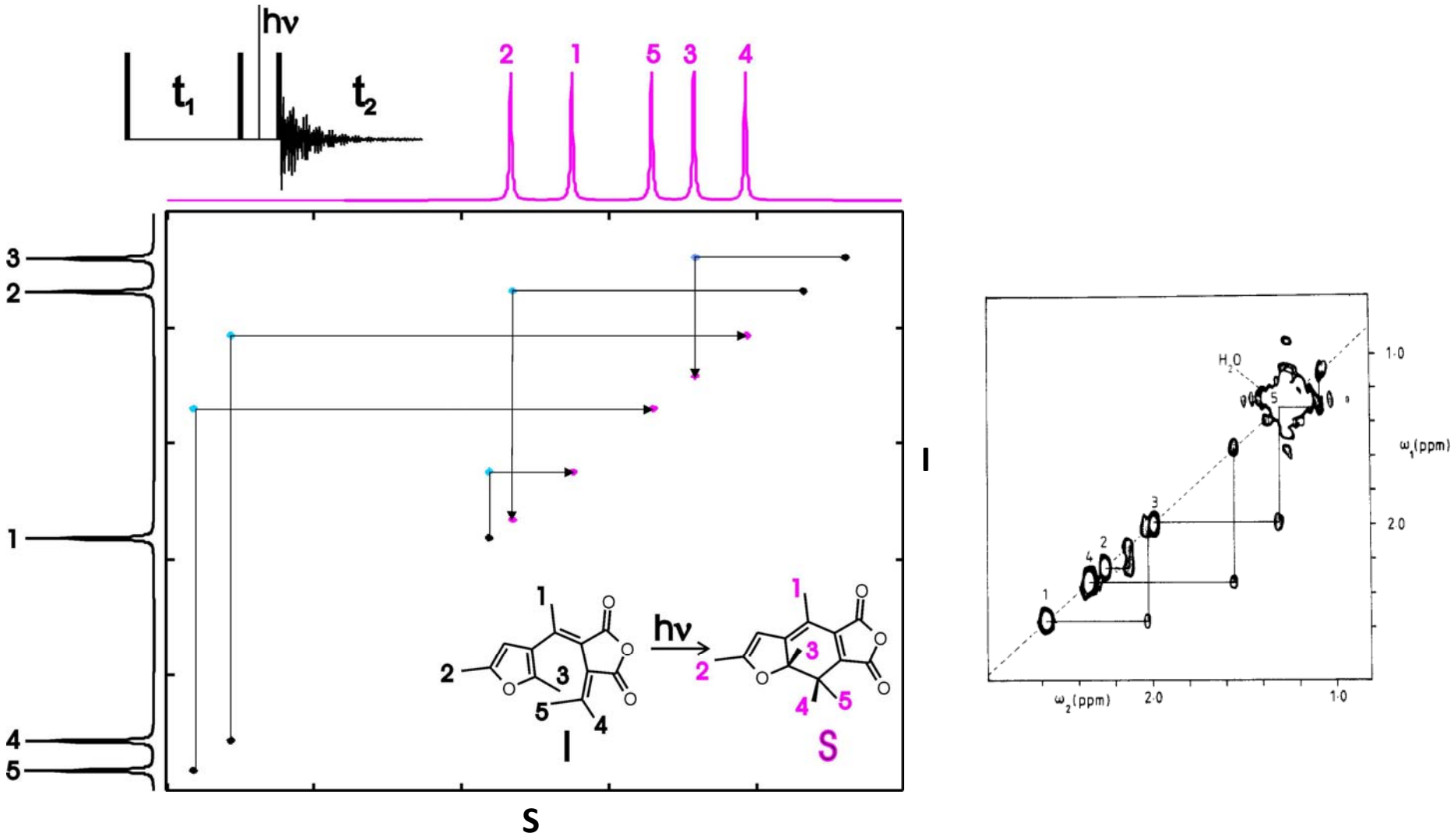
hν
t1
t2
2 1 5 3 4
3
2
1
4
5
I
S
1
2
3
5
4
I
hν
1
2
3
4
5
S
H2O
1·0
2·0
ω1(ppm)
ω2(ppm)
2·0
1·0

Scalar coupling

Scalar coupling and multiplicity

CH

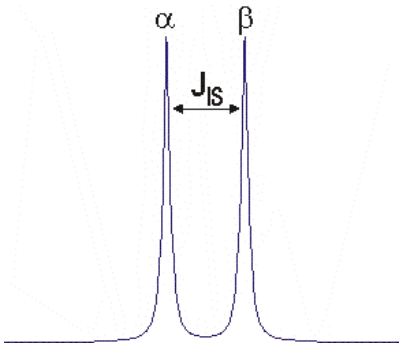

Doublet formed from the coupling of one spin (I) with another spin ½ nucleus (S). The α and β labels refer to the spin states of the coupled nucleus that give rise to different local magnetic fields and thus different frequencies for the coupled spin.

$I - S_\alpha$

$I - S_\beta$

CH_2

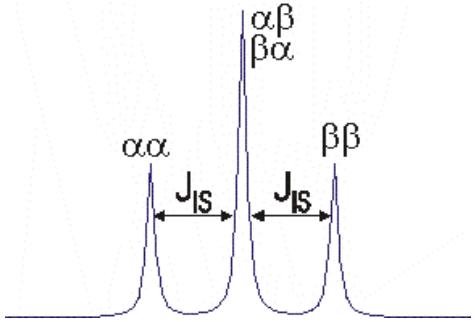

Triplet formed from the coupling of one spin (I) with two other spin ½ nuclei (S,S'). The coupling constants to the two coupled spins are identical. If the coupling constants were not identical then the αβ and βα states would differ in energy giving rise to 4 peaks.

$I - S_\alpha S'_\alpha$

$I - S_\alpha S'_\beta$ & $S_\beta S'_\alpha$

$I - S_\beta S'_\beta$

CH_3

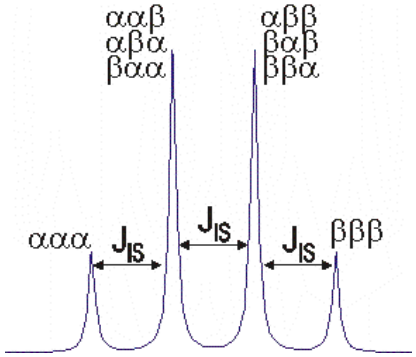

Quartet formed from the coupling of one spin (I) with three other spin ½ nuclei(S,S',S''). The coupling constants to the two coupled spins are identical.

$I - S_\alpha S'_\alpha S'_\alpha$

$I - S_\alpha S'_\alpha S''_\beta + S_\alpha S'_\beta S''_\alpha + S_\beta S'_\alpha S''_\alpha$

$I - S_\beta S'_\beta S''_\alpha + S_\beta S'_\alpha S''_\beta + S_\alpha S'_\beta S''_\beta$

$I - S_\beta S'_\beta S''_\beta$

Isolated spins I and S

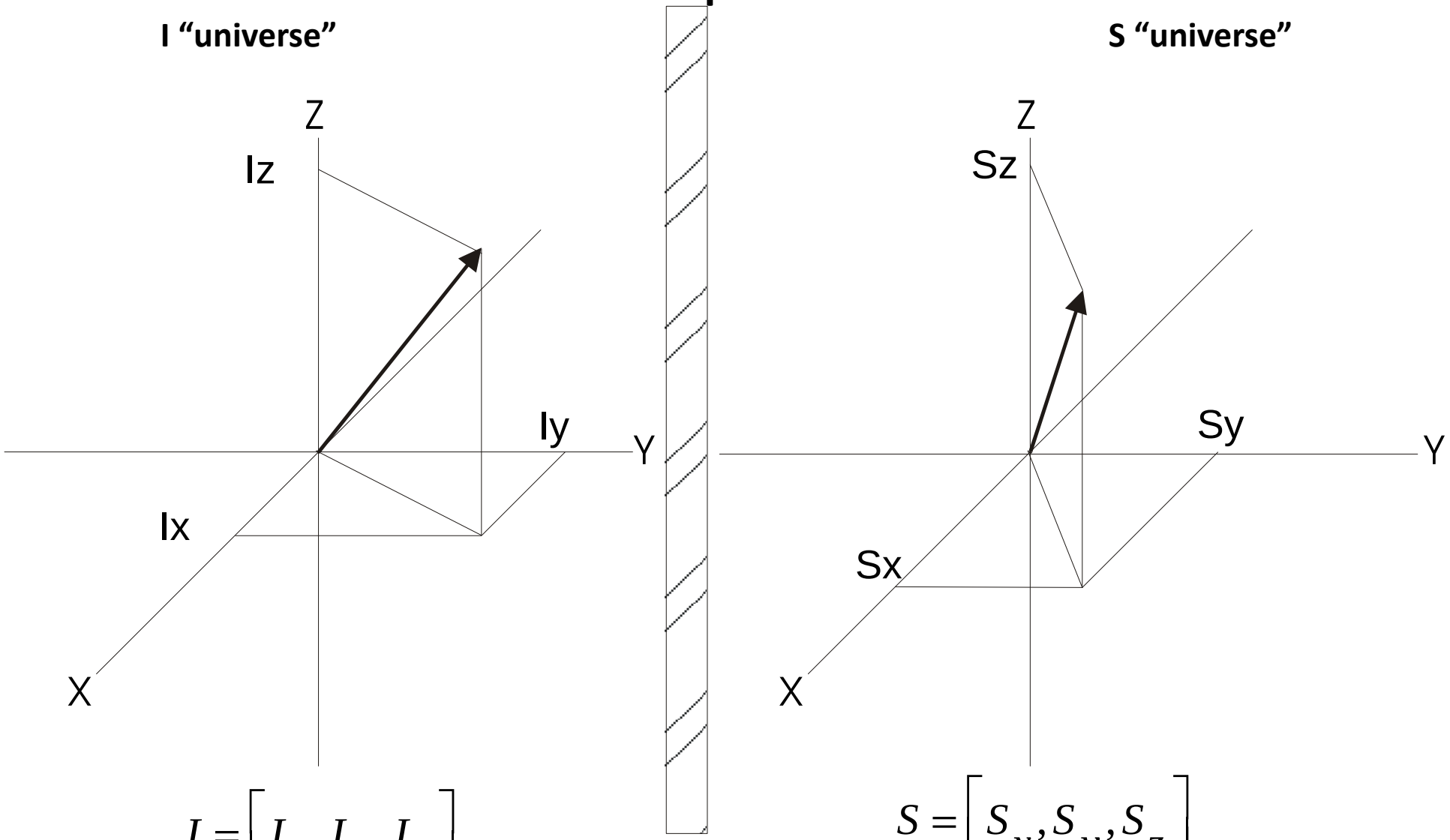

$$I = \left[I_x, I_y, I_z \right]$$

$$S = \left[S_x, S_y, S_z \right]$$

Representation of two isolated spins I and S.
There is no interaction between the spins.

Coupled IS spin system

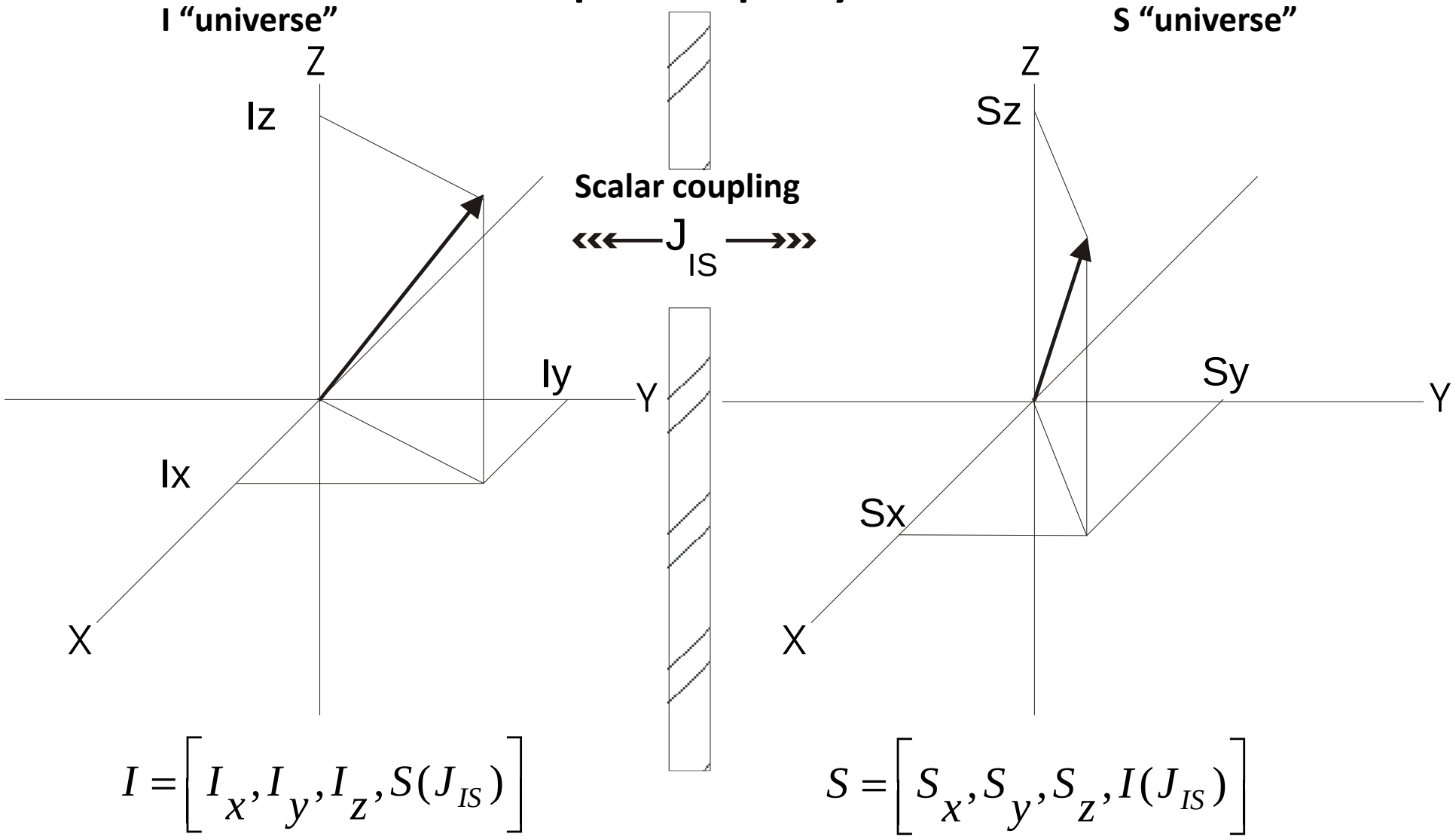

$$I = \left[I_x, I_y, I_z, S(J_{IS}) \right]$$

$$S = \left[S_x, S_y, S_z, I(J_{IS}) \right]$$

Representation of two coupled spins I and S. The hole in the barrier represents the coupling interaction between the spins. Now one spin can "feel" the other spin.

Spins are in communication

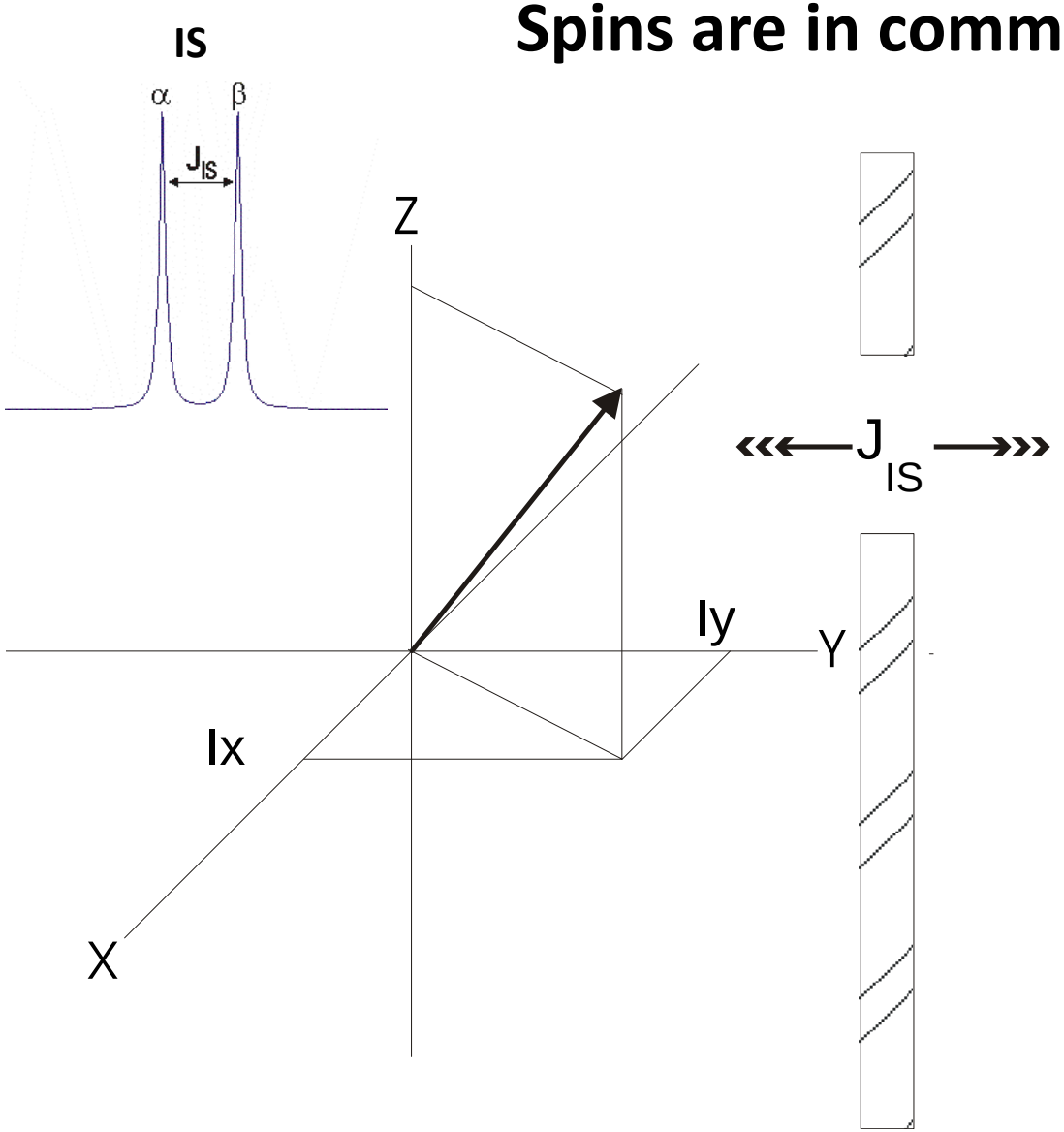

$S_z = S_\alpha - S_\beta$

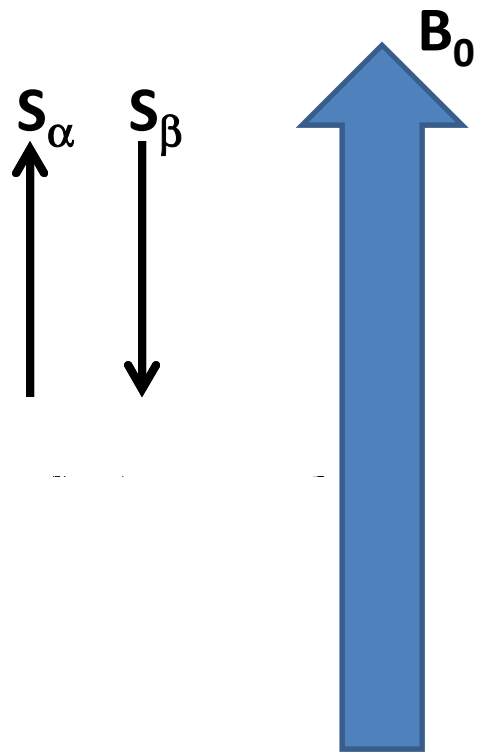

Representation of two coupled spins I and S. Here the S spin is in the S_z state. In individual molecules, the I spin "sees" the S spin in either the α or β state. The frequencies of the I spin different by J_{IS} for those states.

Evolution of coupled spins (observing I only)

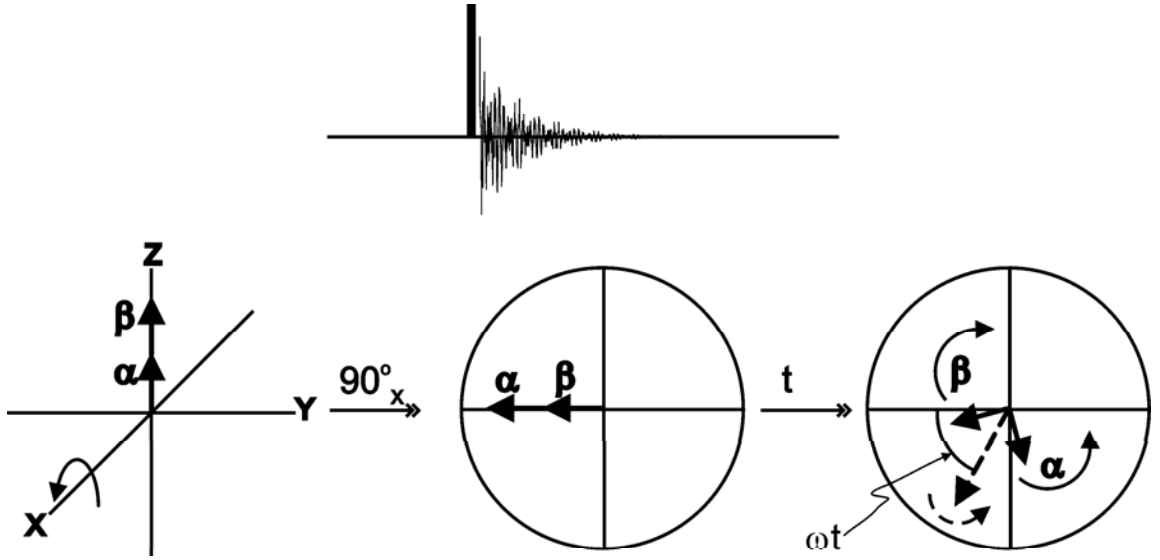

Pulse sequence and vector picture of the evolution of a **IS** coupled spin system. The dashed vector at an angle of ωt in the rightmost panel represents the chemical shift of the spin system in the absence of coupling. The vectors labeled α and β are the two components of the doublet.

$$I_z \xrightarrow{\frac{\pi}{2}\hat{I}_x} \left\{ \xrightarrow{\omega t \hat{I}_z} \xrightarrow{"J"t} \right\}$$

Simultaneous Chemical shift and coupling evolution

Scalar coupling evolution- ω_I=0

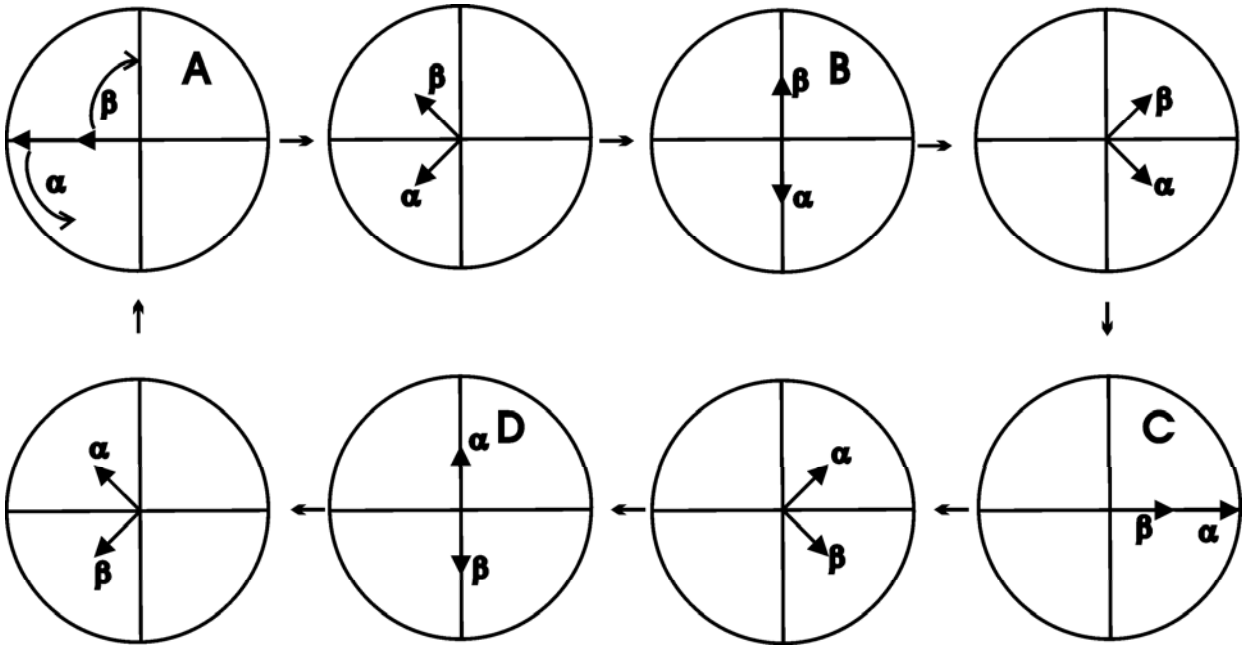

Evolution of a transverse spin I that is coupled to another spin S with states α and β. For clarity, the transverse spin (I) has a chemical shift of 0 Hz.

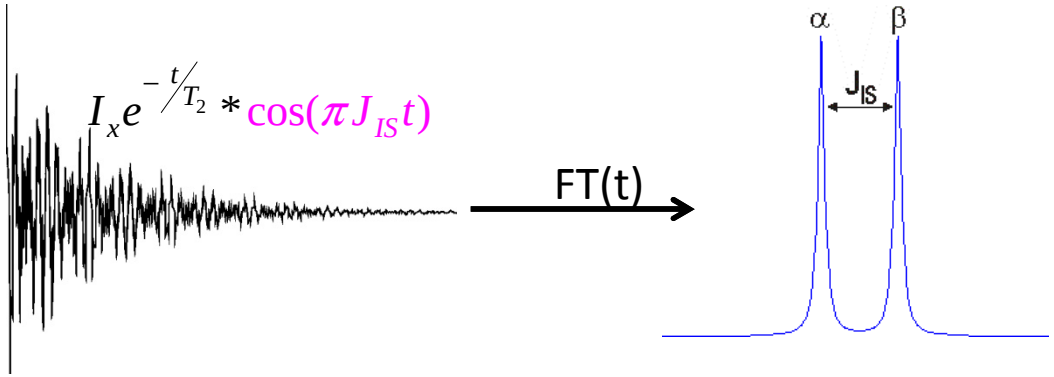

Coupled IS spins, free precession (observe I)

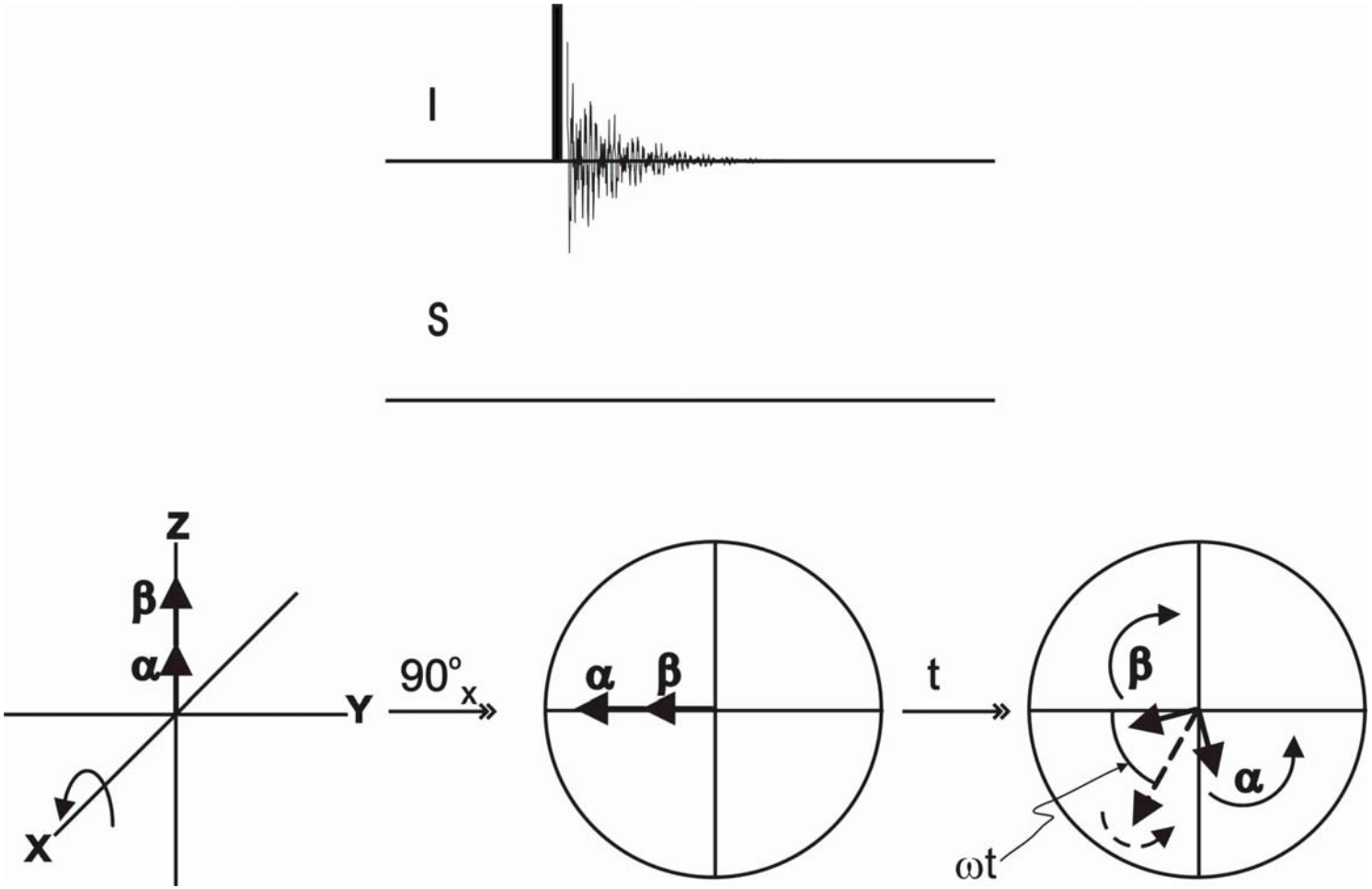

Coupled IS spins, free precession (observe I)

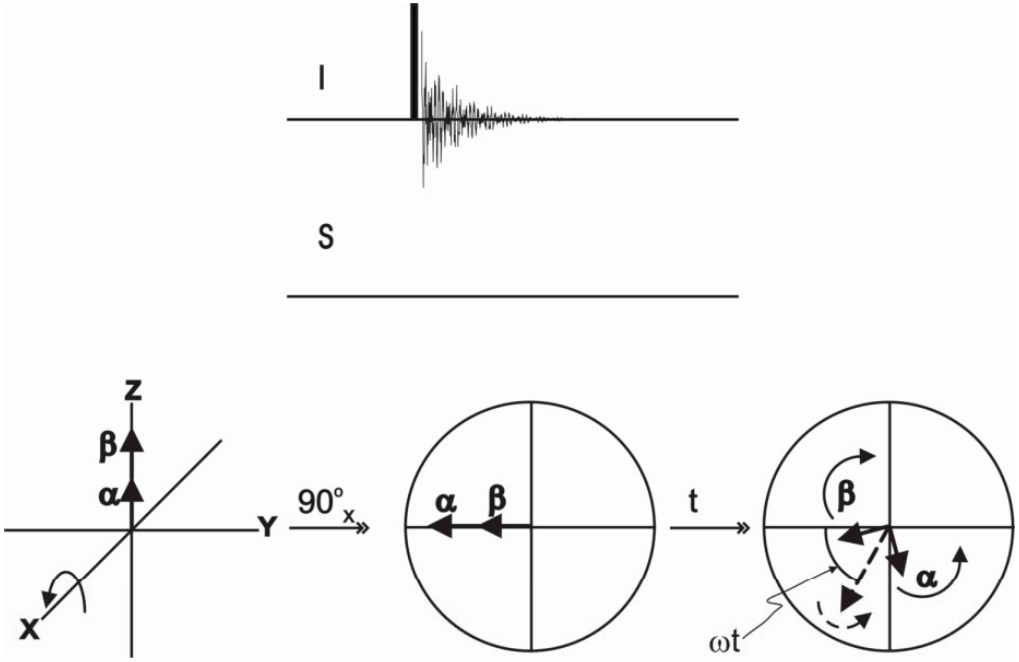

$$
\begin{aligned}
I_z + S_z \xrightarrow{\pi/2\widehat{I_x}} \quad & -I_y + S_z \\
\xrightarrow{\omega_I t \widehat{I_z}} \quad & -I_y\cos(\omega_I t_1) + I_x \sin(\omega_I t_1) + S_z \\
\xrightarrow{\omega_S t \widehat{S_z}} \quad & -I_y\cos(\omega_I t_1) + I_x \sin(\omega_I t_1) + S_z \\
\xrightarrow{\pi J_{IS} t_1 \widehat{I_z S_z}} \quad & \left[-I_y\cos(\pi J_{IS} t_1) + I_x S_z \sin(\pi J_{IS} t_1)\right]\cos(\omega_I t_1) \\
& + \left[I_x\cos(\pi J_{IS} t_1) + I_y S_z \sin(\pi J_{IS} t_1)\right]\sin(\omega_I t_1) + S_z
\end{aligned}
$$

Coupled IS spins, free precession (observe I)

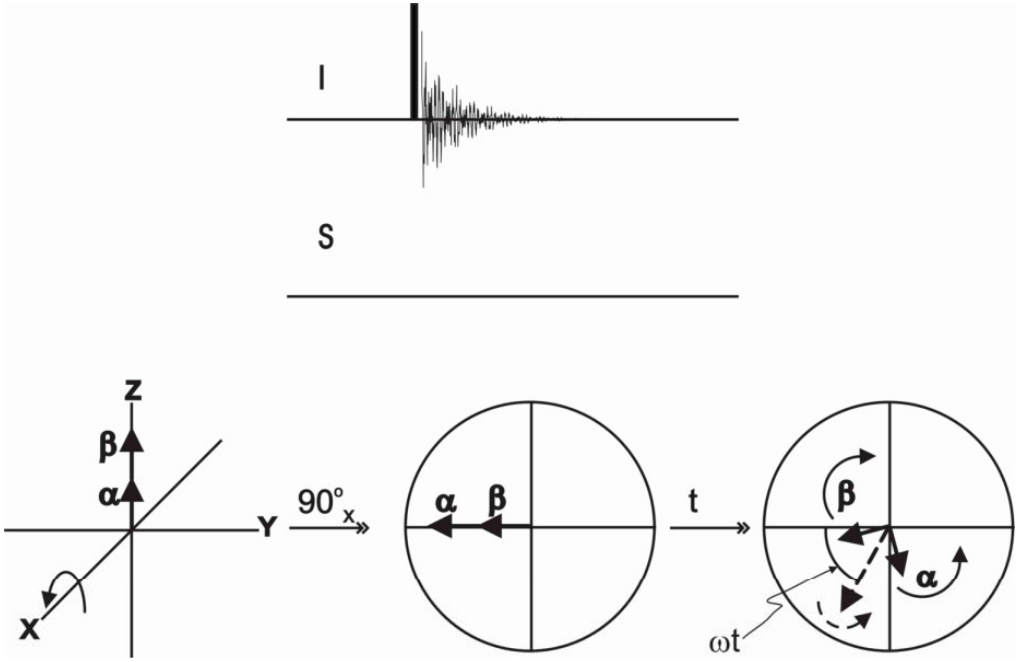

$\delta_I <> 0$

$\delta_S <> 0$

$J_{IS} <> 0$

$$I_z + S_z \xrightarrow{\pi/2\widehat{I_x}} -I_y + S_z$$

$$\xrightarrow{\omega_I t\widehat{I_z}} -I_y\cos(\omega_I t_1) + I_x\sin(\omega_I t_1) + S_z$$

$$\xrightarrow{\omega_S t\widehat{S_z}} -I_y\cos(\omega_I t_1) + I_x\sin(\omega_I t_1) + S_z$$

$$\xrightarrow{\pi J_{IS} t_1 \widehat{I_z S_z}} \left[-I_y\cos(\pi J_{IS} t_1) + I_x S_z \sin(\pi J_{IS} t_1)\right]\cos(\omega_I t_1)$$

$$+\left[I_x\cos(\pi J_{IS} t_1) + I_y S_z \sin(\pi J_{IS} t_1)\right]\sin(\omega_I t_1) + S_z$$

Evolution periods

Isolated

$\delta_I = 0$

$\xrightarrow{\pi \hat{I}_x}$

Coupled

$\delta_I <> 0$

$\delta_S <> 0$

$J_{IS} <> 0$

$\xrightarrow{\{\text{free precession}\}}$

$\xrightarrow{\omega t \hat{I}_z} \xrightarrow{\omega t \hat{S}_z} \xrightarrow{\pi J_{IS} t \hat{I}_z \hat{S}_z}$

$\delta_I = 0$

$\delta_S <> 0$

$J_{IS} = 0$

$\xrightarrow{\{\pi I_x \text{ spin echo}\}}$

$\xrightarrow{\pi I_x} \xrightarrow{2\omega_S t}$

$\delta_I <> 0$

$\delta_S = 0$

$J_{IS} = 0$

$\xrightarrow{\{\pi S_x \text{ spin echo}\}}$

$\xrightarrow{\pi S_x} \xrightarrow{2\omega_I \hat{I}_z}$

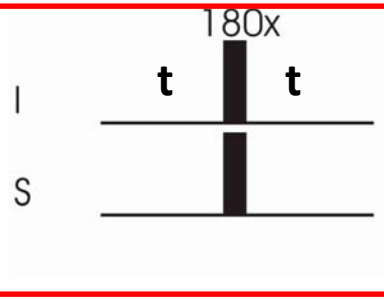

$\delta_I = 0$

$\delta_S = 0$

$J_{IS} <> 0$

$\xrightarrow{\{\pi I_x, S_x \text{ spin echo}\}}$

$\xrightarrow[\pi \hat{S}_x]{\pi \hat{I}_x}$

Iπ spin echo, coupled IS

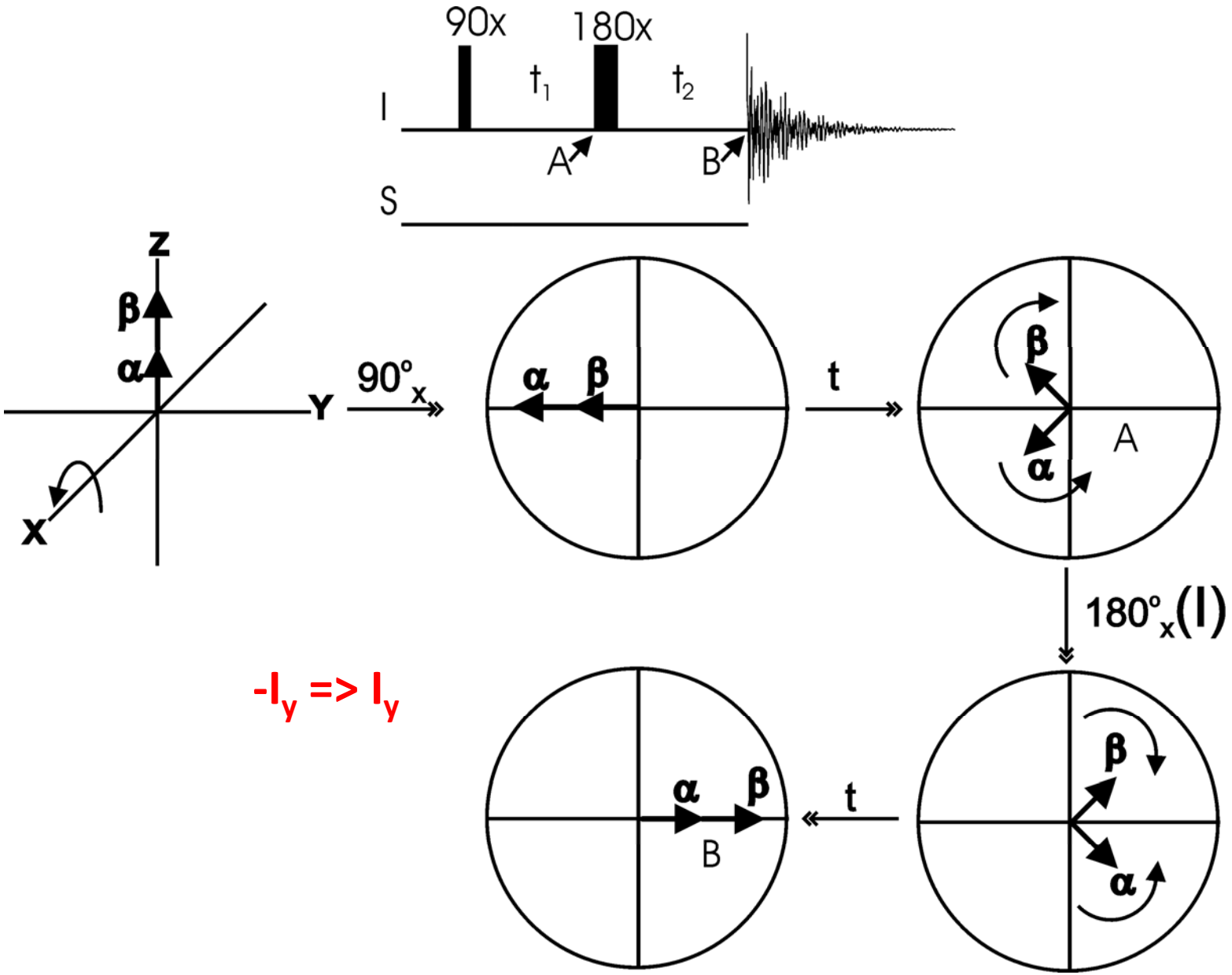

Iπ spin echo, coupled IS

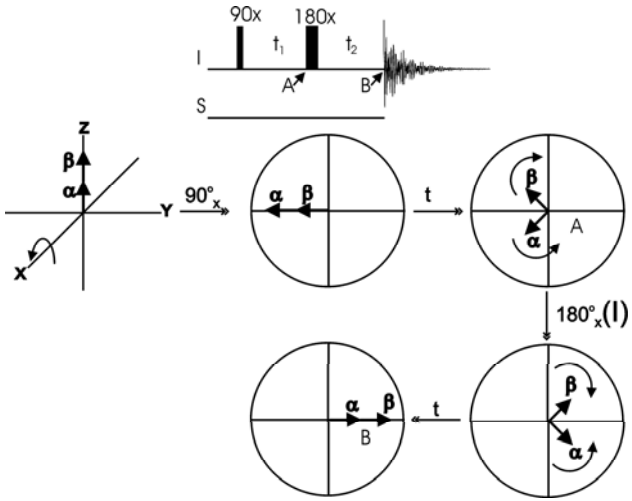

$$I_z \xrightarrow{\pi \hat{I}_x}$$

$$\left[I_y\cos(\pi J_{IS}t_1)+I_xS_z\sin(\pi J_{IS}t_1)\right]\cos(\omega_I t_1)$$
$$+\left[I_x\cos(\pi J_{IS}t_1)-I_yS_z\sin(\pi J_{IS}t_1)\right]\sin(\omega_I t_1)+S_z$$

$$\xrightarrow{\omega_I t_2 \hat{I}_z}$$

$$\left[I_y\cos(\omega_I t_2)-I_x\sin(\omega_I t_2)\right]\cos(\pi J_{IS}t_1)\cos(\omega_I t_1)$$
$$+\left[I_xS_z\cos(\omega_I t_2)-I_yS_z\sin(\omega_I t_2)\right]\sin(\pi J_{IS}t_1)\cos(\omega_I t_1)$$
$$+\left[I_x\cos(\omega_I t_2)+I_y\sin(\omega_I t_2)\right]\cos(\pi J_{IS}t_1)\sin(\omega_I t_1)$$
$$+\left[-I_yS_z\cos(\omega_I t_2)+I_xS_z\sin(\omega_I t_2)\right]\sin(\pi J_{IS}t_1)\sin(\omega_I t_1)+S_z$$

$$\xrightarrow{\pi J_{IS}t_2 \widehat{I_zS_z}}$$

$$\left[I_y\cos(\pi J_{IS}t_2)-I_xS_z\sin(\pi J_{IS}t_1)\right]\cos(\pi J_{IS}t_1)\cos(\omega_I t_1)\cos(\omega_I t_2)$$
$$+\left[-I_x\cos(\pi J_{IS}t_2)+I_yS_z\sin(\pi J_{IS}t_2)\right]\cos(\pi J_{IS}t_1)\cos(\omega_I t_1)\sin(\omega_I t_2)$$
$$+\left[I_xS_z\cos(\pi J_{IS}t_2)+I_y\sin(\pi J_{IS}t_2)\right]\sin(\pi J_{IS}t_1)\cos(\omega_I t_1)\cos(\omega_I t_2)$$
$$+\left[-I_yS_z\cos(\pi J_{IS}t_2)+I_x\sin(\pi J_{IS}t_2)\right]\sin(\pi J_{IS}t_1)\cos(\omega_I t_1)\sin(\omega_I t_2)$$
$$+\left[I_x\cos(\pi J_{IS}t_2)+I_yS_z\sin(\pi J_{IS}t_2)\right]\cos(\pi J_{IS}t_1)\sin(\omega_I t_1)\cos(\omega_I t_2)$$
$$+\left[I_y\cos(\pi J_{IS}t_2)-I_xS_z\sin(\pi J_{IS}t_2)\right]\cos(\pi J_{IS}t_1)\sin(\omega_I t_1)\sin(\omega_I t_2)$$
$$+\left[-I_yS_z\cos(\pi J_{IS}t_2)+I_x\sin(\pi J_{IS}t_2)\right]\sin(\pi J_{IS}t_1)\sin(\omega_I t_1)\cos(\omega_I t_2)$$
$$+\left[I_xS_z\cos(\pi J_{IS}t_2)+I_y\sin(\pi J_{IS}t_2)\right]\sin(\pi J_{IS}t_1)\sin(\omega_I t_1)\sin(\omega_I t_2)$$
$$+S_z$$

$$I_y[c_J^2c_\omega^2+s_J^2c_\omega^2+c_J^2s_\omega^2+s_J^2s_\omega^2]$$
$$=I_y[(c_J^2+s_J^2)c_\omega^2+(c_J^2+s_J^2)s_\omega^2] \qquad = I_y + S_z$$
$$=I_y[(1)c_\omega^2+(1)s_\omega^2]=I_y$$

Again, there must be a simpler way!

Spin echo editing

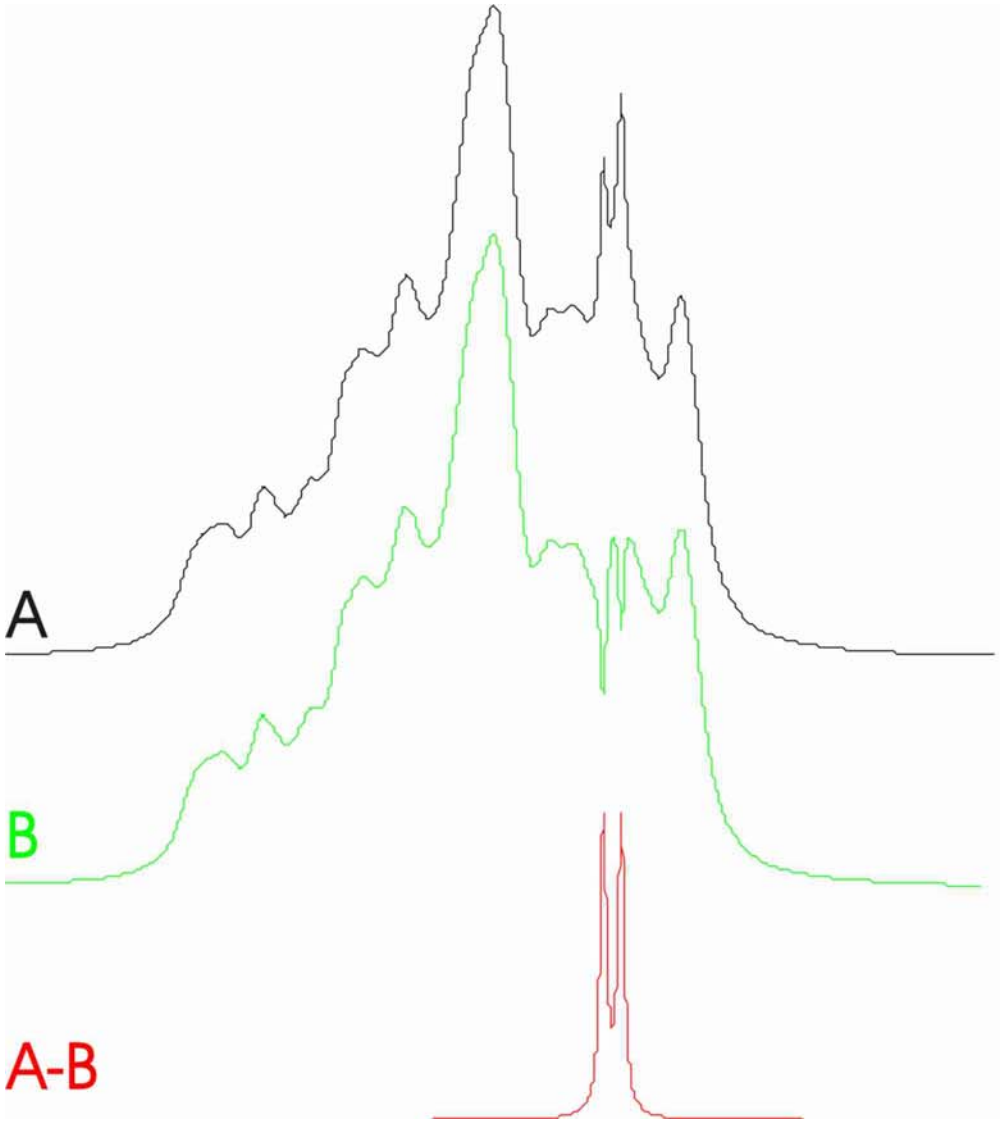

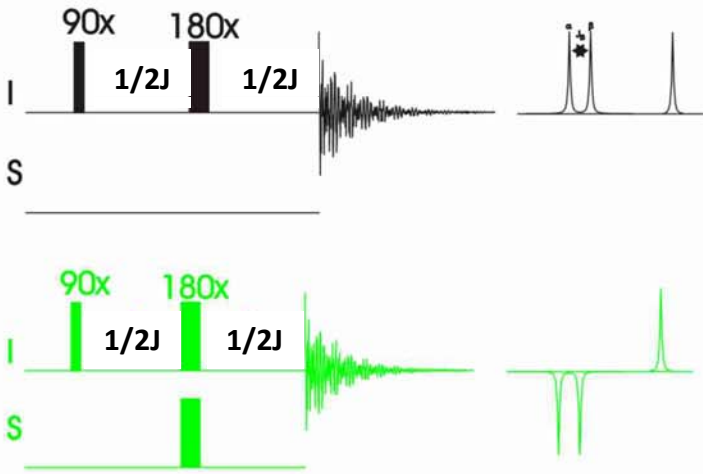

Sπ spin echo, coupled IS

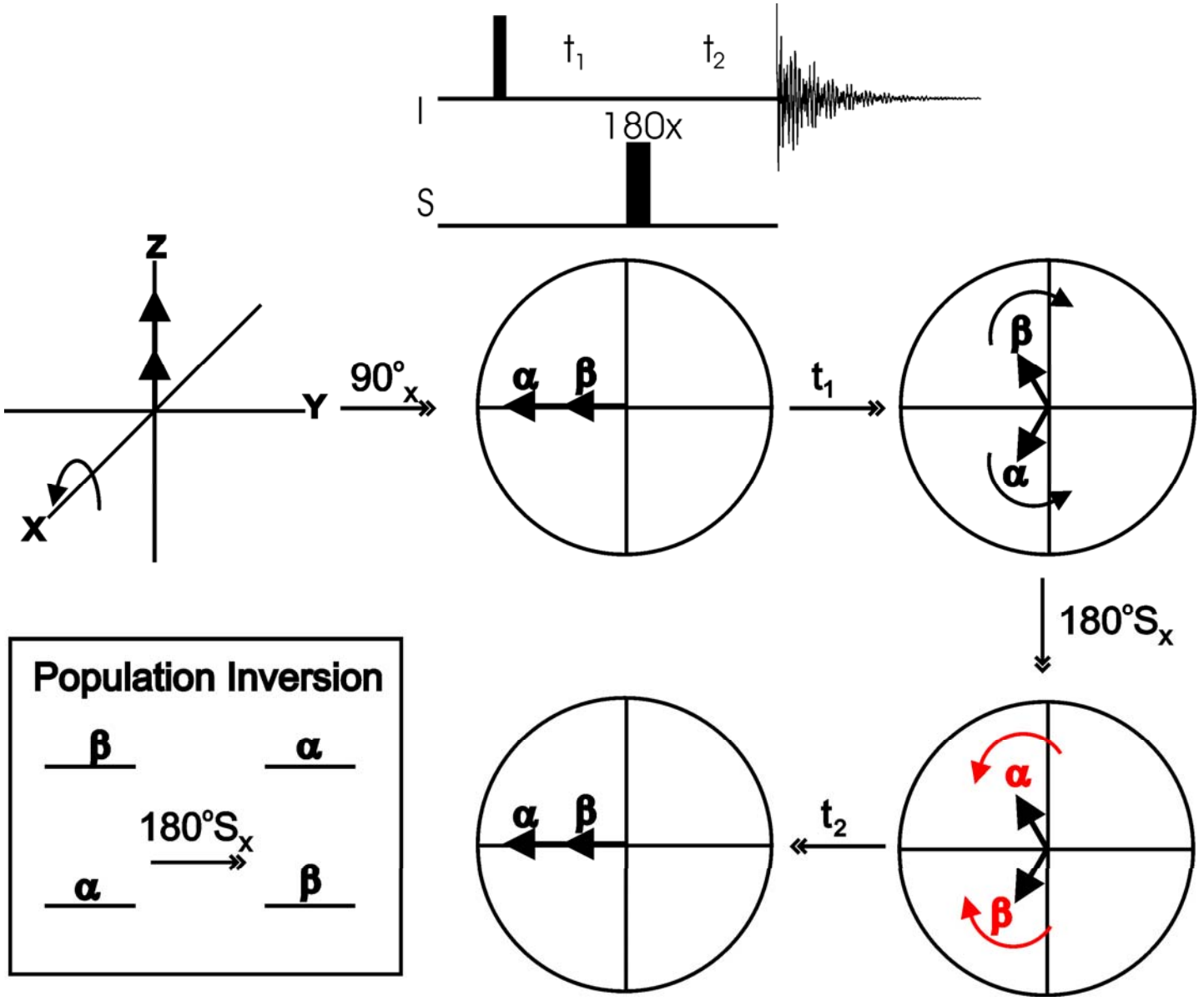

Decoupling

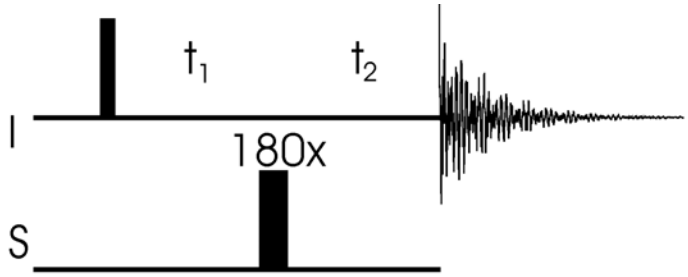

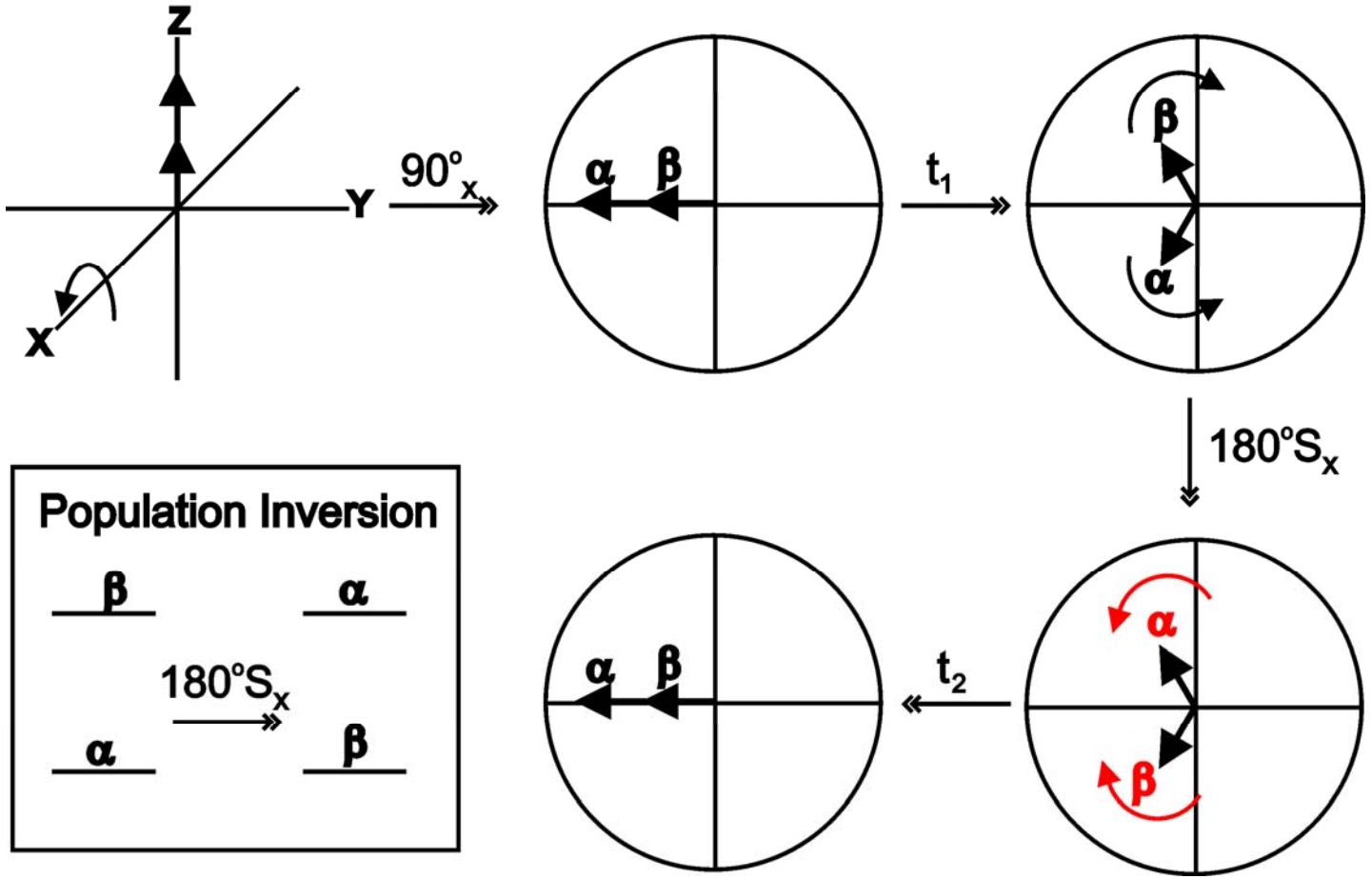

$\delta_I <> 0$

$\delta_S = 0$

$J_{IS} = 0$

Population Inversion

β α

180°S_x

α β

IπSπ spin echo, coupled IS (with I chemical shift)

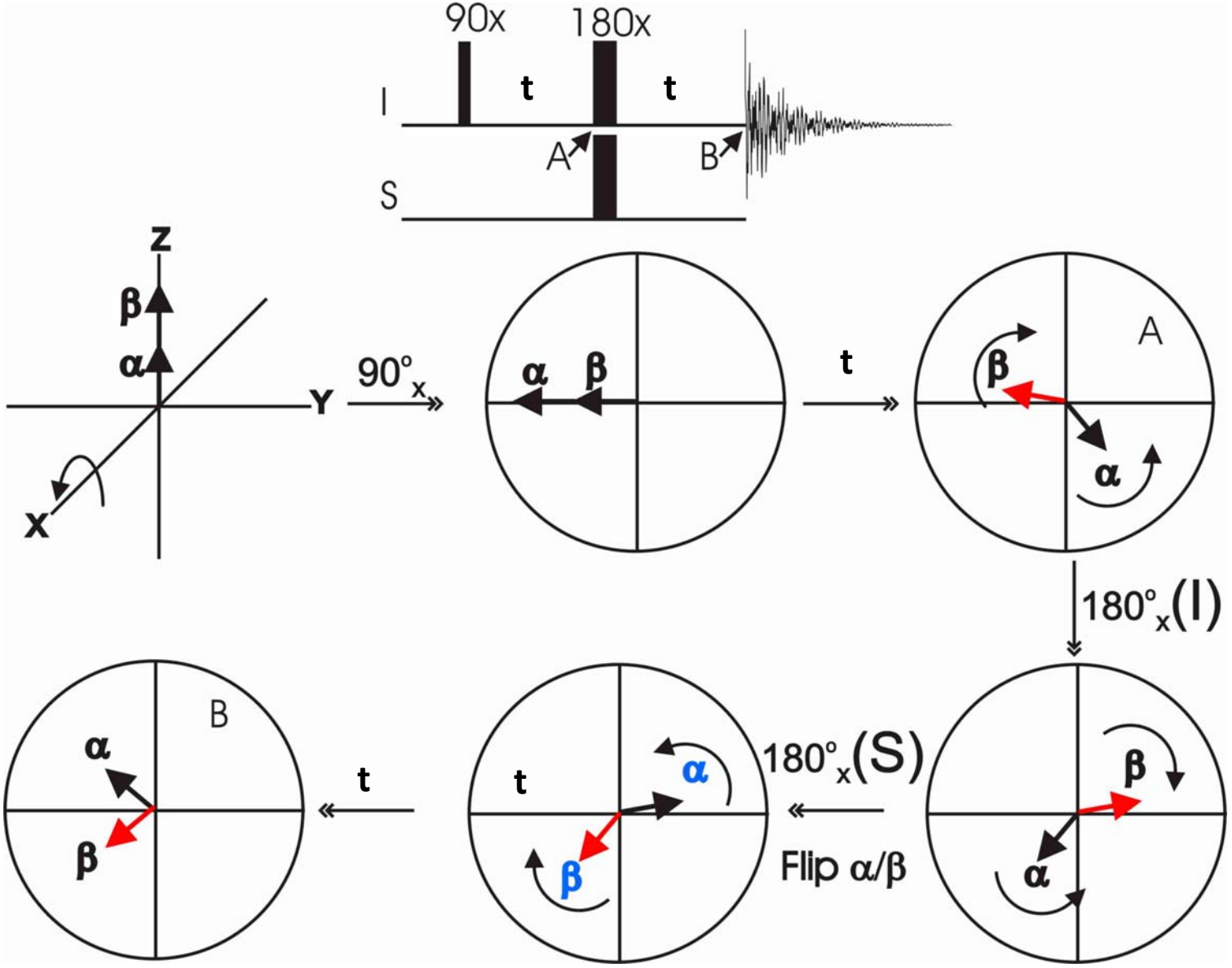

Semi-classical description of INEPT

transfer of coherence between coupled spins

H chemical shift = 0
(180 refocuses H chemical shift)

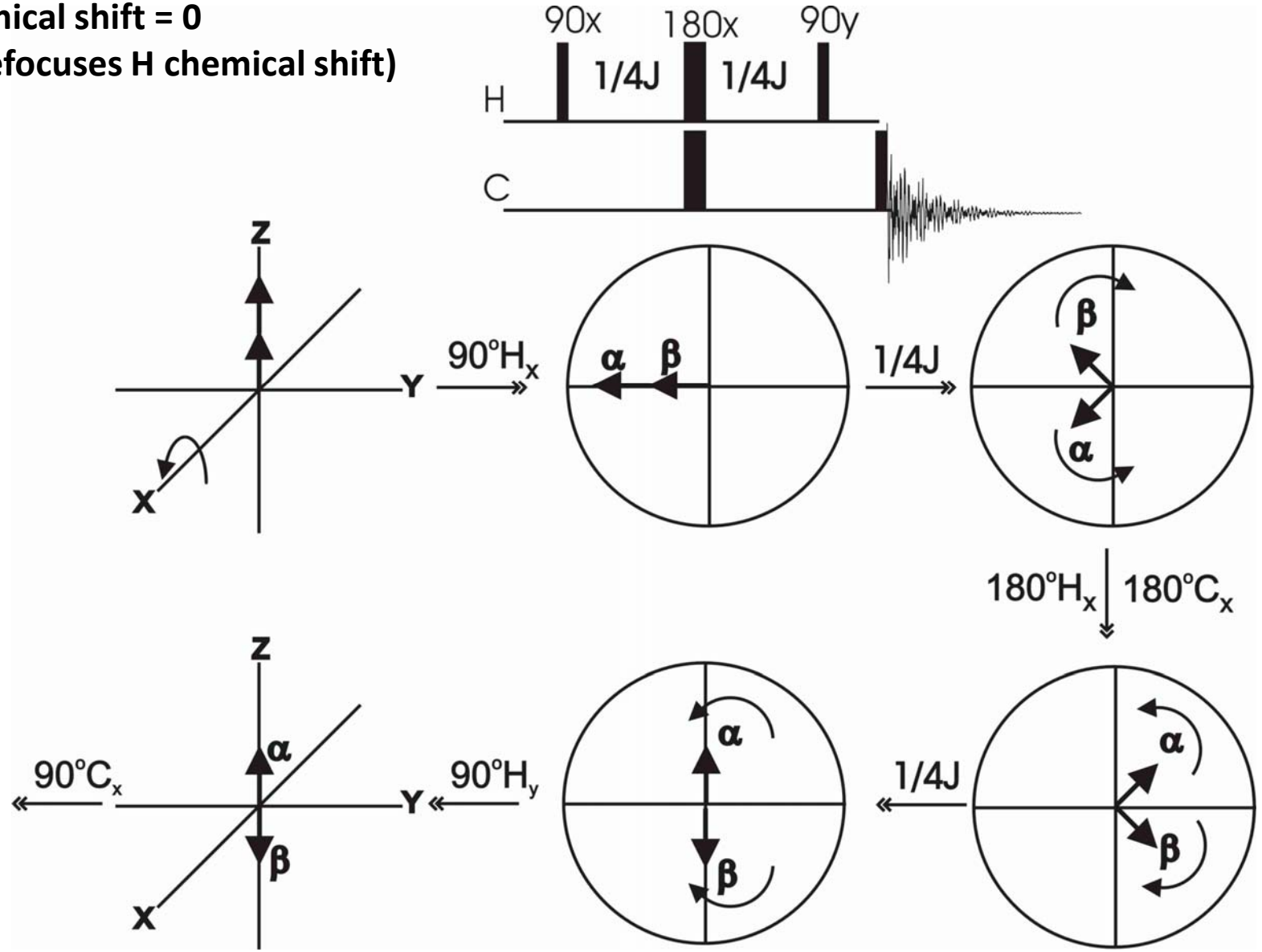

Semi-classical description of INEPT

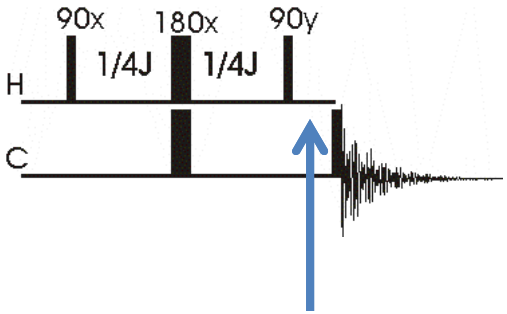

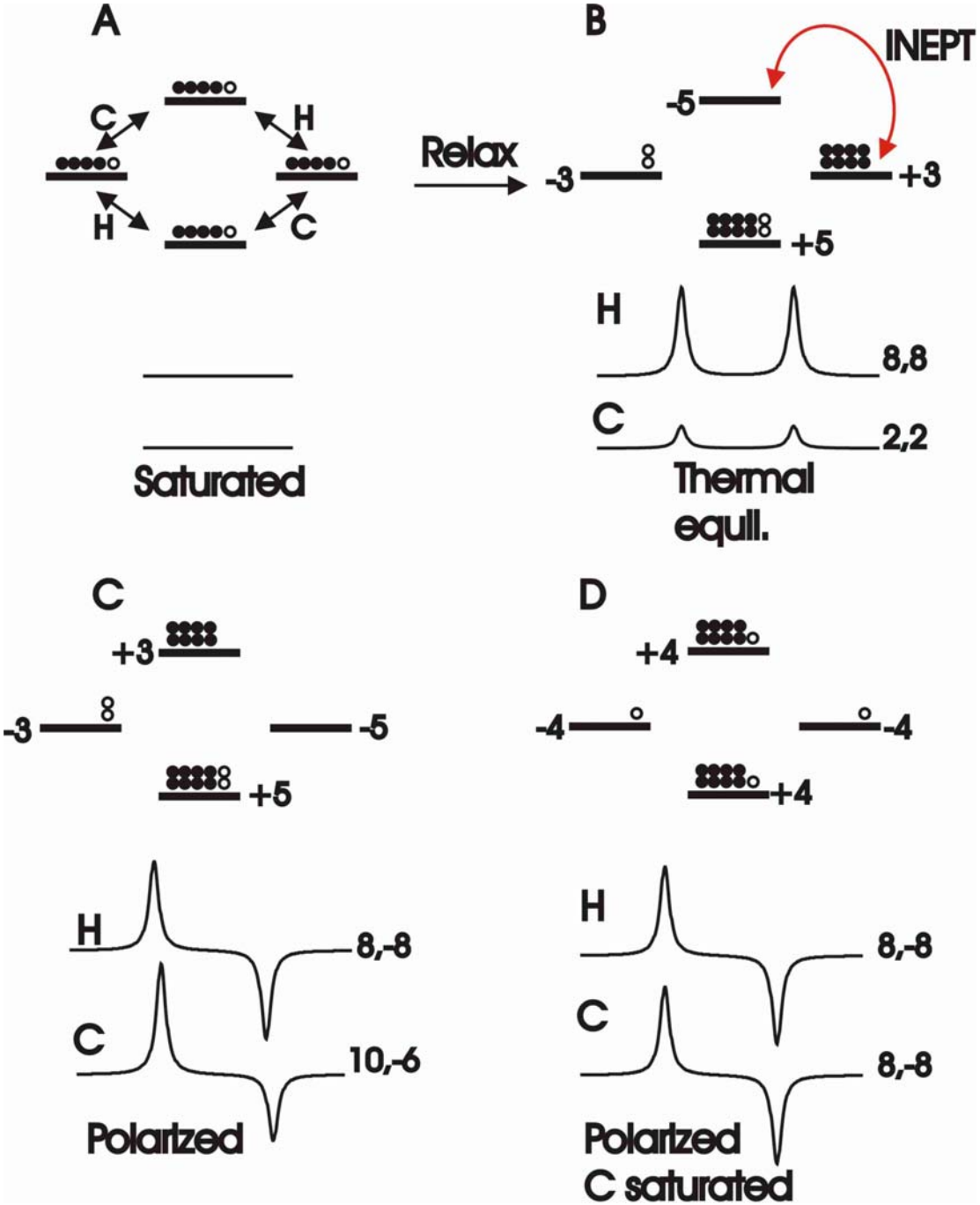

Relative sensitivity of S detection (C) versus S detection with I polarization

Coherence transfer

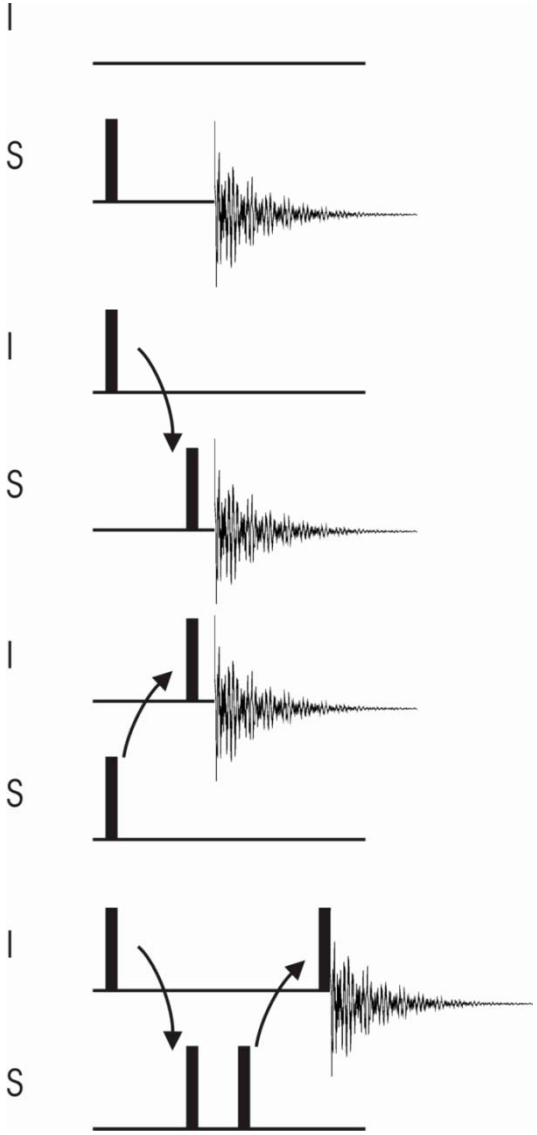

$$\gamma_S^{5/2}\left(1-e^{-T_R/T_1^S}\right)$$

$$\gamma_I\gamma_S^{3/2}\left(1-e^{-T_R/T_1^I}\right)$$

$$\gamma_I^{3/2}\gamma_S\left(1-e^{-T_R/T_1^S}\right)$$

$$\gamma_I^{5/2}\left(1-e^{-T_R/T_1^I}\right)$$

$$\frac{\gamma_H}{\gamma_C} = 4$$

$$\frac{\gamma_H}{\gamma_N} = 10$$

2D HSQC (Heteronuclear single quantum correlation)

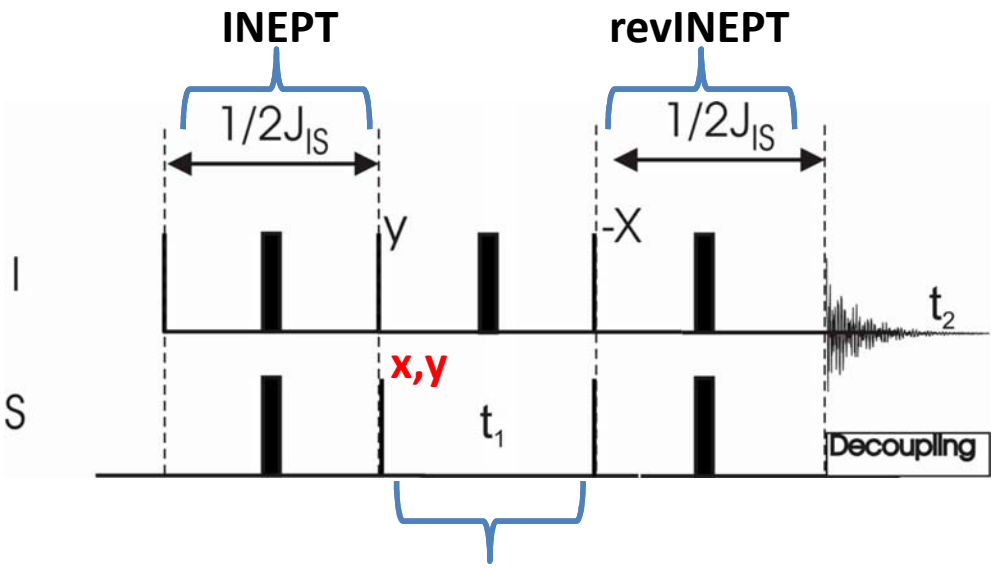

ω_S evol.

$$I_z \xrightarrow{\{\text{INEPT}\}} -I_z S_y$$

$$\left\{ \xrightarrow{\omega_S t_1 \widehat{S_z}} -I_z S_y \cos(\omega_S t_1) + I_z S_x \sin(\omega_S t_1) \right\}$$

$$\xrightarrow{\{\text{revINEPT}\}} I_y \cos(\omega_S t_1)$$

In combination with the Sy pulse experiment

$$I^{\pm} e^{\mp i\omega_I t_2} e^{\mp i\omega_S t_1}$$

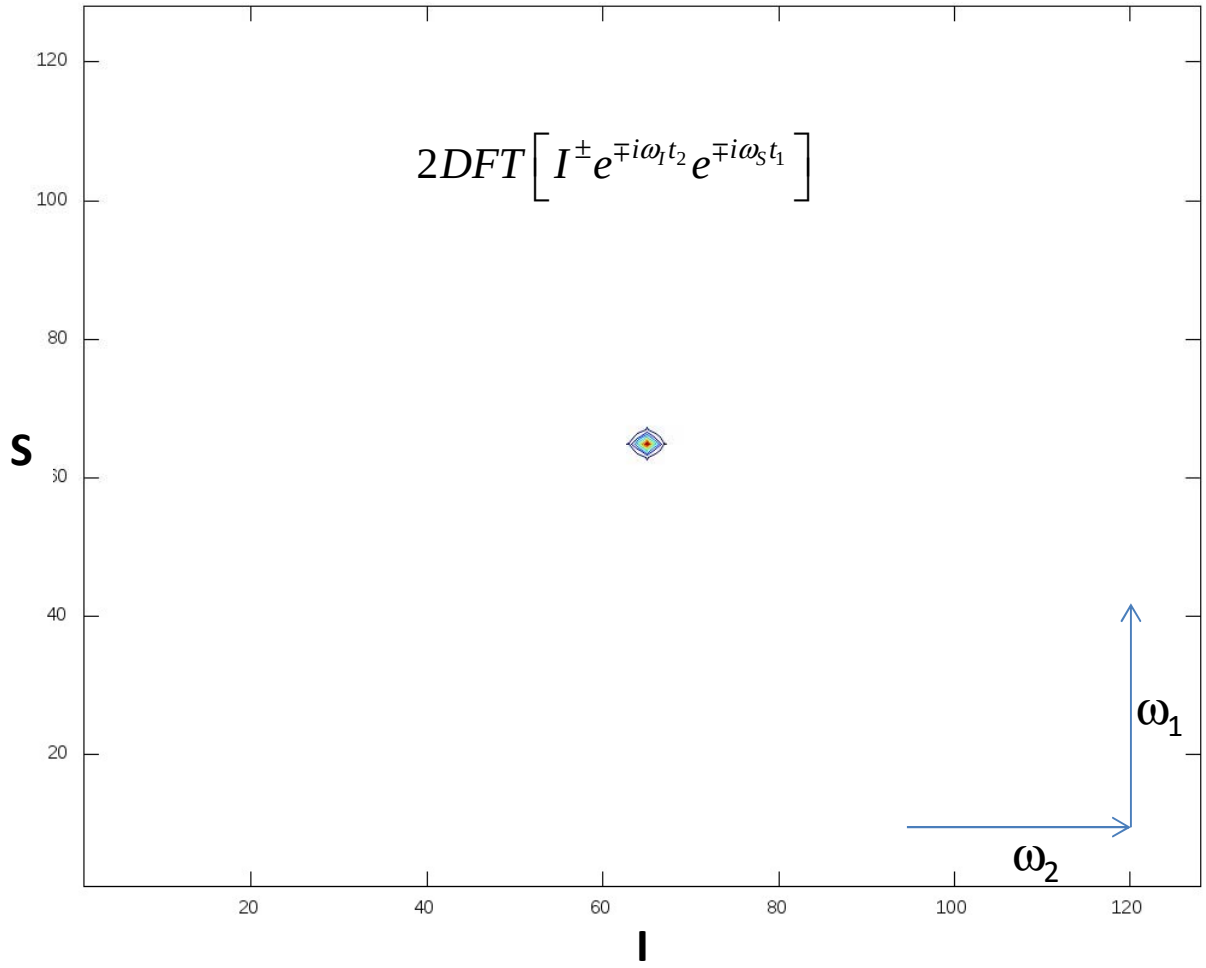
$2DFT\left[I^{\pm} e^{\mp i\omega_I t_2} e^{\mp i\omega_S t_1} \right]$
120
100
80
S
40
20
20
40
60
80
100
120
I
ω_1
ω_2

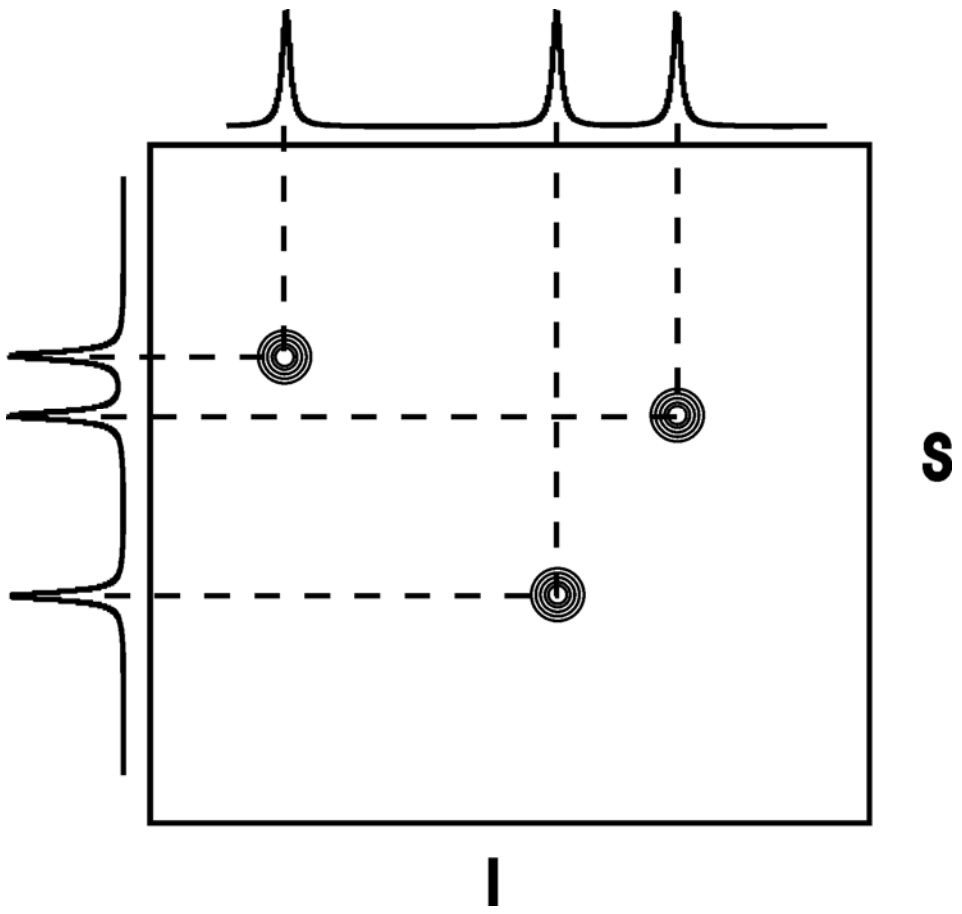
S
I

HMQC (Heteronuclear Multiple Quantum Correlation)

Editing

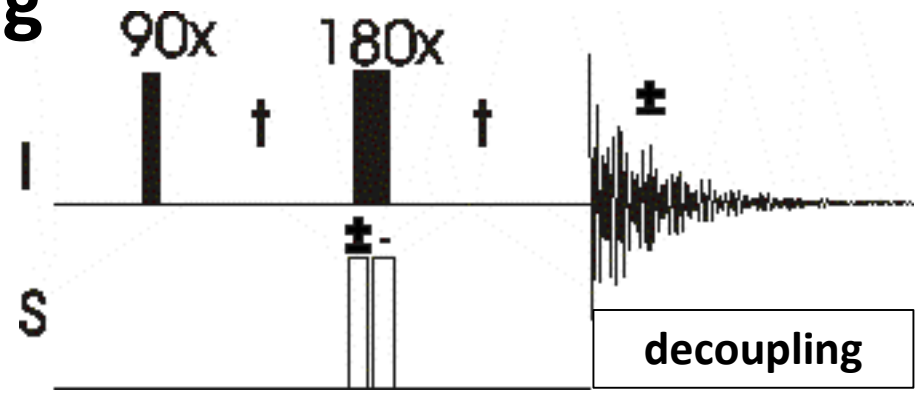

HMQC

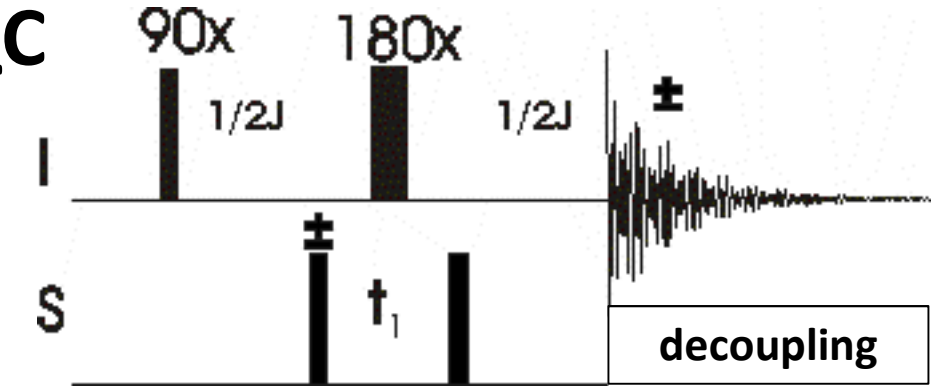

HMBC triple lowpass grad selected (Echo-antiecho)

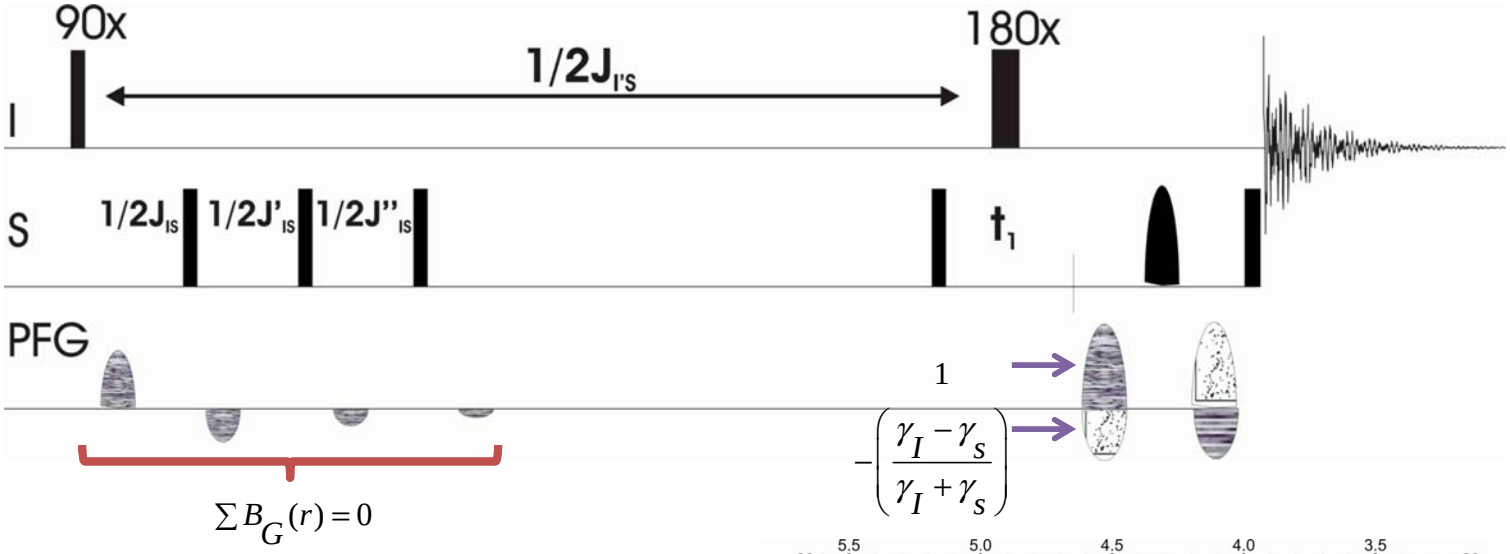

I is gradient refocused

$I^+ S_{x,y}$ is defocused

Bruker: hmbcetgpl3nd

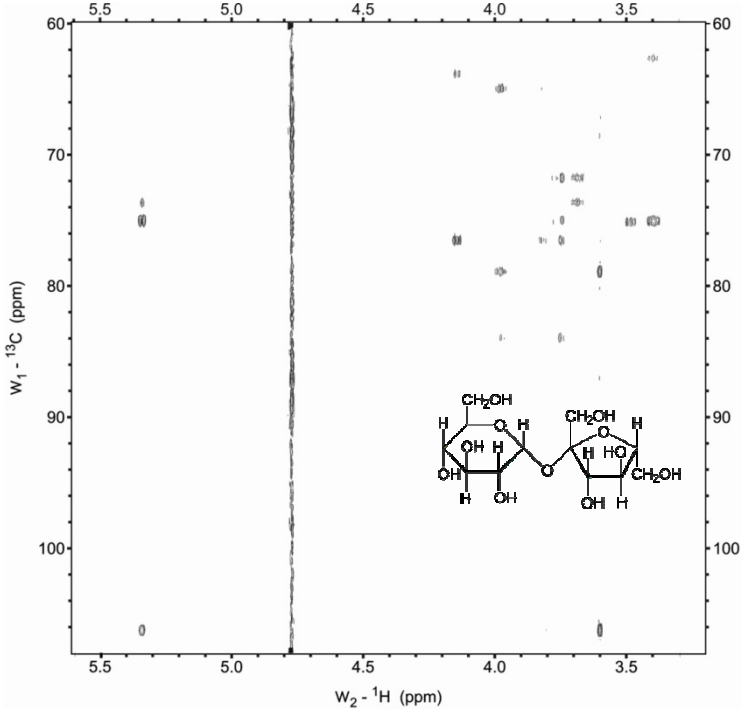

Double Quantum Filtered – HH COSY

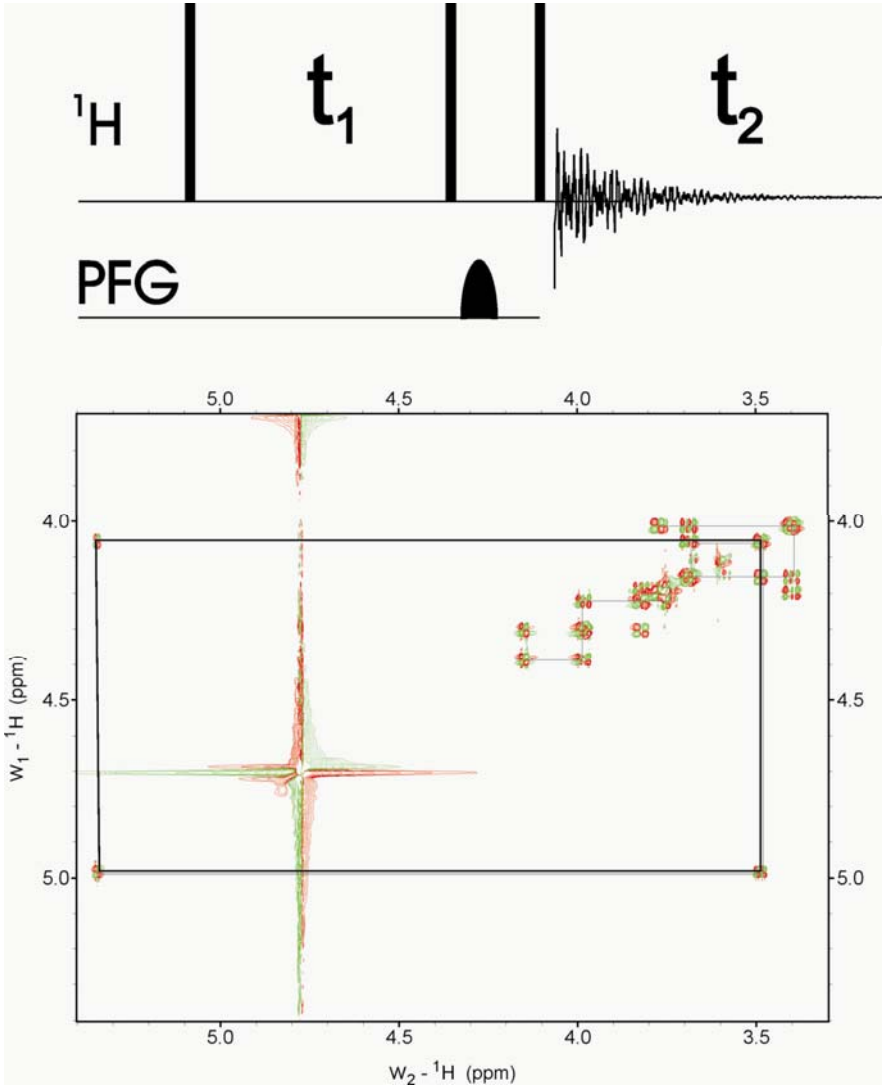

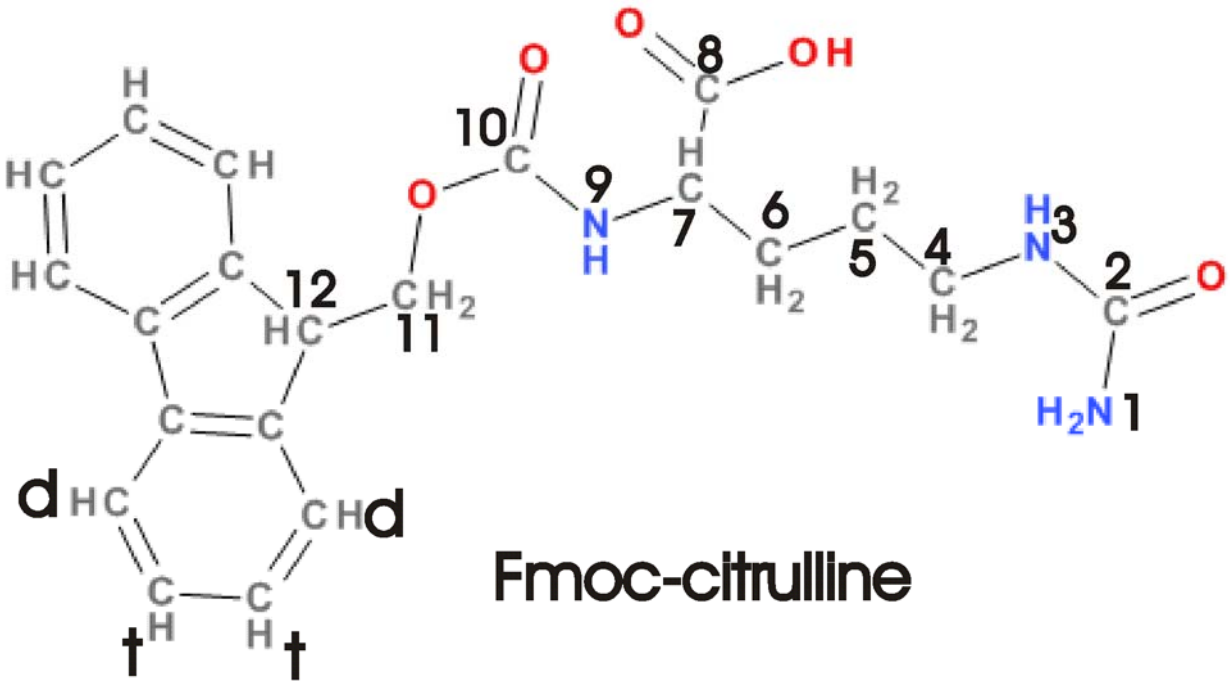
Fmoc-citrulline

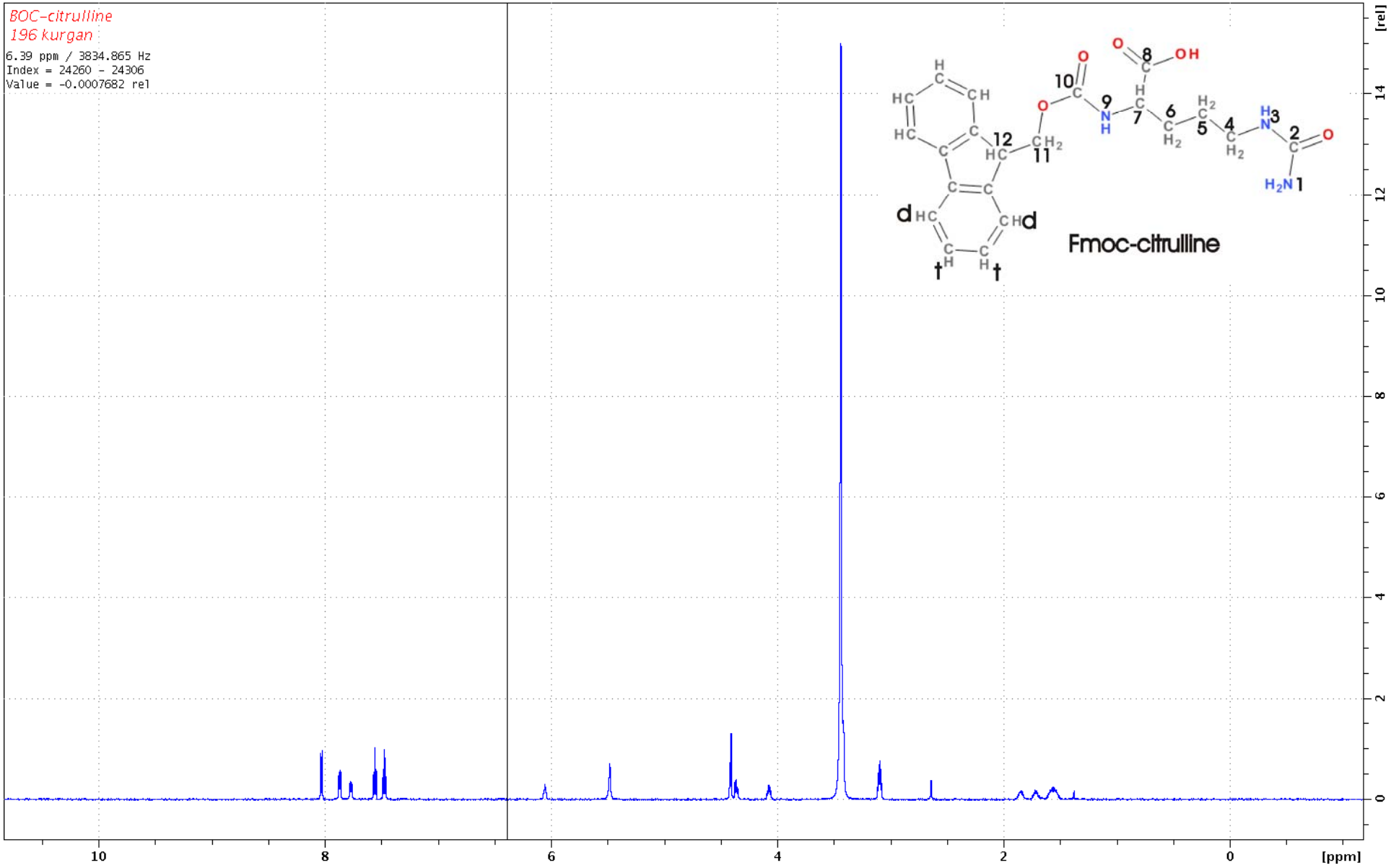
BOC-citrulline
196 kurgan
6.39 ppm / 3834.865 Hz
Index = 24260 - 24306
Value = -0.0007682 rel
Fmoc-citrulline
[rel]
[ppm]
10
8
6
4
2
0

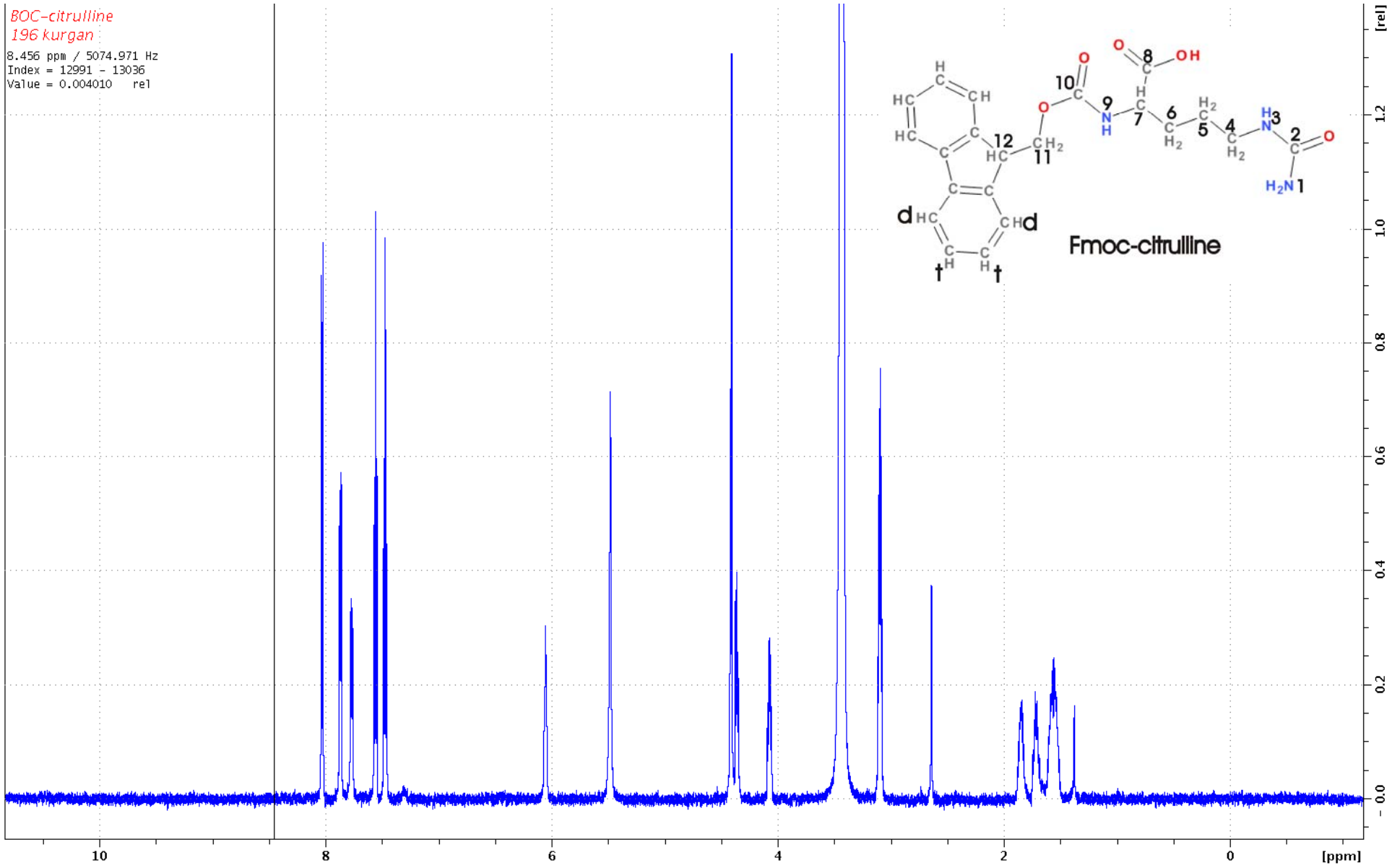
BOC-citrulline
196 kurgan
8.456 ppm / 5074.971 Hz
Index = 12991 - 13036
Value = 0.004010 rel
Fmoc-citrulline
[rel]
[ppm]

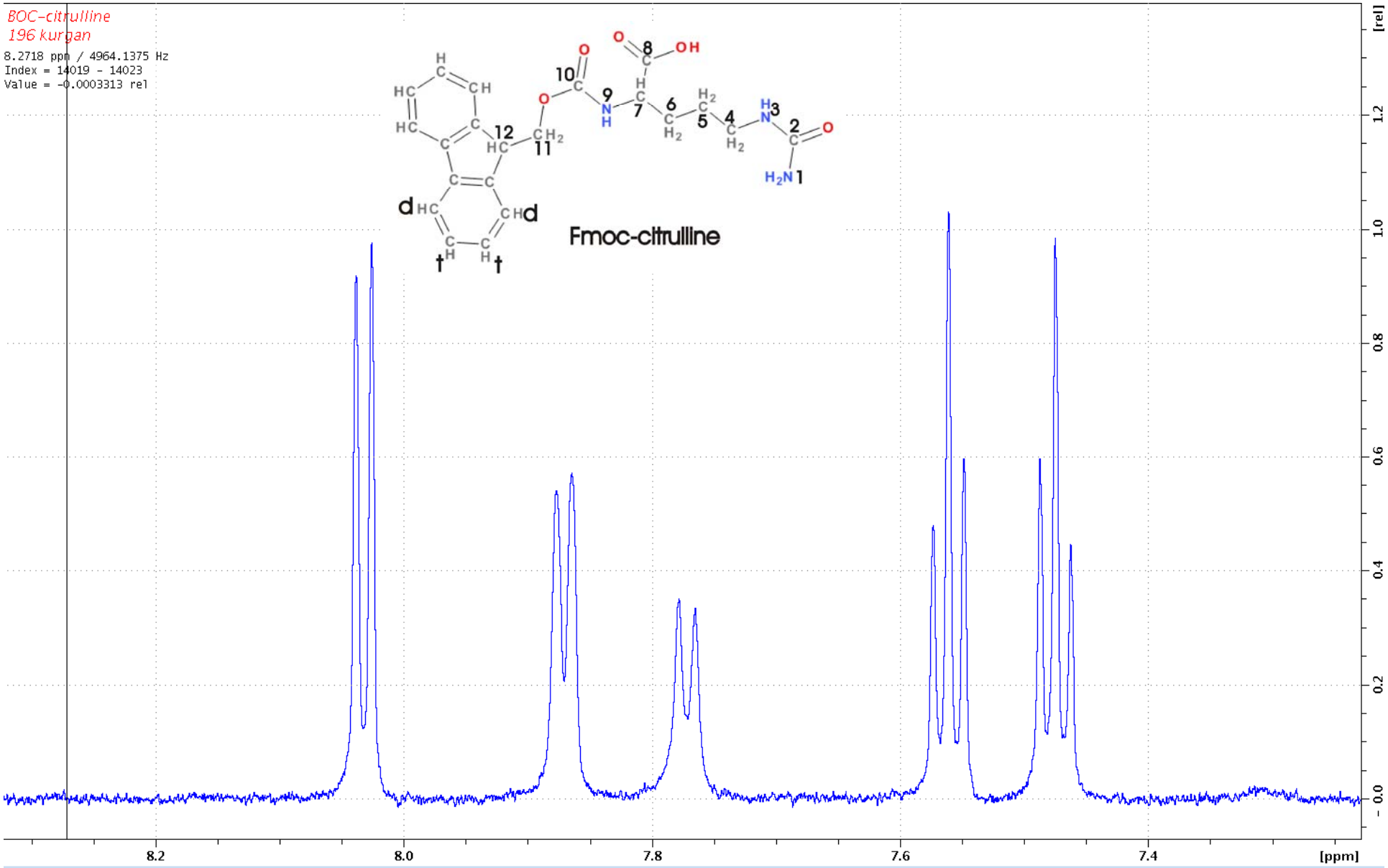
BOC-citrulline
196 kurgan
8.2718 ppm / 4964.1375 Hz
Index = 14019 - 14023
Value = -0.0003313 rel
Fmoc-citrulline
[rel]
1.2
1.0
0.8
0.6
0.4
0.2
- 0.0
8.2
8.0
7.8
7.6
7.4
[ppm]

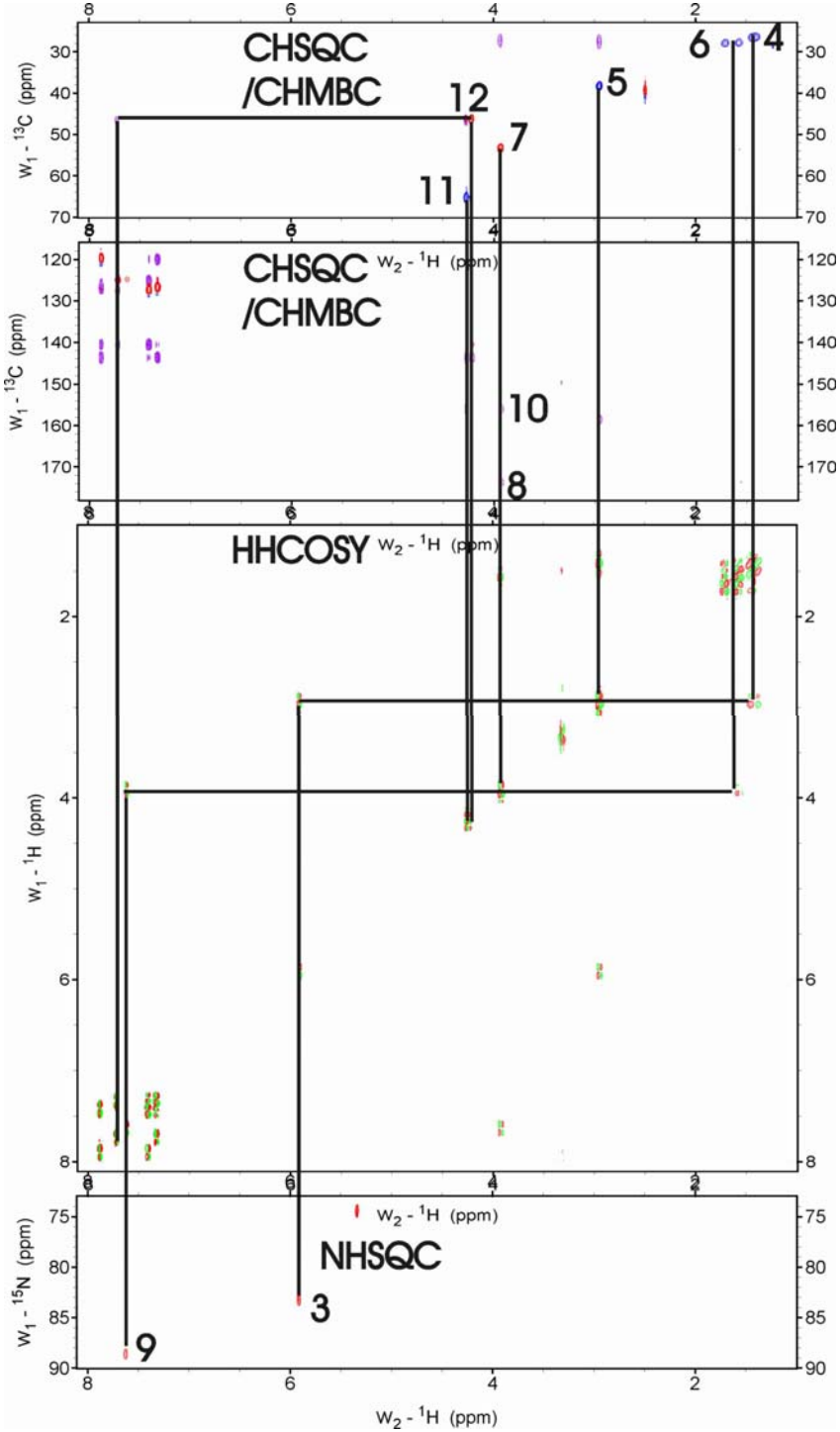
CHSQC
/CHMBC
12
7
11
5
6
4
CHSQC
/CHMBC
10
8
HHCOSY
NHSQC
3
9
W1 - 13C (ppm)
W2 - 1H (ppm)
W1 - 1H (ppm)
W1 - 15N (ppm)

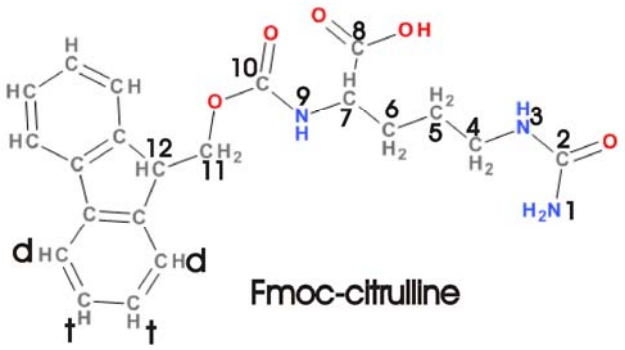
Fmoc-citrulline

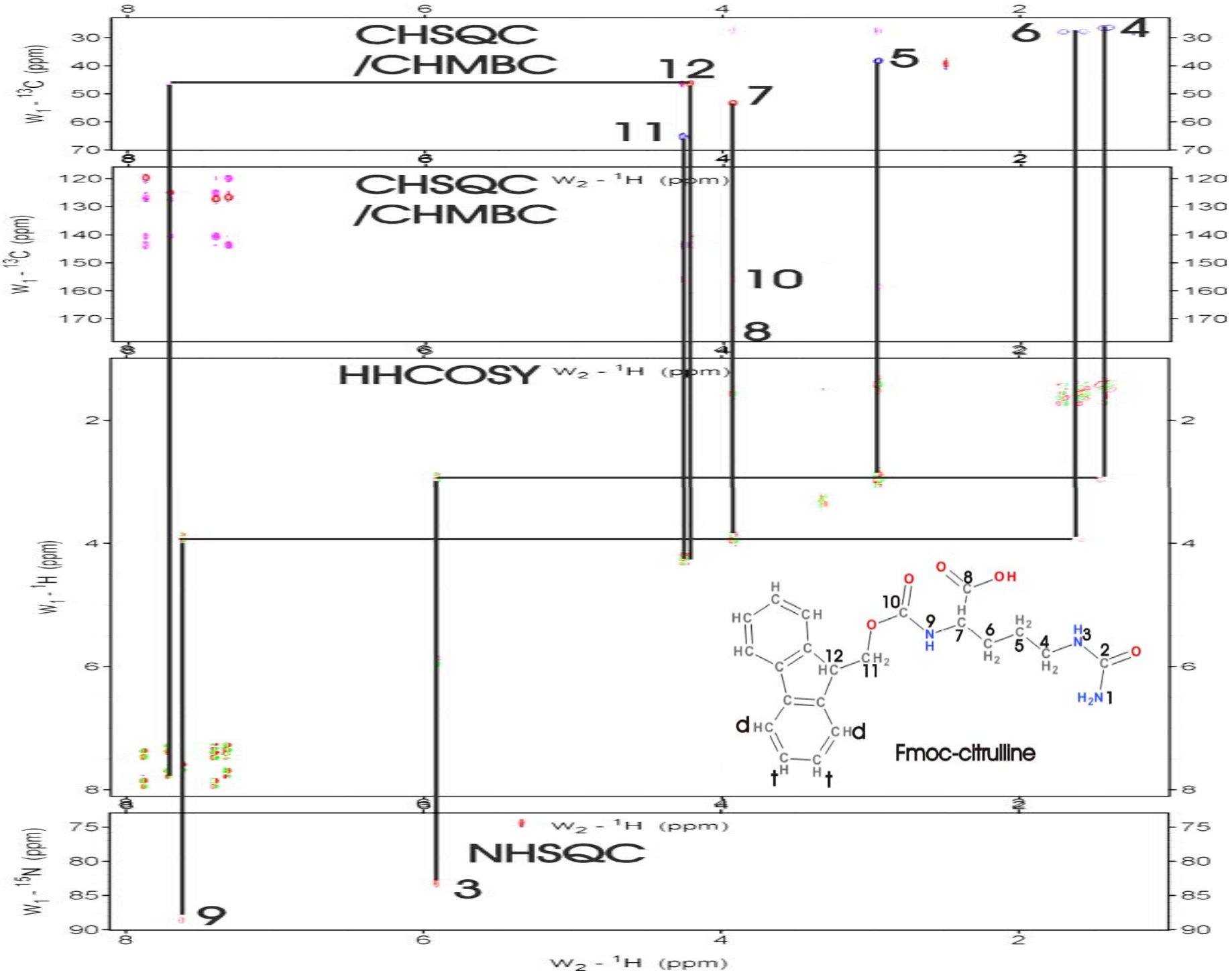
CHSQC
/CHMBC
12
7
11
5
6
4
CHSQC
/CHMBC
10
8
HHCOSY
NHSQC
3
9
W2 - 1H (ppm)
W1 - 13C (ppm)
W1 - 1H (ppm)
W1 - 15N (ppm)
Fmoc-citrulline

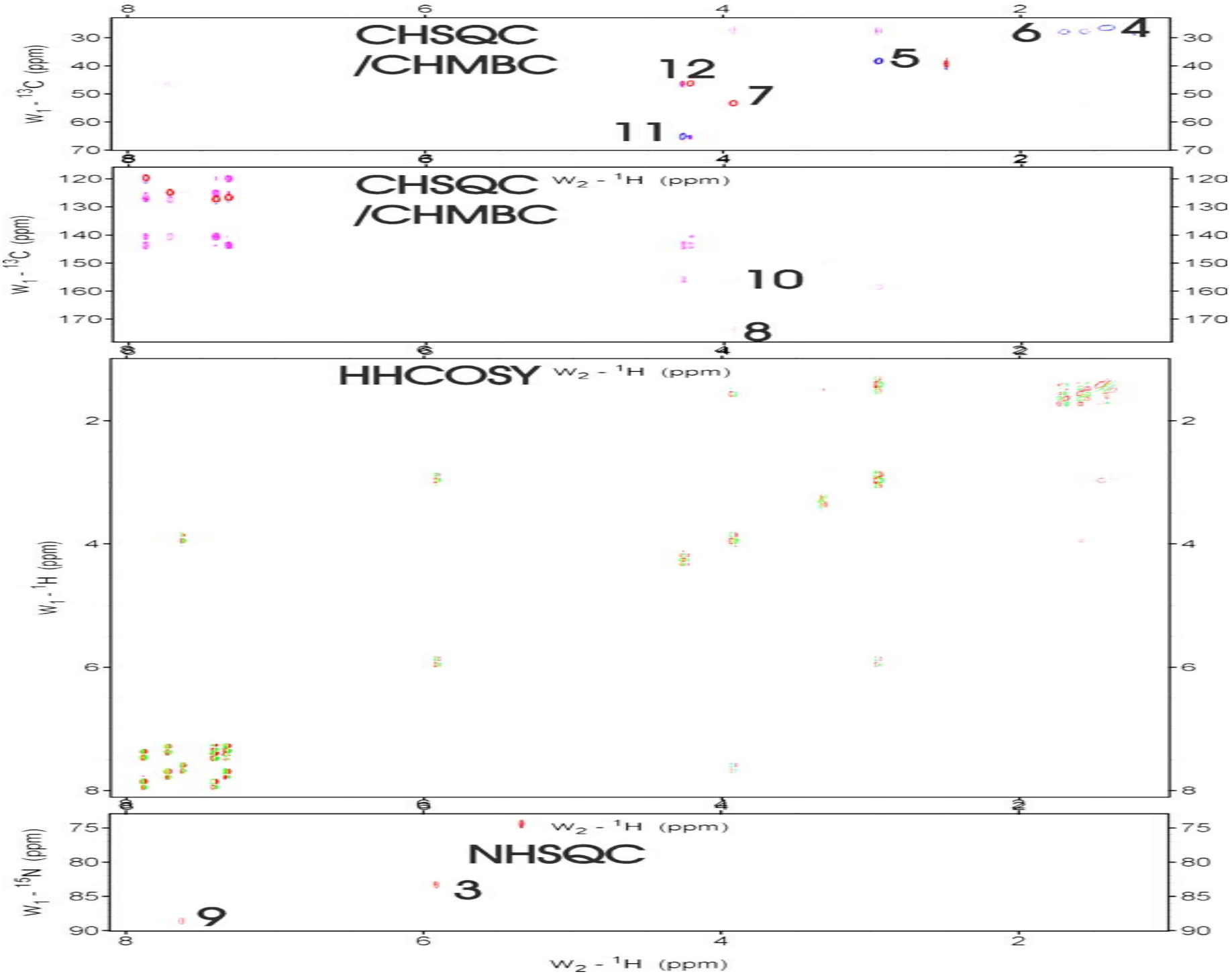
CHSQC
/CHMBC
12
7
11
6
4
5
CHSQC
/CHMBC
10
8
HHCOSY
NHSQC
3
9
W2 - 1H (ppm)
W1 - 13C (ppm)
W1 - 1H (ppm)
W1 - 15N (ppm)

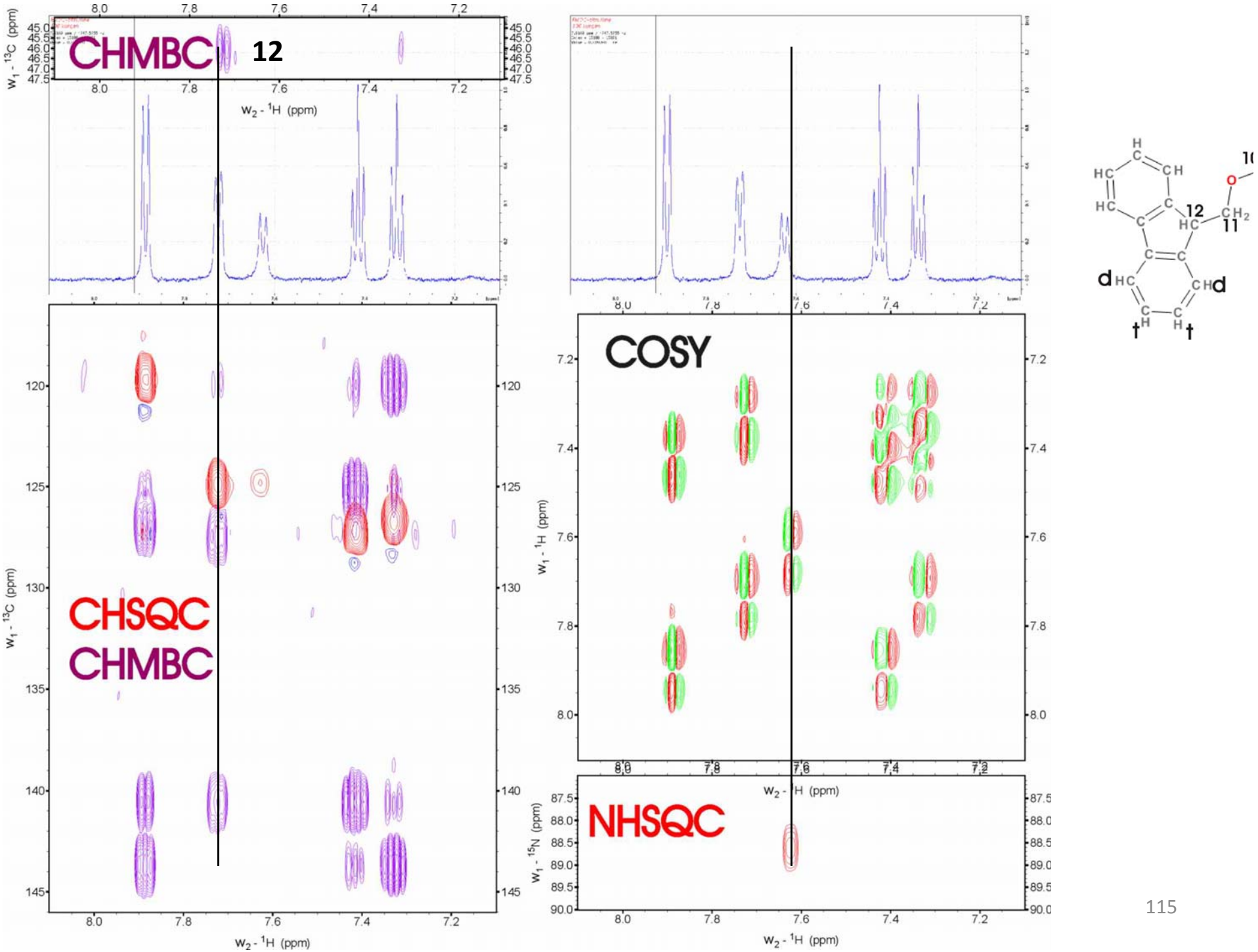
CHMBC
12
w_1 - ^{13}C (ppm)
w_2 - ^{1}H (ppm)
CHSQC
CHMBC
COSY
NHSQC
w_1 - ^{1}H (ppm)
w_1 - ^{15}N (ppm)
12
11
d
d
t
t